SELF-ASSEMBLED MONOLAYERS GENERATED FROM CHOLESTEROL-BASED THIOLS

A Dissertation

Presented to

the Faculty of the Department of Chemistry

University of Houston

In Partial Fulfillment

of the Requirements for the Degree of

Doctor of Philosophy

By

Lynn Michelle Tarkington

August 2012

SELF-ASSEMBLED MONOLAYERS GENERATED FROM CHOLESTEROL-BASED THIOLS

_____

Lynn Michelle Tarkington

APPROVED:

_____

Dr. T. Randall Lee, Chairman

_____

Dr. Scott R. Gilbertson

_____

Dr. Chengzhi Cai

_____

Dr. David M. Hoffman

_____

Dr. Rebecca L. Forrest

_____

Dr. Mark A. Smith, Dean, College of Natural Sciences and Mathematics

ACKNOWLEDGMENTS

My deepest appreciation goes to Dr. T. Randall Lee for his guidance and support throughout my graduate study as my research advisor. I would also like to express my gratitude to the entire committee members, including Dr. Scott Gilbertson, Dr. Olafs Daugulis, Dr. Chengzhi Cai, Dr. Rigoberto Advincula, Dr. David Hoffman, and Dr. Rebecca Forest for their time and valuable feedback.

I applaud my group members, both graduated and current. Without their support, both socially and educationally, I would not have been able to complete this degree. I would like to thank Budapol Singhana and Oussama Zenasi for their synthetic advising, instrumental direction, and constant encouragement. I'd like to thank Crystal Young and Arati Kolhatkar for their lunch time collaboration which out which, I mentally would not have survived graduate school. My greatest appreciation goes to Dr. Andrew C. Jameson, for without whom, this dissertation would not exist. His advice, editing, and constant conversations have been the most helpful.

I am appreciative of my parents, Mr & Mrs. Larry Tarkington, for their support and prayers. Without their constant encouragement, I would not be where I am today.

I am affectionately grateful for Edward Foster and his patience, support, and love.

SELF-ASSEMBLED MONOLAYERS GENERATED FROM CHOLESTEROL-BASED THIOLS

An Abstract of a Dissertation

Presented to

the Faculty of the Department of Chemistry

University of Houston

In Partial Fulfillment

of the Requirements for the Degree of

Doctor of Philosophy

By

Lynn Michelle Tarkington

August 2012

ABSTRACT

Self-assembled monolayers (SAMs) generated from adsorption of the single-chained cholesterol-based and unsymmetrical double-chained cholesterol-based thiols on gold substrates were examined. The single-chained cholesterol-based thiols have a thiol headgroup, hydrocarbon spacer consisting of 3 – 12 methylene units, and a cholesterol tailgroup. The double-chained cholesterol-based thiols consist of a thiol headgroup and two tailgroups: an alkyl chain and a cholesterol-based moiety. Two series of single-component SAMs were formed from the cholesterol-based thiols. Analysis of the pure SAM shows that the added methylene spacer for the single-chained thiols allows for the formation of a better monolayer than that formed from thiocholesterol. The pure SAMs formed from the double-chained cholesterol-based thiols also produce a monolayer that is denser than the SAM generated from thiocholesterol, with interfacial properties resembling a SAM formed from normal alkanethiols. A series of binary SAMs generated from the single-chained cholesterol-based thiols and *n*-octadecanethiol exhibit properties of the cholesterol condensing effect. The SAMs were characterized using ellipsometry, contact angle goniometry, polarization modulation infrared reflection absorption spectroscopy (PM-IRRAS), and X-ray photoelectron spectroscopy (XPS). Overall, these cholesterol-based adsorbates were used to generate dense monolayers despite a mixed composition of cholesterol moieties and trans-extended alkyl chains. The cholesterol condensing effect was observed in self-assembled monolayers for the first time.

TABLE OF CONTENTS

APPENDIX I.

APPENDIX II.

LIST OF FIGURES

LIST OF SCHEMES

LIST OF TABLES

LIST OF ABBREVIATIONS

DLPC	1,2-Dilauroyl-*sn*-glycero-3-phosphocholine
DMPC	1,2-Dimyristoyl-*sn*-glycero-3-phosphocholine
DOPC	1,2-Dioleoyl-*sn*-glycero-3-phosphocholine
DPPC	1,2-Dipalmitoyl-*sn*-glycero-3-phosphocholine
DSPC	1,2-Distearoyl-*sn*-glycero-3-phosphocholine
EtOH	Ethanol
HCl	Hydrochloric acid
LB	Langmuir-Blodgett
LiAlH	Lithium aluminum hydride
MsCl	Methanesulfonyl chloride
MeOH	Methanol
MCT	Mercury-cadmium telluride
MD	Molecular Dynamics
MC	Monte-Carlo
DMF	N,N-dimethylformamide
NMR	Nuclear Magnetic Resonance
PMPC	1-Palmitoyl-2-myristoyl-*sn*-glycero-3-phosphocholine
POPC	1-Palmitoyl-2-oleoyl-*sn*-glycero-3-phosphocholine
PM-IRRAS	Polarization Modulation Infrared Reflection Absorption Spectroscopy
KSAc	Potassium thioacetate

SAMs	Self-assembled monolayers
NaH	Sodium hydride
NaOH	Sodium hydroxide
NaI	Sodium iodide
SOPC	1-Stearoyl-2-oleoyl-*sn*-glycero-3-phosphocholine
THF	Tetrahydrofuran
TLC	Thin-layer chromatography
TsCl	*p*-Toluenesulfonyl chloride
NEt_3	Triethylamine
UPS	Ultraviolet Photoelectron Spectroscopy
XPS	X-ray Photoelectron Spectroscopy

Chapter 1: Cholesterol and Monolayers: The Condensing Effect

1.1. Introduction

1.1.1. Cholesterol

Cholesterol has drawn the interest of researchers in chemistry, biology, and related fields of research since its first structural characterization in 1932.[1] Cholesterol is an important biological molecule and serves many functions in nature due to its chemical structure and corresponding physical properties. In humans, the majority of cholesterol is found in cellular membranes; furthermore, high concentrations within the cardiovascular system often lead to health problems. For example, excess cholesterol is believed to be the main cause of coronary heart disease, and many healthcare professionals recognize the potential consequences of consuming large amounts of cholesterol.[2-5] Cholesterol is also involved in the metabolism of biological molecules such as vitamin D, but the greatest impact of cholesterol can be traced to its effects on biological membranes.

Cholesterol is composed of three main functional elements: a hydrophilic hydroxyl-containing headgroup, a rigid group of polycyclic steroid rings, and a flexible short hydrocarbon tail (Figure 1.1). The hydrocarbon tail consists of a flexible isooctyl group. In the three dimensional conformation, the hydrocarbon tail is curved, providing a slight overall bend to the molecule. The rigid polycyclic system consists of four rings, a common characteristic of steroids. The rings are *trans* to each other and thus form a

relatively flat, rigid system. There are two methyl groups attached to the ring system, creating a smooth α-face and rough β-face, both of which influence the interaction of cholesterol with biological membranes.[6] The hydrophilic hydroxyl headgroup is part of the β-face of the molecule. Other steroid compounds have additional, different, or lack one of these basic functional groups.[7]

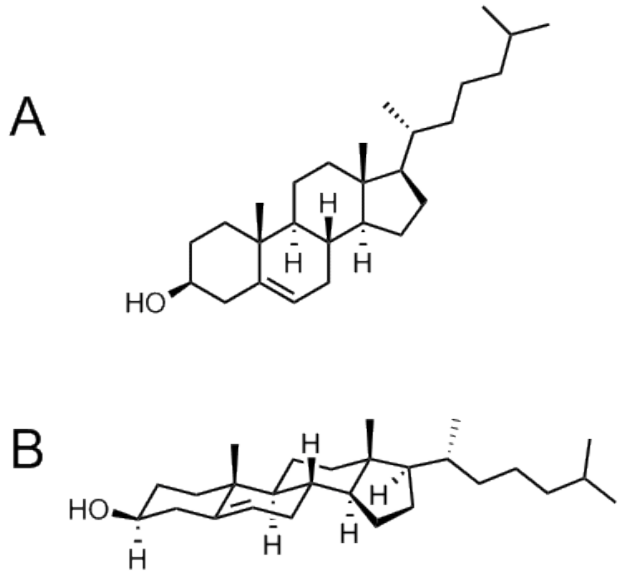

Figure 1.1. Chemical structure of cholesterol: (A) in the plane of the paper and (B) in the chair formation showing the α-face (below the plane of the molecule) and β-face (above the plane of the molecule).

1.1.2. Biological Membranes

In nature, cholesterol is found predominantly in the membranes of animal cells. The majority of eukaryotes utilize cholesterol, but they do so to different extents.

Cholesterol can also be found in bacteria, but the source of this cholesterol is subject to debate.[8-10] Animals can ingest cholesterol or biosynthesize it through a thirty-seven step process in the cytoplasm and the endoplasmic reticulum.[11,12] Cholesterol is also a precursor for vitamin D, bile acids, and other steroids. Other than synthesis, cholesterol is involved in several cellular functions, including cell signaling and membrane fluidity.[12,13] The concentration of cholesterol in a membrane will affect the fluidity of the membrane. At higher concentrations of cholesterol, the membrane is more rigid and is therefore more effective at cell signaling, active transport, facilitated diffusion across the membrane, and other membrane functions.[13]

Except in a few species of archaea, all biological membranes are bilayers that contain two molecular layers (i.e., two head-to-head monolayers). Natural bilayers consist of phospholipid arrays that are interspersed with proteins, cholesterol, and other signaling molecules. About 4 nanometers thick, phospholipid bilayers provide an enclosure for cells that allows regulation of their cellular activity.[14] Cholesterol is an important component of natural bilayers, controlling membrane strength, phase behavior, permeability to water and other small molecules, and membrane fluidity.[11,15-20] These properties arise from cholesterol's condensing effect, which occurs when the concentration of cholesterol is higher in a relatively small area of the membrane than in the remaining area of the membrane. The condensing effect causes the molecules within the membrane to order and become more densely packed. Well-ordered areas of biological membranes are known as lipid rafts.

Lipid rafts (Figure 1.2) are microdomains within a natural bilayer that promote cellular processes, such as signaling, protein activation and deactivation, and transport across the membrane.[21,22] Lipid rafts are freely floating, tightly packed regions. First discovered in 1972 by Singer and Nicolson,[23] the definition of lipid rafts was changed in 2006 at the Keystone Symposium of Lipid Rafts and Cell Function, "Membrane rafts are

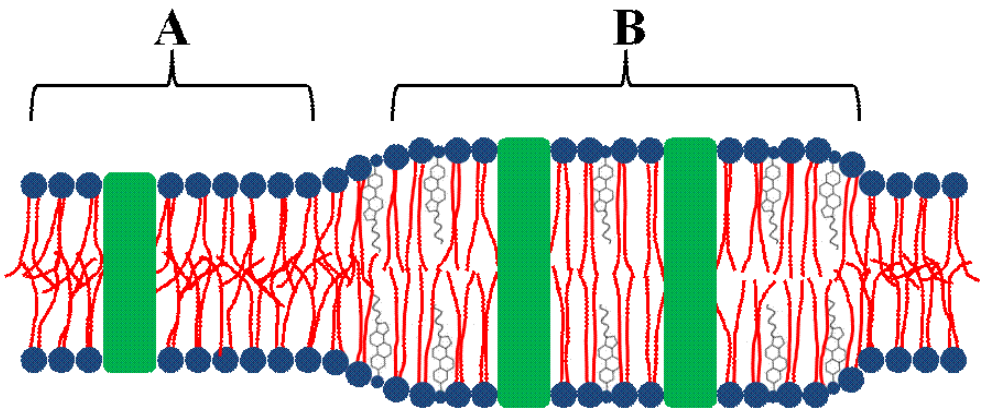

Figure 1.2. A drawing of a biological membrane with (A) a standard lipid bilayer and (B) a lipid raft. The blue circles represent polar headgroups, the red lines represent hydrocarbon tailgroups, the green rectangles represent proteins and other transmembrane molecules, and the black chemical structures represent cholesterol.

small (10 – 200 nm), heterogeneous, highly dynamic, sterol- and sphingolipid-enriched domains that compartmentalize cellular processes. Small rafts can sometimes be stabilized to form larger platforms through protein-protein and protein-lipid interactions."[22] Lipid rafts contain high levels of cholesterol and sphingolipids as compared to the surrounding membrane.[24,25] The high levels of cholesterol in lipid rafts

are believed to be responsible for the raft's high density and stability; correspondingly, cholesterol is considered to have the capacity to condense membranes.

1.1.3. The Condensing Effect

In 1925, Leathes reported for the first time the cholesterol condensing effect at the air-water interface with mixed monolayer systems.[26] He described the interaction as something other than a "chemical union", but clearly noted the attraction of cholesterol and lipids. Since this discovery, extensive research has attempted to explain the mechanism by which the phenomenon occurs. First defined as an increase in surface density caused by cholesterol,[27] the phenomenon is now defined as a decrease in surface area of a mixed lipid monolayer containing cholesterol.[28] In other words, when comparing two monolayers, the monolayer mixed with cholesterol will have less surface area than a monolayer without cholesterol.

The process of condensing a membrane involves the ordering of molecules and inducing a tilt angle. When cholesterol is added to a lipid monolayer, the lipid molecules rotate and move, which is ordering, and the molecules tilt to a given angle that maximizes packing. A well-ordered monolayer is typically crystalline in nature. As the molecules begin to order, van der Waals interactions between hydrocarbons of adjacent molecules causes them to tilt and become closer together in the monolayer. The tilt of a molecule is measured by the angle of the axis of the molecule from the surface normal and allows for molecules to become closer together. When monolayers, or bilayers, have tilt and order,

they form condensed structures. The magnitude of the condensing phenomenon has been observed in mixtures of cholesterol with sphingomyelin, phosphatides, or phosphatidylcholine. Small condensing effects have been observed with other membrane lipids.

A few other sterols, which are shown in Figure 1.3, produce a condensing effect; however, none condense lipid monolayers as effectively as cholesterol. At low concentrations, lanosterol has slightly less ordering ability than cholesterol, but lanosterol produces a larger tilt angle and thus gives rise to films that are less condensed.[29] When

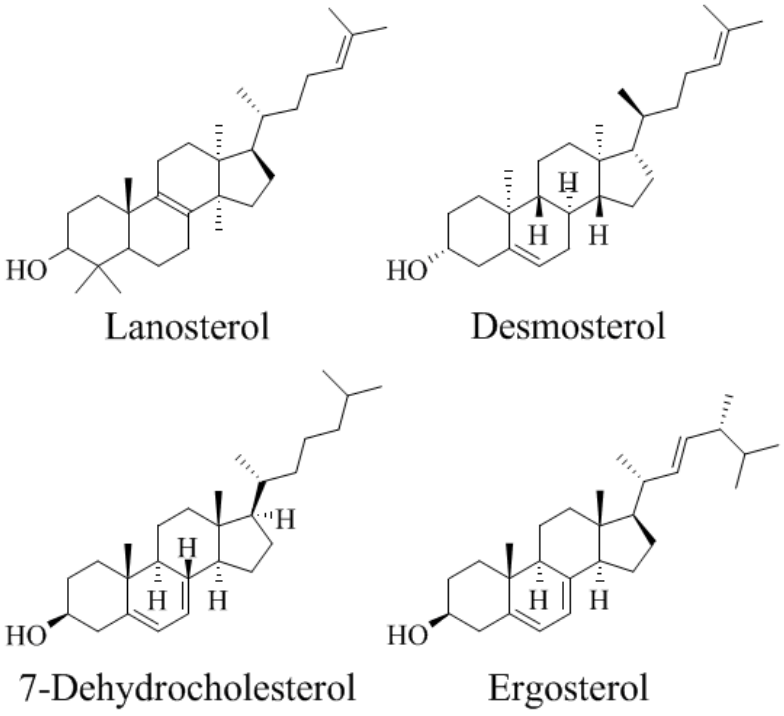

Figure 1.3. Structures of steroids that show an effect on a lipid monolayer similar to cholesterol.

compared to cholesterol, desmosterol has a relatively equal condensing effect on unsaturated lipids; however, its effect on saturated lipids is less than that of cholesterol.[30-33] The compound 7-dehydrocholesterol condenses monolayers to a slightly lesser extent than cholesterol.[32,34] Ergosterol, commonly found in fungi and protozoa species, exhibits a greater ordering effect than cholesterol, regardless of the lipid; however, it induces a larger tilt angle and thus a smaller condensing effect.[35-37] Manipulation of the hydroxyl headgroup fails to enhance the condensing effect, based on studies with cholesterol sulphate,[38] epicholesterol,[39] ketosterone,[40] cholesterol oxygenates,[41] and cholate.[42]

While biological membranes can be extracted with the use of detergents, laboratory studies often utilize experimentally synthesized monolayers and bilayers. In a laboratory setting, monolayers can also be formed at the air-water interface in Langmuir monolayers or at the solid-liquid interface in self-assembled monolayers (SAM), as will be discussed later. Both types of monolayers and bilayers can utilize the cholesterol condensing effect. The cholesterol condensing effect has also been studied with computer simulations, which often shed light on related experimental studies.

1.1.4. Mechanistic Models of the Cholesterol Condensing Effect

Since the discovery of the cholesterol condensing effect, scientists have been trying to understand the phenomenon through mechanistic models. In 1972, Singer and Nicholson proposed the idea of a Fluid-Mosaic Model for biological membranes.[23] The Fluid-Mosaic Model allows for microdomains, such as lipid rafts, but declares that

membranes are heterogeneous with respect to their components, which include lipids, proteins, and transport channels. A purely heterogeneous model, however, fails to rationalize fully the cholesterol condensing effect. Other models that are supported by experimental evidence have been suggested for the cholesterol condensing effect.

The Superlattice Model, first described by Chong in 1994, argues that sterols regularly distribute throughout the monolayer and are not random as suggested by the Fluid-Mosaic Model (Figure 1.4).[43] It is believed that molecules form lattices within the monolayer; for example, cholesterol forms center rectangular or center hexagonal structures in phosphatidylcholine monolayers (Figure 1.5). The Superlattice Model rationalizes why intercellular membranes do not continually merge as suggested by the Fluid-Mosaic Model. In the Superlattice Model, the combination of attractive and

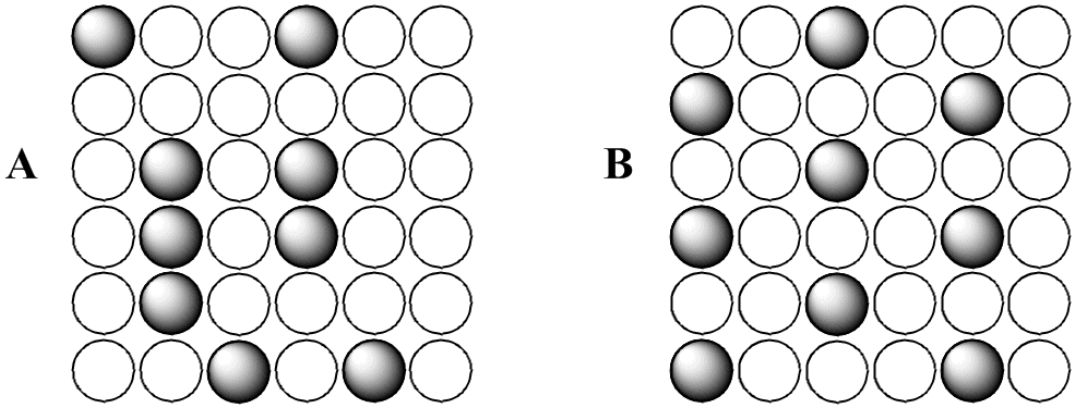

Figure 1.4. A schematic drawing for (A) the Fluid-Mosaic Model and (B) the Superlattice Model for a binary mixed monolayer.

repulsive forces within a mixed monolayer account for lattice formation. Hydrogen bonding between cholesterol and sphingolipids,[44] van der Waals attraction between the rigid polycyclic cholesterol and the flexible hydrocarbon tailgroups on lipids,[45] and Coulombic forces between acidic lipids and positively charged amino acids[46] all contribute to the attractive forces in the Superlattice Model. On the other hand, the repulsive forces arise largely from lattice strain, which can have relatively long-range intermolecular effects associated with lattice formation.[47] The Superlattice Model explains the close interaction of cholesterol and lipids with respect to the sizes of the headgroups and tailgroups: the headgroup for lipids is rather large, and the hydroxyl group of cholesterol is small; in contrast, the tailgroup for lipids is small, and the tailgroup for cholesterol is rather large.[48,49] Thus, a lattice is formed that compensates for the small-large and large-small molecular dimensions to form a condensed monolayer.

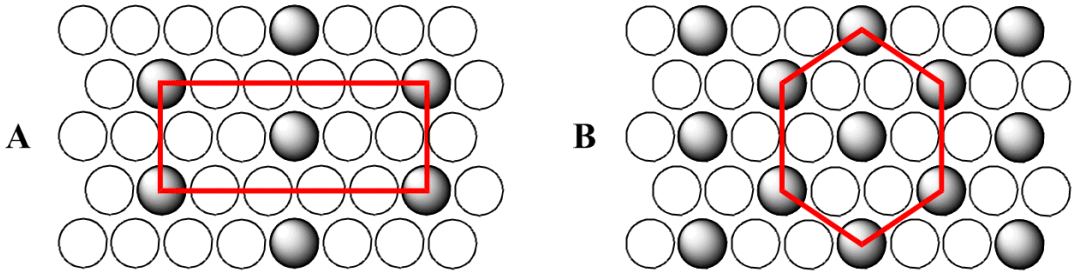

Figure 1.5. A schematic drawing of (A) center rectangular and (B) center hexagonal structures in the Superlattice Model for a binary mixed monolayer.[43-49]

The Superlattice Model is based on surface patterning and variations in the physical properties of monolayers, which are also taken into account in the Condensed

Complex Model.[50] First described in 1953 by Finean, the Condensed Complex Model states that mixtures of cholesterol and lipids form complexes with specific stoichiometries.[51,52] Based on phase diagrams for a binary mixture, the Condensed Complex Model is supported by the unusual evidence of three phases: a rich cholesterol phase, a rich lipid phase, and a mixed phase.[53,54] The phase diagram of a mixed monolayer system shows two upper critical points; consequently, all three phases are observed at the same time, which is unusual for a mixed system. It is believed that most complexes fit into one of three stoichiometric categories: (1) CP_2, where C represents cholesterol and P represents a lipid, (2) C_3P_6, and (3) C_nP_{2n}, where the oligomers can couple to form infinite series of large complexes.[55] The different stoichiometric ratios for the Condensed Complex Model were developed from the critical sterol mole fractions (*e.g.*, 20.0, 22.2, 25.0, 33.3, 40.0, and 50.0 mol % sterol), which are the ratios of cholesterol to lipid at the maximum observed mixed phases in monolayers, as compared to a rich cholesterol phase and a rich lipid phase. The Condensed Complex Model explains the transformation of circular domains into stripes in monolayers of cholesterol and lipids as the horizontal pressure is increased in a Langmuir monolayer.[56] At present, however, experimental observation (*e.g.*, images, crystallography, or analytical analysis) of cholesterol-lipid complexes has yet to be reported.

The Condensed Complex Model and Superlattice Model fail to consider the insolubility of cholesterol in water. Exposure of the hydrophobic region of cholesterol (i.e., everything except the hydroxyl group) would yield an extremely unfavorable contribution to the free energy of the system.[57] The Umbrella Model, introduced in 1999

by Huang and Feigenson, supports the cholesterol condensing effect by hypothesizing that the large headgroups of lipids shield the hydrophobic cholesterol from water, while the rigid hydrophobic region of cholesterol provides ordering, tilting, and thus condensing of the hydrocarbon tailgroups of lipids (see Figure 1.6).[58] The small hydrophilic hydroxyl group of cholesterol is an insufficient cover for the rigid hydrophobic region of cholesterol from a water interface, and thus cholesterol must

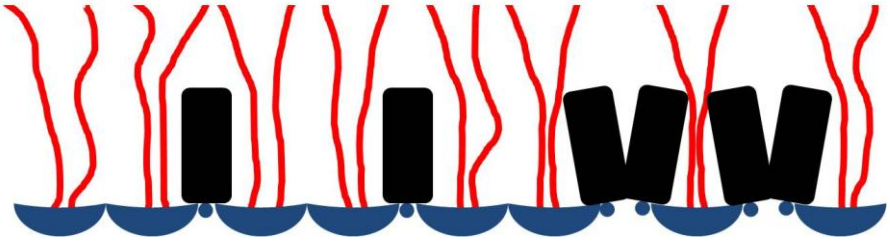

Figure 1.6. A drawing of the Umbrella Model, where the blue hemispheres represent the hydrophilic headgroups of lipids, the red lines represent the hydrophobic tailgroups, the blue circles represent the hydroxyl groups of cholesterol, and the black rectangles represent the hydrophobic region of cholesterol.

associate with the large hydrophilic headgroup of lipids.[58,59] This model is supported by the fact that pure cholesterol does not form stable monolayers or bilayers at surface pressures higher than 20 dynes/cm nor at elevated temperatures.[60] As the Umbrella Model suggests, the hydrophobic region of cholesterol is shielded from the aqueous phase by the headgroup of a lipid. However, at high concentrations of cholesterol (e.g., > 45 mol %), the lipid headgroups are no longer capable of shielding cholesterol from the

water interface, and thus it precipitates to form monohydrate crystals.[59] The Umbrella Model also explains the decrease in permeability of condensed mixed bilayers by the increase in density of the hydrophobic portion of a bilayer due to the limited space covered by the hydrophilic headgroup of the lipids and the shared space of the hydrocarbon tailgroups and hydrophobic region of cholesterol.[58,61] The "Umbrella Effect" (*e.g.*, condensing, ordering, and tilt) is strongest for nearest-neighbors, although it can be felt for the third-nearest neighbor.[62] Computer simulations show support for the Umbrella Model with both saturated and unsaturated hydrocarbons.[63,64]

The three aforementioned models apply to the majority of studies; nevertheless, not all data fit these models. Gidalevitz *et al.* proposed a model that is a mixture of the Umbrella Model and the Condensed Complex Model.[65] These researchers found that the hydroxyl groups of cholesterol were positioned at the interface methodically in accordance with the concentration of cholesterol in the solution but not in stoichiometric ratios. Sugahara *et al.* suggested a "Template Model" where the flexible hydrocarbon tailgroups of lipids complement the planar rigid cholesterol, which leads to a high number of hydrophobic contacts and thus condensing.[66] As a whole, more studies are needed to support or disprove these mechanistic models.

1.1.5. Computer Simulations of the Cholesterol Condensing Effect

Unable to develop a complete understanding of the cholesterol condensing effect from experimental observations, scientists have turned to computer simulations. The

most common simulations used to study the cholesterol condensing effect are molecular dynamics (MD) and Monte-Carlo (MC). Molecular dynamic studies were first developed for lipid systems in the 1980s.[67-69] MD simulations treats all atoms within the system classically using force fields, meaning that interactions between atoms are divided into bonded (*e.g.*, covalent and ionic) and non-bonded interactions (*e.g.*, van der Waals and electrostatic). Complex formulations allow for the potential function, or a projected trajectory, of all atoms in a system to be determined based on forces on the atoms and with respect to time. MD simulations require large quantities of variables, and a limit to this type of simulation is that these variables will not always provide accurate results. Another drawback of MD simulations is the long computational time associated with the time scale of the system. MD simulations are based on model systems and thus must be supported by experimental data.

1,2-Dipalmitoyl-*sn*-glycero-3-phosphocholine (DPPC, Figure 1.7 A) is the most commonly used lipid in MD studies and is therefore considered a standard among molecules.[70-77] When comparing the cholesterol condensing effect on DPPC bilayers versus 1,2-dimyristoyl-*sn*-glycero-3-phosphocholine (DMPC, Figure 1.7 B) bilayers through MD simulations, cholesterol has a greater influence on DPPC, which correlates with experimental observations.[78-82] The ordering effect of cholesterol on lipids has been studied using MD simulations.[83] The MD simulation tilt angle of cholesterol on the DMPC bilayer is 17° from the surface normal, while DPPC-cholesterol bilayers have a calculated tilt angle of 20°.[84,85] The packing differences between the α-face and β-face of cholesterol have been accurately predicted with MD simulations.[84,86] The effect of

cholesterol concentration in a lipid bilayer with respect to the cholesterol condensing effect has also been studied by MD simulations and gives results that are similar to experimental results.[87-90]

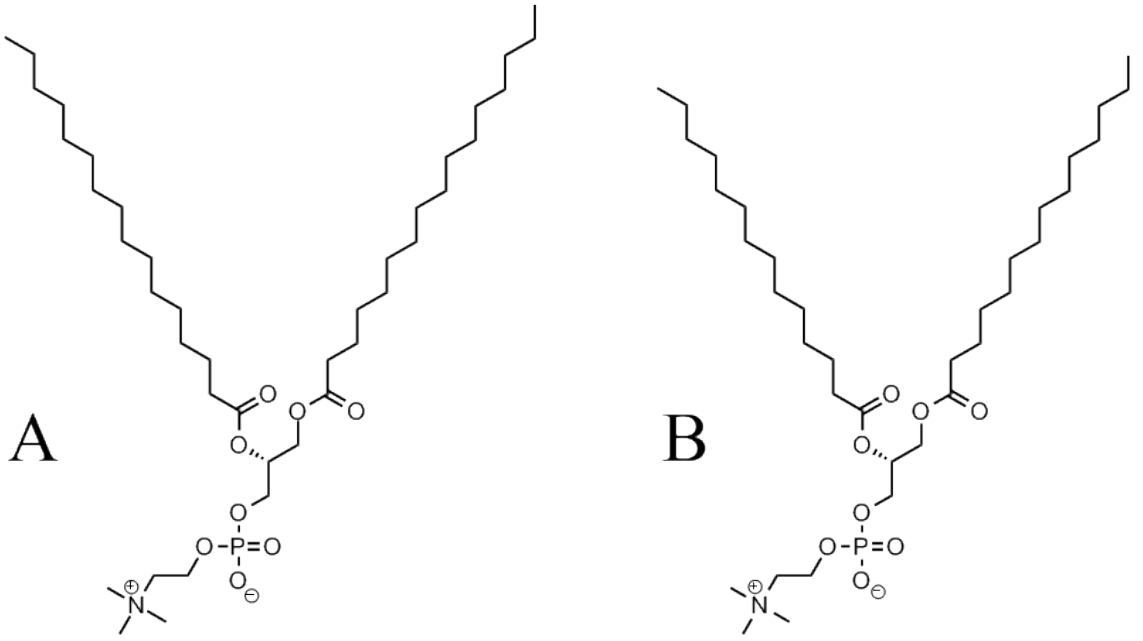

Figure 1.7. Chemical structures of (A) 1,2-dipalmitoyl-*sn*-glycero-3-phosphocholine (DPPC) and (B) 1,2-dimyristoyl-*sn*-glycero-3-phosphocholine (DMPC). Note that the difference between to the two molecules is the number of hydrocarbons in the two tailgroups: DPPC has 16 carbons in each tailgroup, while DMPC has 14 carbons in each tailgroup.

MD simulations are considered deterministic by predicting the trajectory of the system over a given time as calculated by the average probability for the system as a whole in each event (*e.g.*, movement and interaction). Monte-Carlo simulations are

considered stochastic by providing a random probability for the molecular system. In MC simulations, the probability for each event (*e.g.*, movement and interaction) is calculated and then averaged for the whole system. Although MC simulations were developed in the 1950s by scientists at the Los Alamos National Labs,[91] they were first used on lipid bilayers in the 1970s.[92] When studying the cholesterol condensing effect, it has been suggested that the diffusion of cholesterol and lipids is too slow for accurate MD simulations, and thus only MC should be utilized. However, MC simulations tend to focus on localized phenomena, while MD simulations shed light on a broader picture.[93]

Similar to MD studies, MC simulations have provided a great deal of insight into the cholesterol condensing effect. In 1977, the first lipid bilayer MC study by Scott *et al.* paved the way for MC simulations in this field.[92] Twelve years later, these researchers showed the ordering effect of cholesterol on lipids and supported the experimental data that cholesterol has a greater affect on DPPC than other disaturated phosphatidylcholine molecules.[94] In 1991, Scott *et al.* used MC simulation to demonstrate the affect of cholesterol concentration on the condensing effect and ordering of a lipid bilayer.[95] In the last decade, MC studies have supported experimental data that describe the difference in condensing between cholesterol and lanosterol,[96] the difference in ability to condense lipids with respect to cholesterol concentration,[59] and the difference in ordering of lipids with respect to the α-face and β-face of cholesterol.[97] Computer simulation studies are a useful approach to understanding the cholesterol condensing effect; however, experimental data are still required to understand fully the mechanist models and theories behind the phenomenon.

1.2. Experimental Studies of the Cholesterol Condensing Effect

1.2.1. Langmuir-Blodgett Monolayers

In cells, biological membranes exist at liquid-liquid interfaces. Replicating a liquid-liquid interface requires two immiscible liquids; however, creating a monolayer in a liquid-air interface can be accomplished by using a Langmuir trough. Since 1917, replicating biological monolayers at the air-water interface has been thoroughly studied.[98] In brief, a Langmuir monolayer is formed by dissolving the desired molecules in a volatile solvent and then adding that mixture to pure water in a Langmuir trough. After the solvent has evaporated, the monolayer is formed by adding pressure to the system through compression of the water area during which the molecules align and diffuse throughout the monolayer. The molecules transform from a low-density lying down state to a well-packed upright state. The monolayer can be transferred to a solid substrate, known as a Langmuir-Blodgett monolayer, and even form several layers, known as a multilayer film. Langmuir-Blodgett (LB) monolayers are the most studied type of monolayer with respect to the cholesterol condensing effect.

Several aspects of the cholesterol condensing effect can be observed through the use of Langmuir-Blodgett monolayers. The actual condensing of a monolayer can be observed as well as ordering and tilting of a monolayer by the addition of cholesterol. There have been several unique features of the condensing phenomenon that scientist use to validate various mechanistic models. The condensing ability of cholesterol depends

on many variables: the concentration of cholesterol in the mixture, the number of different types of lipids in the mixture, and the difference in lipid structure (*e.g.*, chain length, symmetry of tailgroups, saturation of tailgroups, headgroups, and body structure).

The most common lipid explored in cholesterol condensing studies is DPPC (Figure 1.7 A). DPPC contains two acyl tailgroups that are fully saturated and contain 16 carbons. Kusumi *et al*. used fluorescence spectroscopy to study the effect of chain length and cholesterol's ability to condense monolayers.[79] These researchers studied 1,2-dilauroyl-*sn*-glycero-3-phosphocholine (DLPC), DMPC, DPPC, and 1,2-distearoyl-*sn*-glycero-3-phosphocholine (DSPC), containing 12, 14, 16, and 18 carbons per alkyl chain, respectively. Based on phase diagrams, they concluded that cholesterol has the least effect on DLPC and follows the order: DLPC < DSPC < DMPC < DPPC.[79] McElhaney *et al.* obtained similar results using differential scanning calorimetry.[99] Using X-ray diffraction, McIntosh found that the monolayer thickness increases for DLPC, DMPC, and DPPC, but decreases for DSPC.[100] Presti and Chan used electron spin resonance spectroscopy and found that cholesterol affected DLPC less than DPPC.[101] A supported theory for the increase in cholesterol effect from 12 carbons to 16 carbons is the van der Waals interactions of the hydrophobic region of the lipid and cholesterol. It is theorized that the length of the entire hydrophobic region of cholesterol closely matches the chain length of 16 hydrocarbons on a lipid; the affect of cholesterol on a monolayer increases as the length of the hydrocarbon region increases till 16 hydrocarbons. The diminished condensing effect on 18 carbon lipids is caused by the hydrocarbon extending beyond

cholesterol and the hydrocarbon chain disorienting due to lack of excess van der Waals as provided by cholesterol.

The difference in the cholesterol condensing effect has also been observed with lipids that contain asymmetric tailgroups. DPPC has two tailgroups containing 16 hydrocarbons, while 1-palmitoyl-2-myristoyl-*sn*-glycero-3-phosphocholine (PMPC) has one tailgroup consisting of 16 hydrocarbons and one consisting of 14 hydrocarbons (Figure 1.8). Sabatini *et al.* studied the effect of symmetry on the cholesterol condensing effect.[102] Using compression isotherms, Sabatini concluded that the difference in the condensing effect of cholesterol on asymmetric saturated lipids varies with the cholesterol concentration: DPPC shows a maximum condensing effect at 30 mol %, while PMPC shows a maximum effect at 50 mol %.[102] This significant difference in condensing effect is believed to be caused by the hydrocarbon mix-match associated with tailgroups of different lengths as seen in pure PMPC monolayers.

Another interesting impact of lipid structure on the cholesterol condensing effect is the position of the tailgroups: for phosphatidylcholine, there are two possible positions for the tailgroups, *sn*-1 and *sn*-2 (*sn* stands for stereospecific numbering of the glycerol region), as shown in Figure 1.8. Smaby *et al.* used compression isotherms to determine that the chain length of the *sn*-2 position has no effect on condensing, but the chain length

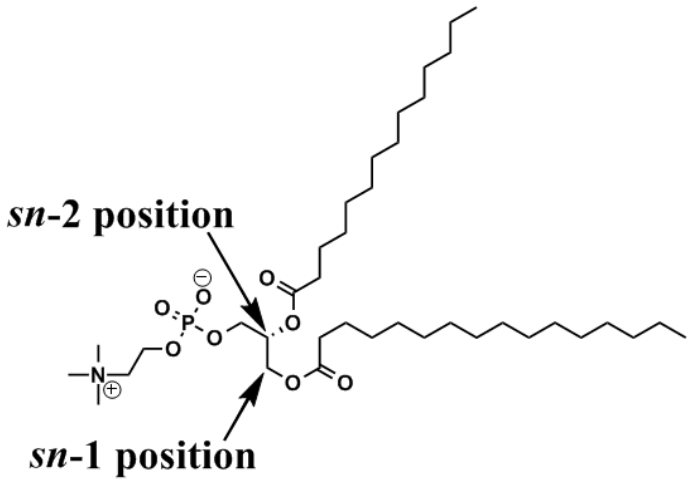

Figure 1.8. Chemical structure of 1-palmitoyl-2-myristoyl-*sn*-glycero-3-phosphocholine, showing the *sn*-1 position and the *sn*-2 position of the tailgroups.

of the *sn*-1 position is critical.[103] The researchers concluded that the hydrocarbon tailgroup at the *sn*-1 position must contain strong van der Waals interactions with cholesterol's planar rigid ring, and the lipid must position itself so that the *sn*-1 tailgroup interacts more with cholesterol than with the *sn*-2 tailgroup.

The ability of cholesterol to condense a monolayer also depends on the degree of saturation of the lipid. It is well known that cholesterol will condense saturated lipids better than unsaturated lipids, and as the degree of unsaturation increases, the extent of condensing decreases.[104] Rog *et al.* supported computational data with experimental data in their study of the weaker effects of cholesterol on monounsaturated 1-palmitoyl-2-oleoyl-*sn*-glycero-3-phosphocholine (POPC) as compared to saturated DMPC in monolayers and bilayers.[105] They also found weaker condensing in 1,2-dioleoyl-*sn*-glycero-3-phosphocholine (DOPC, a di-unsaturated lipid) versus DSPC, which is

comparable in length yet fully saturated.[106] Smaby noted that the cholesterol condensing effect is strong as long as the *sn*-1 position is saturated, with little correlation to the *sn*-2 position, even if it is unsaturated.[103] When the unsaturation is on the *sn*-1 position, the kink from the double bond prevents attractive van der Waals interactions between the tailgroup and cholesterol, and thus cholesterol has reduced effects on these monolayers.

As observed with chain length, lipids rotate so that the *sn*-1 tailgroup is positioned to interact with cholesterol, and therefore unsaturation in the *sn*-2 position has less impact on the phenomenon. Harroun *et al.* studied cholesterol and polyunsaturated lipids and found the lack of attractive van der Waals interactions led to the re-positioning of cholesterol within the monolayer to maximize condensing. The unfavorable interactions of cholesterol and polyunsaturated lipids caused cholesterol to flip upside-down in a one-dimensional neutron scattering study.[107] Hao-Wydro *et al.* showed that other sterols, ergosterol and lanosterol, exhibit condensing effects on unsaturated systems that are similar but smaller than those of cholesterol.[108]

In addition to tailgroup effects, the headgroup and backbone of a lipid also influence the cholesterol condensing effect. Glycerophospholipids can have a several different types of headgroups; phosphate, ethanolamine, choline, and serine are the most common. In 1976, van Dijck used differential scanning calorimetry to show a greater condensing effect in lipids with a choline headgroup as compared to lipids with an ethanolamine headgroup.[109,110] These results were confirmed by measuring vesicle transportation and partition coefficients as well as in bilayers with steady-state fluorescence polarization measurements.[111-113] The solubility limit of cholesterol in

phosphocholine vs. phosphoethanolamine correlates with the greater condensing effect of cholesterol on the former monolayer. Cholesterol in phosphocholine lipids can be as high a 50 – 67 mol %, whereas cholesterol in phosphoethanolamine is 35 – 45 %.[114-116] The solubility difference and effect of cholesterol on these two headgroups is believed to be caused by the difference in size of the headgroups and their capacity to shield the rigid region of cholesterol from the water at the interface.[58] Slotte *et al.* used fluorescence spectroscopy to illustrate the effect of headgroup size on cholesterol's ability to condense a monolayer.[117] Using DPPC as a control, the researchers showed the effect of methylation of the amine of the choline headgroup. They concluded that the smaller the headgroup, the better the ordering of the monolayer by cholesterol – a phenomenon believed to be caused by repulsion of the lipid headgroup and cholesterol's hydroxyl group as the lipid headgroup increases in size and the diminished hydrophilicity of the methylated amine headgroup as compared to the simple amine headgroup.

Until now, all previously mentioned lipids have consisted of glycophospholipids having two acyl tailgroups linked via ester bonds, a glycerol backbone, and a phosphor-containing headgroup. Sphingomyelin, which contains a long chain sphingoid backbone with an amide-linked acyl tailgroup, a second unsaturated tailgroup, and a phosphocholine headgroup (Figure 1.9 B), is a common lipid found in biological membranes. The interfacial region of a sphingolipid is more polar than a glyocphospholipid, and sphingolipids contain regions that are hydrogen-bond donors and acceptors, while glycophospholipids only contain regions that are hydrogen-bond acceptors.[118,119] In natural membranes, cholesterol has a greater effect on sphingolipids

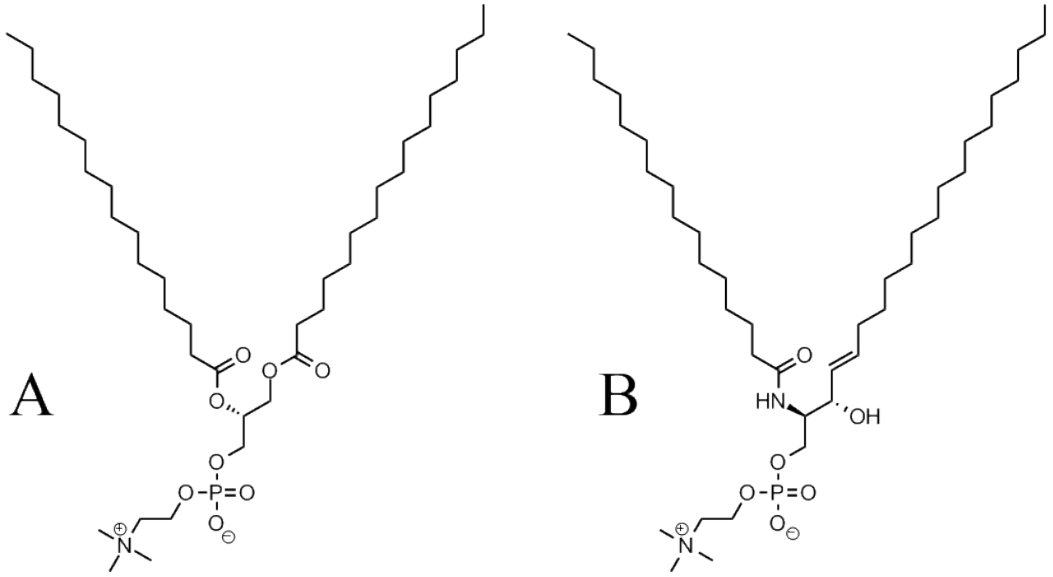

Figure 1.9. Chemical structures of general configurations for (A) glycophosphocholine and (B) sphingomyelin.

as compared to glycophospholipids; however, glycophospholipids tend to be the molecule of choice for studying the cholesterol condensing effect due to the ease in manipulation of the tailgroups as compared to sphingolipids.[119-121] Using differential scanning calorimetry, van Dijck showed that the phospholipids decrease in cholesterol affinity in the following order: sphingomyelin > phosphatidylserine, phosphatidylglycerol > phosphatidylcholine > phosphatidylethanolamine.[110] The extra hydrogen bonding between the sphingomyelin and cholesterol gives rise to the enhanced condensing effect. Li *et al.* recently discovered that the ordering affect of cholesterol at low concentrations is similar between sphingomyelin and glycophospholipids, but at higher concentrations, glycophospholipids are more ordered due to cholesterol.[122] Despite the difference in effects, the mechanism of condensing by cholesterol for sphingolipids is believed to be

the same as that for glycophospholipids; therefore, studies typically focus on cholesterol's effects on glycophospholipids.

The concentration of cholesterol in a monolayer has a strong influence on the condensing phenomenon. Bonn *et al.* used sum frequency generation spectroscopy to determine that the initial increase of cholesterol from 0 – 10 mol % has a greater affect on the order and condensation of a DPPC monolayer than an increase in cholesterol from 10 – 50 mol %.[123] In studies where the concentrations were varied, Hung *et al.* determined that the maximum monolayer thickness is achieved prior to the maximum solubility of cholesterol in DMPC, 1-stearoyl-2-oleoyl-*sn*-glycero-3-phosphocholine (SOPC), and DOPC monolayers.[124] Pan *et al.* used X-ray scattering techniques to determine that cholesterol greatly affects thickness and ordering of DPPC, DMPC, SOPC, and DOPC monolayers at 0 – 30 mol % and continues to affect the monolayer until cholesterol saturation is attained.[125]

As with all experiments, the variables can differ from group to group (e.g., temperature, pressure, and relative humidity) and thus affect the results. One major difference in experimental studies of the cholesterol condensing effect is the concentration of cholesterol in a monolayer or bilayer. The most common concentration ranges are a mole fraction = [0, 0.1, 0.3, 0.5, 0.7, 0.9, 1.0] and the critical sterol mole fraction = [0.200, 0.222, 0.250, 0.333, 0.400, 0.500]. The critical sterol mole fraction range is supported by experimental techniques, where the maximum sterol superlattice formation is observed.[43] When studying the effects of concentration on the cholesterol

condensing effect, each research group chooses their preference, most likely based off of their support for the Superlattice Model or another mechanistic model.

Historically, most membrane studies have focused on binary mixtures to simplify the study and eliminate unknown variables. As biological membranes consist of several different types of lipids, the current focus of this area of research involves ternary mixtures and multi-component mixtures. Different from binary mixtures, ternary mixtures of DPPC, DOPC, and cholesterol shows phase separation; however, DPPC and DOPC are known to phase separate in binary mixtures with each other.[126,127] Mattjus and Slotte used a ternary monolayer to test the affinity for cholesterol to sphingomyelin or phosphatidylcholine and found that cholesterol prefers sphingomyelin, which is in accordance with the stronger condensing of binary mixtures of sphingomyelin with cholesterol.[128] Veatch *et al.* created phase diagrams for ternary mixtures of cholesterol, DPPC, DOPC, POPC, DSPC, and other lipids that have become a standard for other studies.[126,129,130] Wydro studied the interactions of ternary mixtures of sphingomyelin, glycophosphatidylcholine, and cholesterol, determining that the greatest effect occurs at 30 % of the total lipids. However, there was little difference for a 50 % cholesterol film as compared to a 1:1:1 mixture in a Langmuir-Blodgett monolayer.[131]

1.2.2. Self-assembled Monolayers

Self-assembled monolayers (SAM) are another way to analyze the cholesterol condensing effect; the difference being that the monolayer forms at the liquid-solid

interface. SAMs contain fewer degrees of freedom than LBs in that the molecules undergo relatively little lateral movement within the monolayer once formed. SAMs are formed by the chemisorption of a hydrophilic headgroup of a molecule onto a solid (typically metallic) surface followed by the organization of the molecules into a monolayer.[132] The most common SAMs are formed from thiols on gold due to the lack of a stable oxide for gold at standard temperature and pressure, and the strong covalent sulfur-gold bond (ca. 40 – 45 kcal/mol).[133,134] SAMs, being on a solid substrate, can be characterized using a range of physical techniques (*e.g.*, ellipsometry, surface plasmon resonance, atomic force microscopy, X-ray diffraction, and surface infrared spectroscopy).[135]

To the best of my knowledge, the cholesterol condensing effect has never been studied directly with SAMs; however, it is possible that SAMs will provide advantages over LB films for studying the cholesterol condensing effect. SAMs, like LB films, exist as a monolayer that is a simplified version of a biological membrane. Although unmodified cholesterol does not form a monolayer on gold, supramolecular assemblies do form at the liquid-solid interface.[136] When the hydroxyl group of cholesterol is replaced with a thiol group to form thiocholesterol (Figure 1.10), a stable SAM on gold is formed via a thiolate.[137,138] Thiocholesterol makes a well-defined but inhomogenous SAM, showing defects approximately 5 – 8 Å in diameter with ~ 65 % surface coverage.[137,139,140] When thiocholesterol is mixed with an alkanethiol containing a carboxylic acid tailgroup, the alkanethiol will preferentially bind to gold even at high concentrations of thiocholesterol, due to the overall steric bulk so close to the thiol

headgroup and the α-face and β-face of thiocholesterol.[139,141] Mixed SAMs of thiocholesterol and a carboxylic acid-terminated alkanethiol appear to mimic the hydrophobic region of a Langmuir monolayer and thus mimic biological membranes. The mixed SAMs showed preferential phase separation of the thiocholesterol molecules from the alkanethiol molecules -- a characteristic found for LB monolayers when studying the cholesterol condensing effect. Despite cholesterol's inability to form a stable monolayer on water at higher surface pressures and temperatures, thiocholesterol's unique ability to form monolayers on a gold surface might prove useful for the study of the cholesterol condensing effect. To the best of my knowledge, mixed SAMs of thiocholesterol and normal alkanethiols have yet to be studied.

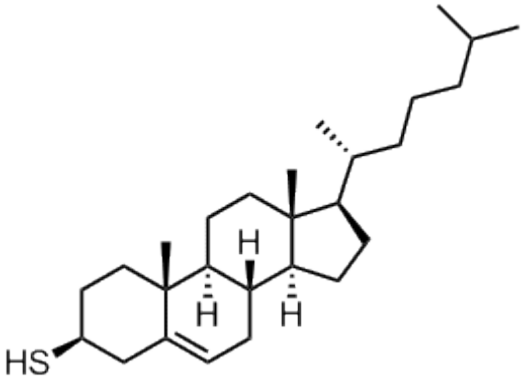

Figure 1.10. Chemical structure of thiocholesterol.

Other studies of SAMs that mimic biological membranes involve the use of cholesterol as a tether for creating a bilayer. Tethering a membrane to a solid surface utilizes the condensing effect, as the cholesterol moiety will intercalate into the

phospholipid membrane without disrupting the membrane. Through molecular design of the thiol headgroup, long spacer region, and cholesterol tailgroup, SAMs can be formed, analyzed, and then used to create bilayers of biological vesicles, which can be studied using various techniques.[135] Molecular tethers with a cholesterol tailgroup can be used to create a mixed SAM, which contains a second molecule that is shorter than the molecular tether, where the cholesterol group is extended beyond the interface of the monolayer. A membrane, micelle, or other biological vesicle can then deposit on top of the monolayer through the intercalation of cholesterol to a lipid layer.[135] Jeuken *et al.* used a cholesterol based tether to adhere a membrane from *Bacillus subtilis* to a gold substrate for analysis by atomic force microscopy and surface plasmon resonance spectroscopy.[142] This analysis allows for the characterization of the studied membrane from which proteins and other materials can be identified within the membrane.

The cholesterol-based tether used by Jeuken *et al.* consists of a thiol headgroup, a spacer comprised of three repeating units of ethylene glycol, and cholesterol as the tailgroup. The length of the hydrophilic spacer unit is essential to the attachment of a membrane, micelle, or other biological vesicle and prevents the biological vesicle from interacting with the metallic substrate, as some metals cause lysis of biological membranes. The spacer unit must be long enough for cholesterol to reach the optimal position within the biological vesicle. Others have examined up to seven repeating ethylene glycol units; the length of the spacer chosen was based on the goals of the study.[143-147] Indrieri *et al.* used a similarly designed molecule that contains 22 repeating units of ethylene glycol as a membrane tether on glass.[148] The long poly(ethylene glycol)

chain provides amphiphilic properties to the monolayer, protein resistance, and a rather large separation between the surface of the monolayer and the substrate. Cholesterol-based tethers have been used in microcontact printing for sensing applications and for attachment of a biomembrane.[149,150] The successful use of cholesterol in molecular tethers in SAMs shows the ability of cholesterol to intersperse within a lipid membrane without disrupting the functionality of the membrane while being fixed to a solid surface. As SAMs can be used to tether membranes to solid surfaces, cholesterol-based molecules can be used to study the cholesterol condensing effect in mixed SAM systems.

SAMs show great potential for the study of the cholesterol condensing effect. It is our directive to merge the molecular design of tethers and thiocholesterol to gain knowledge of the cholesterol condensing effect through the use of self-assembled monolayers.

1.3. Goals of Our Research

Understanding the cholesterol condensing effect can lead to ample opportunities within medicinal research,[151-155] sensors,[150,156] molecular modeling,[157,158] thin films,[159,160] and model membranes.[149,161] Utilizing SAMs can provide an understanding of how the rigid region of cholesterol and hydrocarbon chains interact, thus providing insight regarding this phenomenon. The molecules we will use for this research are specifically designed to maximize selected interactions between the rigid region of cholesterol and

the saturated hydrocarbon chains (e.g., positioning the rigid region of cholesterol throughout the monolayer).

1.3.1. Monolayer Formation in Our Research

Utilizing SAMs, we propose a novel study of the cholesterol condensing effect. From an experimental perspective, SAMs are perhaps the most facile method of monolayer formation. SAMs can also be formed more quickly than LB monolayers.[162] SAMs are also more cost effective and have a higher throughput of fabrication. Other drawbacks for LB films are the need for a perfectly planar substrate during LB deposition and sensitivity to environmental contaminants due to the metastable structure of the monolayer at the air-water interface as it is being transferred to a solid substrate.[163] Chemisorption of the headgroup to the gold surface during SAM formation and the design of the molecule (*e.g.,* the length of the spacer region) limit to some extent the vertical degrees of freedom of the rigid cholesterol moiety. In SAMs, all headgroups involved in the system can be positioned in the same vertical plane attached to the solid substrate, which is not necessarily the case for LB monolayers. With these attributes, we believe SAMs will be an ideal system to study the cholesterol condensing effect.

1.3.2. Molecular Design

Self-assembly in SAMs is driven by covalent bonding, van der Waals interactions, and to a lesser extent, solubility effects. The design of a molecule is important to induce self-assembly and sustain a monolayer at the liquid-solid interface. Key structural components to these molecules are the headgroup, the hydrocarbon spacer, and the tailgroup. There are many choices for each component, for which we have chosen thiol headgroups on gold surfaces, a hydrocarbon spacer having a length ranging from 3 to 12 hydrocarbons, and a cholesterol tailgroup connected via an ether linkage (Figure 1.11). Thiols on gold are a known well-studied system for SAM formation.

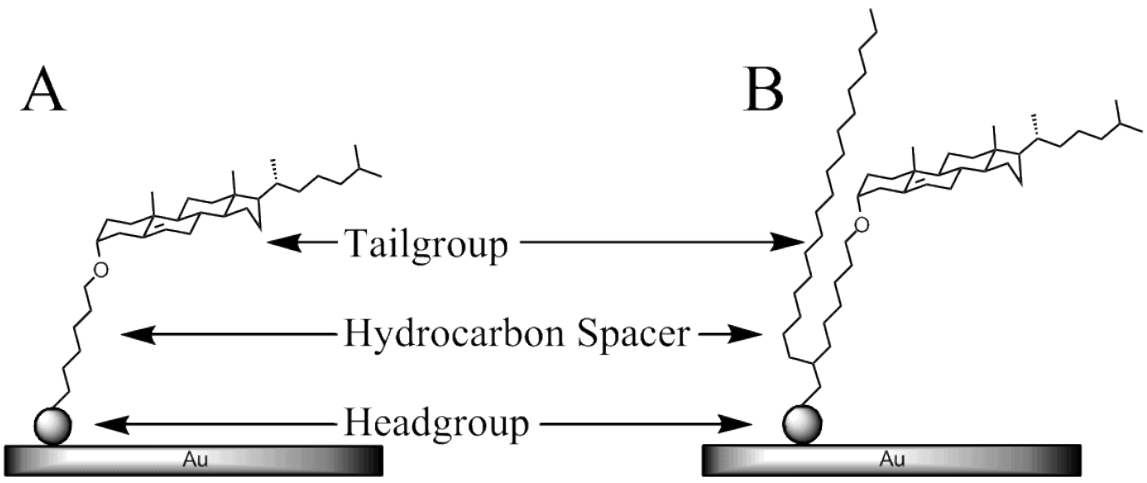

Figure 1.11. A schematic drawing of the molecules designed to study the cholesterol condensing effect in self-assembled monolayers. The molecules shown are (A) single-chained and (B) double-chained.

The hydrocarbon spacer length will position the tailgroup at a specific vertical position in the monolayer. The cholesterol tailgroup is essential to our proposed investigation of the cholesterol condensing effect.

A distinguishing aspect of our molecular design is the use of a single tailgroup (Figure 1.11 A) or two tailgroups (Figure 1.11 B). The single-chain molecule is modeled after cholesterol itself, with the addition of a hydrocarbon spacer. The double-chain molecule is modeled after a "Y" shape, with one tail being cholesterol and the other being a straight alkyl chain. The synthesis of the double-chain molecules utilizes malonic ester synthesis to create a molecule that possesses two tailgroups attached to a single carbon, which is also attached to the headgroup. The asymmetric nature of the two tailgroups -- straight alkyl chain versus polycyclic cholesterol -- should provide for interactions in the monolayer in addition to the cholesterol condensing effect, despite the bulk of the tailgroup region as compared to the headgroup region of the molecule.

Our novel SAM adsorbates will provide insight into the cholesterol condensing effect. Single-component monolayers will be analyzed to provide information concerning the formation of a monolayer based on this particular design. Data from single-component monolayers will be compared to mixed monolayers containing these cholesterol-based molecules and normal alkanethiolates, to determine the effect of cholesterol on the alkyl monolayers. Additionally, the effects of the single tailgroup versus the double tailgroup in these films will be analyzed.

1.3.3. Hypothesis

A self-assembled monolayer study with cholesterol-based thiols on gold will provide insight into the cholesterol condensing effect. The design of the molecules with respect to the length of hydrocarbon spacer region and the use of a single tailgroup versus double tailgroup will provide additional insight into the major mechanistic theories, which will be demonstrated by the ability of these molecules to condense a hydrocarbon monolayer. In a mixed SAM, these molecules, both single tailgroup and double tailgroup, might provide support for the Superlattice Model if they assemble in a specified lattice or the Condensed Complex Model if they assemble in one of the three stoichiometric ratios (CP_2, C_3P_6, or C_nP_{2n}).

1.4. References

(1) Vaupel, E. *Angew. Chem. Int. Ed.* **2007**, *46*, 9154–9179.

(2) deGoma, E. M.; Knowles, J. W.; Angeli, F.; Budoff, M. J.; Rader, D. J. *Cardiol. Rev.* **2012**, *20*, 118–129.

(3) Keys, A. *J. Chron. Dis.* **1956**, *4*, 364–380.

(4) Minder, C. M.; Blaha, M. J.; Horne, A.; Michos, E. D.; Kaul, S.; Blumenthal, R. S. *Am. J. Med.* **2012**, *125*, 440–446.

(5) Ng, D. S. *BBA - Biomembr.* **2012**, *1821*, 654–659.

(6) Huang, C. *Chem. Phys. Lipids* **1977**, *19*, 150–158.

(7) Moss, G. P. *Pure Appl. Chem.* **1989**, *61*, 1783–1822.

(8) Razin, S. *J. Bacteriol.* **1975**, *124*, 570–572.

(9) Hotze, E. M.; Tweten, R. K. *BBA - Biomembr.* **2012**, *1818*, 1028–1038.

(10) Grille, S.; Zaslawski, A.; Thiele, S.; Plat, J.; Warnecke, D. *Prog. Lipid Res.* **2010**, *49*, 262–288.

(11) Goedeke, L.; Fernández-Hernando, C. *Cell. Mol. Life Sci.* **2012**, *69*, 915–930.

(12) Bloch, K. *Annu. Rev. Biochem.* **1987**, *56*, 1–18.

(13) Vance, D. E.; van den Bosch, H. *BBA - Mol. Cell Biol. L.* **2000**, *1529*, 1–8.

(14) Lodish, H.; Berk, A.; Zipursky, S. L.; Matsudaira, P.; Baltimore, D.; Darnell, J., Eds.; *Molecular Cell Biology*; 4th ed.; W H Freeman: New York, 2000.

(15) Bloom, M.; Evans, E.; Mouritsen, O. G. *Q. Rev. Biophys.* **1991**, *24*, 293–397.

(16) Kawakami, K.; Nishihara, Y.; Hirano, K. *Langmuir* **1999**, *15*, 1893–1895.

(17) El-Sayed, M. Y.; Guion, T. A.; Fayer, M. D. *Biochemistry* **1986**, *25*, 4825–4832.

(18) Jedlovszky, P. l.; Mezei, M. *J. Phys. Chem. B* **2003**, *107*, 5322–5332.

(19) Subczynski, W. K.; Wisniewska, A.; Yin, J. J.; Hyde, J. S.; Kusumi, A. *Biochemistry* **1994**, *33*, 7670–7681.

(20) Finkelstein, A.; Cass, A. *Nature* **1967**, *216*, 717–718.

(21) Silvius, J. R.; Giudice, D. d.; Lafleur, M. *Biochemistry* **1996**, *35*, 15198–15208.

(22) Pike, L. J. *J. Lipid Res.* **2006**, *47*, 1597–1598.

(23) Singer, S. J.; Nicolson, G. L. *Science* **1972**, *175*, 720–731.

(24) Brown, D. A.; Rose, J. K. *Cell* **1992**, *68*, 533–544.

(25) Simons, K.; van Meer, G. *Biochemistry* **1988**, *27*, 6197–6202.

(26) Leathes, J. B. *Lancet* **1925**, *208*, 853–856.

(27) Marsh, D.; Smith, I. C. P. *BBA - Biomembr.* **1973**, *298*, 133–144.

(28) Yeagle, P. L. *Biochim. Biophys. Acta* **1985**, *822*, 267–287.

(29) Smondyrev, A. M.; Berkowitz, M. L. *Biophys. J.* **2001**, *80*, 1649–1658.

(30) Vainio, S.; Jansen, M.; Koivusalo, M.; Rog, T.; Karttunen, M.; Vattulainen, I.; Ikonen, E. *J. Biol. Chem.* **2006**, *281*, 348–355.

(31) Aittoniemi, J.; Rog, T.; Niemela, P.; Pasenkiewicz-Gierula, M.; Karttunen, M.; Vattulainen, I. *J. Phys. Chem. B* **2006**, *110*, 25562–25564.

(32) Rog, T.; Vattulainen, I.; Jansen, M.; Ikonen, E.; Karttunen, M. *J. Chem. Phys.* **2008**, *129*, 154508.

(33) Shrivastava, S.; Paila, Y. D.; Dutta, A.; Chattopadhyay, A. *Biochemistry* **2008**, *47*, 5668–5677.

(34) Serfis, A. B.; Brancato, S.; Fliesler, S. J. *BBA - Biomembr.* **2001**, *1511*, 341–348.

(35) Urbina, J. A.; Pekerar, S.; Le, H. b.; Patterson, J.; Montez, B.; Oldfield, E. *BBA - Biomembr.* **1995**, *1238*, 163–176.

(36) Endress, E.; Heller, H.; Casalta, H.; Brown, M. F.; Bayerl, T. M. *Biochemistry* **2002**, *41*, 13078–13086.

(37) Czub, J.; Baginski, M. *Biophys. J.* **2006**, *90*, 2368–2382.

(38) Faure, C.; Dufourc, E. J. *BBA - Biomembr.* **1997**, *1330*, 248–252.

(39) Dufourc, E. J.; Parish, E. J.; Chitrakorn, S.; Smith, I. C. P. *Biochemistry* **1984**, *23*, 6062–6071.

(40) Rog, T.; Stimson, L. M.; Pasenkiewicz-Gierula, M.; Vattulainen, I.; Karttunen, M. *J. Phys. Chem. B* **2008**, *112*, 1946–1952.

(41) Smondyrev, A. M.; Berkowitz, M. L. *Chem. Phys. Lipids* **2001**, *112*, 31–39.

(42) Marrink, S. J.; Mark, A. E. *Biochemistry* **2002**, *41*, 5375–5382.

(43) Chong, P. L. *Proc. Natl. Acad. Sci. U. S. A.* **1994**, *91*, 10069–10073.

(44) Bittman, R.; Kasireddy, C. R.; Mattjus, P.; Slotte, J. P. *Biochemistry* **1994**, *33*, 11776–11781.

(45) McIntosh, T. J.; Simon, S. A.; Needham, D.; Huang, C. H. *Biochemistry* **1992**, *31*, 2012–2020.

(46) Marsh, D. *J. Bioenerg. Biomembr.* **1987**, *19*, 677–689.

(47) Somerharju, P.; Virtanen, J. A.; Cheng, K. H. *BBA - Mol. Cell Biol. L.* **1999**, *1440*, 32–48.

(48) Israelachvili, J. N.; Mitchell, D. J. *BBA - Biomembr.* **1975**, *389*, 13–19.

(49) McIntosh, T. J. *Biophys. J.* **1980**, *29*, 237–245.

(50) Anderson, T. G.; McConnell, H. M. *Colloid Surface A* **2000**, *171*, 13–23.

(51) Finean, J. *Cell. Mol. Life Sci.* **1953**, *9*, 17–19.

(52) Needham, D.; McIntosh, T. J.; Evans, E. *Biochemistry* **1988**, *27*, 4668–4673.

(53) Radhakrishnan, A.; McConnell, H. M. *J. Am. Chem. Soc.* **1999**, *121*, 486–487.

(54) Radhakrishnan, A.; McConnell, H. M. *Biophys. J.* **1999**, *77*, 1507–1517.

(55) McConnell, H. M.; Radhakrishnan, A. *BBA - Biomembr.* **2003**, *1610*, 159–173.

(56) Keller, S. L.; McConnell, H. M. *Phys. Rev. Lett.* **1999**, *82*, 1602–1605.

(57) Privalov, P. L.; Gill, S. J.; Anfinsen, C. B.; Edsall, J. T.; Richards, F. M.; David, S. E. In *Adv. Protein Chem.*; Academic Press: 1988; Vol. Volume 39, p 191–234.

(58) Huang, J.; Feigenson, G. W. *Biophys. J.* **1999**, *76*, 2142–2157.

(59) Parker, A.; Miles, K.; Cheng, K. H.; Huang, J. *Biophys. J.* **2004**, *86*, 1532–1544.

(60) Cadenhead, D. A.; Phillips, M. C. *J. Colloid Interface Sci.* **1967**, *24*, 491-499.

(61) Kinsky, S. C.; Luse, S. A.; Zopf, D.; Van Deenen, L. L. M.; Haxby, J. *BBA - Biomembr.* **1967**, *135*, 844–861.

(62) Kucerka, N.; Perlmutter, J. D.; Pan, J.; Tristram-Nagle, S.; Katsaras, J.; Sachs, J. N. *Biophys. J.* **2008**, *95*, 2792–2805.

(63) Dai, J.; Alwarawrah, M.; Huang, J. *J. Phys. Chem. B* **2009**, *114*, 840–848.

(64) Alwarawrah, M.; Dai, J.; Huang, J. *J. Phys. Chem. B* **2010**, *114*, 7516–7523.

(65) Ivankin, A.; Kuzmenko, I.; Gidalevitz, D. *Phys. Rev. Lett.* **2010**, *104*, 108101–108104.

(66) Sugahara, M.; Uragami, M.; Yan, X.; Regen, S. L. *J. Am. Chem. Soc.* **2001**, *123*, 7939–7940.

(67) Kox, A. J.; Michels, J. P. J.; Wiegel, F. W. *Nature* **1980**, *287*, 317–319.

(68) van der Ploeg, P.; Berendsen, H. J. C. *J. Chem. Phys.* **1982**, *76*, 3271–3276.

(69) van der Ploeg, P.; Berendsen, H. J. C. *Mol. Phys.* **1983**, *49*, 233–248.

(70) Egberts, E.; Marrink, S. J.; Berendsen, H. J. C. *Eur. Biophys. J.* **1994**, *22*, 423–436.

(71) Tieleman, D. P.; Berendsen, H. J. C. *J. Chem. Phys.* **1996**, *105*, 4871–4880.

(72) Berger, O.; Edholm, O.; Jahnig, F. *Biophys. J.* **1997**, *72*, 2002–2013.

(73) Zhang, Y.; Feller, S. E.; Brooks, B. R.; Pastor, R. W. *J. Chem. Phys.* **1995**, *103*, 10252–10266.

(74) Feller, S. E.; Zhang, Y.; Pastor, R. W. *J. Chem. Phys.* **1995**, *103*, 10267–10276.

(75) Tu, K.; Tobias, D. J.; Klein, M. L. *Biophys. J.* **1995**, *69*, 2558–2562.

(76) Venable, R. M.; Zhang, Y.; Hardy, B. J.; Pastor, R. W. *Science* **1993**, *262*, 223–226.

(77) Essmann, U.; Perera, L.; Berkowitz, M. L. *Langmuir* **1995**, *11*, 4519–4531.

(78) Rog, T.; Pasenkiewicz-Gierula, M.; Vattulainen, I.; Karttunen, M. *BBA - Biomembr.* **2009**, *1788*, 97–121.

(79) Kusumi, A.; Subczynski, W. K.; Pasenkiewicz-Gierula, M.; Hyde, J. S.; Merkle, H. *BBA - Biomembr.* **1986**, *854*, 307–317.

(80) Doxastakis, M.; Sum, A. K.; de Pablo, J. J. *J. Phys. Chem. B* **2005**, *109*, 24173–24181.

(81) Jedlovszky, P. l.; Mezei, M. *J. Phys. Chem. B* **2003**, *107*, 5311–5321.

(82) Chiu, S. W.; Jakobsson, E.; Scott, H. L. *J. Chem. Phys.* **2001**, *114*, 5435–5443.

(83) Robinson, A. J.; Richards, W. G.; Thomas, P. J.; Hann, M. M. *Biophys. J.* **1995**, *68*, 164–170.

(84) Rog, T.; Pasenkiewicz-Gierula, M. *Biophys. J.* **2001**, *81*, 2190–2202.

(85) Rog, T.; Pasenkiewicz-Gierula, M.; Vattulainen, I.; Karttunen, M. *Biophys. J.* **2007**, *92*, 3346–3357.

(86) Scott, H. L.; McCullough, W. S. *Biophys. J.* **1993**, *64*, 1398–1404.

(87) Chiu, S. W.; Jakobsson, E.; Mashl, R. J.; Scott, H. L. *Biophys. J.* **2002**, *83*, 1842–1853.

(88) Hofsass, C.; Lindahl, E.; Edholm, O. *Biophys. J.* **2003**, *84*, 2192–2206.

(89) Edholm, O.; Nagle, J. F. *Biophys. J.* **2005**, *89*, 1827–1832.

(90) Sugar, I. P.; Chong, P. L. G. *J. Am. Chem. Soc.* **2011**, *134*, 1164–1171.

(91) Metropolis, N. *Los Alamos Science* **1987**, *15*, 125–130.

(92) Scott Jr, H. L. *BBA - Biomembr.* **1977**, *469*, 264–271.

(93) Elson, E. L.; Fried, E.; Dolbow, J. E.; Genin, G. M. *Ann. Rev. Biophys.* **2010**, *39*, 207–226.

(94) Scott, H. L.; Kalaskar, S. *Biochemistry* **1989**, *28*, 3687–3691.

(95) Scott, H. L. *Biophys. J.* **1991**, *59*, 445–455.

(96) Miao, L.; Nielsen, M.; Thewalt, J.; Ipsen, J. H.; Bloom, M.; Zuckermann, M. J.; Mouritsen, O. G. *Biophys. J.* **2002**, *82*, 1429–1444.

(97) de Joannis, J.; Coppock, P. S.; Yin, F.; Mori, M.; Zamorano, A.; Kindt, J. T. *J. Am. Chem. Soc.* **2011**, *133*, 3625–3634.

(98) Langmuir, I. *J. Am. Chem. Soc.* **1917**, *39*, 1848–1906.

(99) McMullen, T. P. W.; Lewis, R. N. A. H.; McElhaney, R. N. *Biochemistry* **1993**, *32*, 516–522.

(100) McIntosh, T. *Biochim. Biophys. Acta* **1978**, *513*, 43–58.

(101) Presti, F. T.; Chan, S. I. *Biochemistry* **1982**, *21*, 3821–3830.

(102) Sabatini, K.; Mattila, J. P.; Kinnunen, P. K. J. *Biophys. J.* **2008**, *95*, 2340–2355.

(103) Smaby, J. M.; Brockman, H. L.; Brown, R. E. *Biochemistry* **1994**, *33*, 9135–9142.

(104) Needham, D.; Nunn, R. S. *Biophys. J.* **1990**, *58*, 997–1009.

(105) Rog, T.; Pasenkiewicz-Gierula, M. *Biochimie* **2006**, *88*, 449–460.

(106) Martinez-Seara, H.; Rog, T.; Pasenkiewicz-Gierula, M.; Vattulainen, I.; Karttunen, M.; Reigada, R. *Biophys. J.* **2008**, *95*, 3295–3305.

(107) Harroun, T. A.; Katsaras, J.; Wassall, S. R. *Biochemistry* **2006**, *45*, 1227–1233.

(108) Dynarowicz-Latka, P.; Hac-Wydro, K. *Colloid Surface B* **2004**, *37*, 21–25.

(109) van Dijck, P. W. M.; De Kruijff, B.; van Deenen, L. L. M.; De Gier, J.; Demel, R. A. *BBA - Biomembr.* **1976**, *455*, 576–587.

(110) van Dijck, P. W. M. *BBA - Biomembr.* **1979**, *555*, 89–101.

(111) Yeagle, P. L.; Young, J. E. *J. Biol. Chem.* **1986**, *261*, 8175–8181.

(112) Niu, S. L.; Litman, B. J. *Biophys. J.* **2002**, *83*, 3408–3415.

(113) van Blitterswijk, W. J.; van der Meer, B. W.; Hilkmann, H. *Biochemistry* **1987**, *26*, 1746–1756.

(114) Collins, J. J.; Phillips, M. C. *J. Lipid Res.* **1982**, *23*, 291–298.

(115) Cheetham, J. J.; Wachtel, E.; Bach, D.; Epand, R. M. *Biochemistry* **1989**, *28*, 8928–8934.

(116) Huang, J.; Buboltz, J. T.; Feigenson, G. W. *BBA - Biomembr.* **1999**, *1417*, 89–100.

(117) Bjorkbom, A.; Rog, T.; Kaszuba, K.; Kurita, M.; Yamaguchi, S.; Lonnfors, M.; Nyholm, Thomas K. M.; Vattulainen, I.; Katsumura, S.; Slotte, J. P. *Biophys. J.* **2010**, *99*, 3300–3308.

(118) Brown, R. E. *J. Cell Sci.* **1998**, *111*, 1–9.

(119) Ohvo-Rekila, H.; Ramstedt, B.; Leppimaki, P.; Peter Slotte, J. *Prog. Lipid Res.* **2002**, *41*, 66–97.

(120) Slotte, J. P. *Chem. Phys. Lipids* **1999**, *102*, 13–27.

(121) McMullen, T. P. W.; McElhaney, R. N. *Curr. Opin. Colloid Interface Sci.* **1996**, *1*, 83–90.

(122) Li, X. M.; Momsen, M. M.; Smaby, J. M.; Brockman, H. L.; Brown, R. E. *Biochemistry* **2001**, *40*, 5954–5963.

(123) Bonn, M.; Roke, S.; Berg, O.; Juurlink, L. B. F.; Stamouli, A.; Muller, M. *J. Phys. Chem. B* **2004**, *108*, 19083–19085.

(124) Hung, W. C.; Lee, M. T.; Chen, F. Y.; Huang, H. W. *Biophys. J.* **2007**, *92*, 3960–3967.

(125) Pan, J.; Mills, T. T.; Tristram-Nagle, S.; Nagle, J. F. *Phys. Rev. Lett.* **2008**, *100*, 198103/198104.

(126) Veatch, S. L.; Polozov, I. V.; Gawrisch, K.; Keller, S. L. *Biophys. J.* **2004**, *86*, 2910–2922.

(127) Tsamaloukas, A.; Szadkowska, H.; Heerklotz, H. *Biophys. J.* **2006**, *90*, 4479–4487.

(128) Mattjus, P.; Slotte, J. P. *Chem. Phys. Lipids* **1996**, *81*, 69–80.

(129) Veatch, S. L.; Keller, S. L. *Biophys. J.* **2003**, *85*, 3074–3083.

(130) Almeida, P. F. F. *BBA - Biomembr.* **2009**, *1788*, 72–85.

(131) Wydro, P. *Colloid Surface B* **2012**, *93*, 174–179.

(132) Ulman, A. *An Introduction to Ultrathin Organic Films: From Langmuir-Blodgett to Self-Assembly*; Academic Press: San Diego, 1991.

(133) Ulman, A. *Self-Assembled Monolayers of Thiols*; Academic Press: San Diego, CA, 1998.

(134) Garg, N.; Lee, T. R. *Langmuir* **1998**, *14*, 3815–3819.

(135) Achalkumar, A. S.; Bushby, R. J.; Evans, S. D. *Soft Matter* **2010**, *6*, 6036–6051.

(136) Segura, A.; Batina, N. *NSTI Nanotechnology* **2006**, *1*, 261–264.

(137) Yang, Z. P.; Engquist, I.; Kauffmann, J. M.; Liedberg, B. *Langmuir* **1996**, *12*, 1704–1707.

(138) Trevor, J. L.; Lykke, K. R.; Pellin, M. J.; Hanley, L. *Langmuir* **1998**, *14*, 1664–1673.

(139) Yang, Z.; Engquist, I.; Wirde, M.; Kauffmann, J. M.; Gelius, U.; Liedberg, B. *Langmuir* **1997**, *13*, 3210–3218.

(140) Yang, Z.; Engquist, I.; Liedberg, B.; Kauffmann, J. M. *J. Electroanal. Chem.* **1997**, *430*, 189–195.

(141) Bittoun, E.; Marmur, A.; Ostblom, M.; Ederth, T.; Liedberg, B. *Langmuir* **2009**, *25*, 12374–12379.

(142) Jeuken, L. J. C.; Connell, S. D.; Nurnabi, M.; O'Reilly, J.; Henderson, P. J. F.; Evans, S. D.; Bushby, R. J. *Langmuir* **2005**, *21*, 1481–1488.

(143) Boden, N.; Bushby, R. J.; Clarkson, S.; Evans, S. D.; Knowles, P. F.; Marsh, A. *Tetrahedron* **1997**, *53*, 10939–10952.

(144) Williams, L. M.; Evans, S. D.; Flynn, T. M.; Marsh, A.; Knowles, P. F.; Bushby, R. J.; Boden, N. *Langmuir* **1997**, *13*, 751–757.

(145) Cheng, Y.; Boden, N.; Bushby, R. J.; Clarkson, S.; Evans, S. D.; Knowles, P. F.; Marsh, A.; Miles, R. E. *Langmuir* **1998**, *14*, 839–844.

(146) Jenkins, A. T. A.; Bushby, R. J.; Boden, N.; Evans, S. D.; Knowles, P. F.; Liu, Q.; Miles, R. E.; Ogier, S. D. *Langmuir* **1998**, *14*, 4675–4678.

(147) Sheikh, K. H.; Christenson, H. K.; Bushby, R. J.; Evans, S. D. *J. Phys. Chem. B* **2006**, *111*, 379–386.

(148) Indrieri, M.; Suardi, M.; Podesta, A.; Ranucci, E.; Ferruti, P.; Milani, P. *Langmuir* **2008**, *24*, 7830–7841.

(149) Blasi, L.; Pisignano, D.; Di Benedetto, F.; Maruccio, G.; Ciccarella, G.; Maffei, A.; Vasapollo, G.; Cingolani, R.; Rinaldi, R. *BBA - Biomembr.* **2005**, *1714*, 93–102.

(150) Andersson, O.; Ulrich, C.; Bjorefors, F.; Liedberg, B. *Sensor. Actuat. B - Chem.* **2008**, *134*, 545–550.

(151) Luthi, A. J.; Zhang, H.; Kim, D.; Giljohann, D. A.; Mirkin, C. A.; Thaxton, C. S. *ACS Nano* **2011**, *6*, 276–285.

(152) Yu, G.; Ji, J.; Shen, J. *J. Mater. Sci.: Mater. Med.* **2006**, *17*, 899–909.

(153) Woll, K. A.; Schuchardt, E. J.; Willis, C. R.; Ortengren, C. D.; Hendricks, N.; Johnson, M.; Gaidamauskas, E.; Baruah, B.; Sostarecz, A. G.; Worley, D. R.; Osborne, D. W.; Crans, D. C. *Chem. Biodivers.* **2011**, *8*, 2195–2210.

(154) Xie, A. J.; Shen, Y. H.; Xia, B.; Chen, H. B.; Ouyang, J. M. *Thin Solid Films* **2005**, *472*, 227–231.

(155) Ambike, A.; Rosilio, V.; Stella, B.; Lepetre-Mouelhi, S.; Couvreur, P. *Langmuir* **2011**, *27*, 4891–4899.

(156) Shin, M. J.; Hong, W. H. *Biochem. Eng. J.* **2011**, *54*, 57–61.

(157) Sugar, I. P.; Chong, P. L. G. *J. Am. Chem. Soc.* **2012**, *134*, 1164–1171.

(158) Alwarawrah, M.; Dai, J.; Huang, J. *J. Chem. Theory Comput.* **2012**, *8*, 749–758.

(159) Zhou, G.; Li, Y.; Yu, X.; Yu, D.; Yin, Y. *Supramol. Chem.* **2012**, *24*, 234–237.

(160) Jiao, T.; Wang, Y.; Gao, F.; Zhou, J.; Gao, F. *Prog. Nat. Sci.* **2012**, *22*, 64–70.

(161) Han, X.; Achalkumar, A. S.; Bushby, R. J.; Evans, S. D. *Chem. - Eur. J.* **2009**, *15*, 6363–6370.

(162) Arndt, T.; Schupp, H.; Schrepp, W. *Thin Solid Films* **1989**, *178*, 319–326.

(163) Blodgett, K. B. *J. Am. Chem. Soc.* **1935**, *57*, 1007–1022.

Chapter 2. Self-assembled Monolayers Generated from Single-chained Cholesterol-based Thiols on Gold

2.1. Introduction

Cholesterol is an important biological molecule involved in many physiological processes in eukaryotic cells.[1] It is most commonly associated with the plasma membrane and lipoproteins.[1,2] The molecular interactions between molecules of cholesterol and lipids can greatly affect the biophysical properties of a lipid membrane. One of the most important effects of cholesterol on lipid membranes is the cholesterol condensing effect: the surface area of a cholesterol-containing lipid bilayer is less than the sum of the areas of the individual bilayer components.[3] This condensing phenomenon is believed to be caused by the molecular mismatch within the membrane. Cholesterol, Figure 2.1, consists of a hydrophobic, rigid, almost planar body containing a fused hydrocarbon four ring system and a hydrophilic, hydroxyl headgroup. Lipids contain a linear hydrophobic saturated or unsaturated hydrocarbon tailgroup and a hydrophilic headgroup, producing a mismatch between the bulkier cholesterol and lipids.

This condensing effect was first discovered in monolayer experiments at the air-water interface where the area per phospholipid was found to decrease in the presence of cholesterol.[3-5] Since these initial experiments, the effect has also been seen on lipid bilayers.[6-9] The mechanism for the condensing effect is subject to debate, however it has been shown to occur at a wide range of concentrations for cholesterol to the total lipid

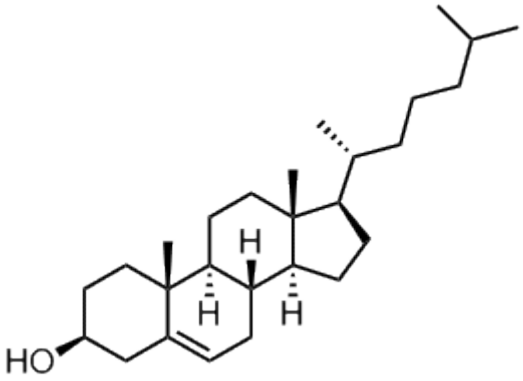

Figure 2.1. Chemical structure of cholesterol.

concentration. At 2 mol %, cholesterol can influence the membrane packing density; however, the upper limit of cholesterol concentration varies based on the lipid studied, as influenced by the combination of the tailgroup and headgroup.[10-12] In mammalian membranes, cholesterol can affect the biophysical properties of membranes up to 70 mol % of total lipids.[13,14] Considering only the interaction between cholesterol and lipids, several models are proposed for the mechanism of the cholesterol condensing effect: the Superlattice Model,[15] the Condensed Complex Model,[16] the Umbrella Model,[17] and others.[18] Several experimental techniques and computer simulations have been used to provide support for each model.

Most cholesterol studies involve Langmuir and Langmuir-Blodgett (LB) monolayers which are formed at the air-water interface and mimic biological membranes. With an ease of synthesis, cholesterol-based model membrane systems utilize phosphocholine as a headgroup. While the amount of saturation and chain length can vary from study to study, the most commonly utilized phosphatidylcholines comprise

saturated tailgroups with chain lengths equaling 14, 16, or 18 hydrocarbons.[9,19-21] Studies involving unmodified cholesterol show that it does not form a stable Langmuir monolayer at higher surface pressures;[22] when deposited on a hydrophilic substrate and the solvent evaporated, cholesterol precipitates to form monohydrate crystals as the hydroxyl headgroup is insufficient to shield the hydrophobic region of the molecule from the substrate.[23] To address this problem, Gupta *et al.* combined thiocholesterol and cholesterol in a Langmuir monolayer which was transferred to a solid substrate as a LB monolayer.[24] Thiocholesterol is structurally similar to cholesterol with a substitution of the –OH group with a –SH group at the 3β-position. Gutpa *et al.* found that thiocholesterol does not form a monolayer at the air-water interface owing to the weakly acidic nature of the thiol headgroup, as compared to an alcohol functional group, and the inability of the thiol headgroup to shield the rigid hydrophobic region of thiocholesterol from the water interface, however thiocholesterol and cholesterol do form a stable mixed Langmuir monolayer. Most Langmuir and LB monolayers utilize hydrophilic headgroups while less hydrophilic to hydrophobic headgroups, like thiols, are generally used to form self-assembled monolayers (SAMs).

The adsorbates that form SAMs on a solid substrate have fewer degrees of freedom during the monolayer formation process, as compared to Langmuir monolayers, and therefore provide an alternative route to the monolayer formation for surfactants that fail to assemble at an air-liquid interface. Cholesterol, with a –OH group at the 3β-position, will not form a homogenous SAM on gold. This was demonstrated by Segura *et al.* who used a scanning tunneling microscopy to show that cholesterol will not form a

homogeneous monolayer rather the molecule positions parallel to the metal interface to form supramolecular assemblies on Au(111).[25] However, thiocholesterol forms a stable single-component SAM on Au(111).[26] With the thiol headgroup positioning at the Au interface, the rigid polycyclic steroid ring extends nearly perpendicular to the surface creating a monolayer 16 Å in thickness. Yang *et al.* characterized the monolayer by collecting ellipsometic data, infrared reflection-adsorption spectroscopy, contact angle goniometry, and cyclic voltamometry.[26] They concluded that thiocholesterol forms homogenous SAMs with structural defects associated with the self-assembling of the rigid polycyclic steroid rings. These structural defects could be filled with other molecules, such as 11-mercaptoundecanoic acid, indicating defects with a 5 – 9 Å diameter.[26-29] The success of the SAM format for incorporating cholesterol into a monolayer structure has led to an extensive number of studies of mixed SAMs involving cholesterol, thiocholesterol, and cholesterol moieties, in the last decade.[30-34] Boden *et al.* synthesized a cholesterol moiety for use as a tether for biomembranes.[34] The molecules used in the mixed SAM study consisted of a cholesterol tailgroup, an ethylene glycol spacer, and a thiol headgroup. Molecules with similar structures have been used to study biomembranes yet have not been utilized for the study of the cholesterol condensing effect. To the author's knowledge, these cholesterol-based molecules have never been used to form a single-component SAM. By generating SAMs from single-chained cholesterol-based thiols, we wished to examine the interfacial properties of homogeneous monolayers utilizing the cholesterol condensing effect.

Within this work, we generated SAMs on gold from single-chained molecules containing a cholesterol moiety (**CholCnSH**) composed of a thiol headgroup, a hydrocarbon spacer, and cholesterol tailgroup. The specific structure of this series of molecules utilizes the hydrocarbon spacer to carry the cholesterol away from the gold substrate and into the SAM. The **CholCnSH** series of molecules has a hydrocarbon spacer with n = 3, 4, 5, 6, 9, and 12. Since the hydrocarbon spacer promotes the formation of a well-organized monolayer, the cholesterol unit should participate in an increased packing density, as compared to thiolcholesterol (see Figure 2.2).

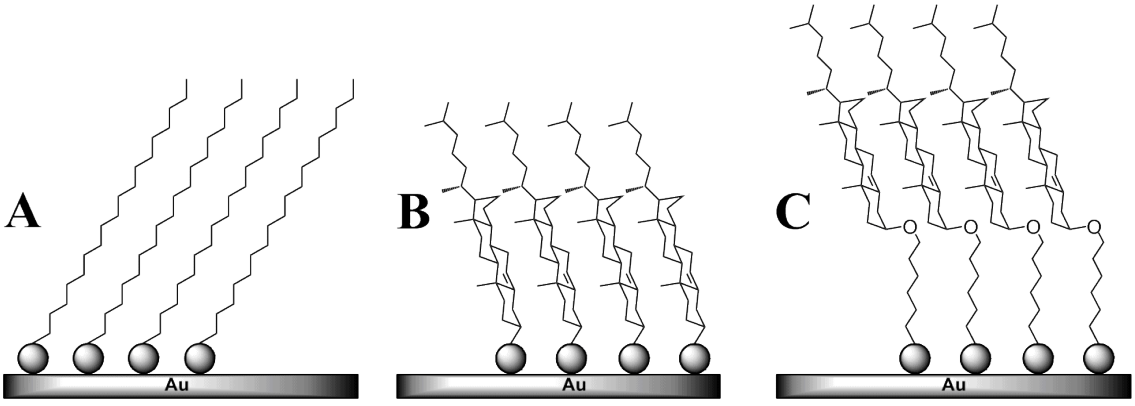

Figure 2.2. Illustration of the structures of SAMs generated from: (A) $CH_3(CH_2)_{17}SH$ (**C18SH**) with trans-extended conformation; (B) thiocholesterol (**CholSH**); and (C) the new cholesterol-based moieties (**CholCnSH**). The image shows **CholC6SH** as an example of the cholesterol-based thiols. Molecular sizes and dimensions are not drawn to scale.

The structure and interfacial properties of the resultant monolayers were characterized using optical contact angle goniometry, ellipsometry, X-ray photoelectron spectroscopy (XPS), and polarization modulation infrared reflection absorption spectroscopy (PM-IRRAS). Additionally, we prepared SAMs from *n*-octadecanethiol ($CH_3(CH_2)_{17}SH$, **C18SH**) and thiocholesterol (5-cholestene-3β-thiol, **CholSH**). The data collected from the **CholCnSH** were compared to that collected from films formed from **C18SH** and **CholSH**.

2.2. Experimental Section

2.2.1 Nomenclature

We denote the names of the thiol adsorbates used in this study as follows: *n*-octadecanethiol ($CH_3(CH_2)_{17}SH$), **C18SH**; thiocholesterol (5-cholestene-3β-thiol), **CholSH**; cholest-5-en-3β-oxypropan-3-thiol, **CholC3SH**; cholest-5-en-3β-oxybutan-4-thiol, **CholC4SH**; cholest-5-en-3β-oxypentan-5-thiol, **CholC5SH**; cholest-5-en-3β-oxyhexan-6-thiol, **CholC6SH**; cholest-5-en-3β-oxynonan-9-thiol, **CholC9SH**; and **c**holest-5-en-3β-oxydodecan-12-thiol, **CholC12SH**. The letter indicates the chemical composition of the adsorbate: **Chol** denotes a cholesterol moiety, **C** denotes methylene units (CH_2) within the hydrocarbon spacer, and **SH** denotes thiol structure. The number indicates the number of methylene units in the hydrocarbon spacer.

2.2.2. Materials

Gold shot (99.99 %) was purchased from Kamis Inc. Nickle-chromium canes (80 % nickel: 20 % chromium) were purchased from Kurt J. Lesker Company. Polished single-crystal Si(100) wafers were purchased from Silicon Sense, Inc. and rinsed with absolute ethanol (EtOH, Aaper Alcohol and Chemical Co.) before use. The contacting liquids used for wettability measurements were of the highest purity available from the following sources and were used as received: water generated from Milli Q Water System with resistance of 18.2 MΩ, Millipore Corporation; and hexadecane from Aldrich Chemical Co.. *n*-Octadecanethiol (**C18SH**) and thiocholesterol (**CholSH**) were purchased from Aldrich Chemical Co. and used without further purification. Tetrahydrofuran (THF) was purchased from Mallinckrodt Baker, Inc, distilled over calcium hydride, and stored under argon. Anhydrous dioxane, anhydrous *N*,*N*-dimethylformamide (DMF), methanol, cholesterol, sodium hydride (NaH, 60 % dispersion in mineral oil), 1,3-propanediol, 1,4-butanediol, 1,5-pentanediol, 1,6-hexanediol, 1,9-nonanediol, 1,12-dodecanediol, triethylamine (NEt_3), and potassium thioacetate (KSAc) were purchased from Aldrich Chemical Co. and used as received. Lithium aluminum hydride (LiAlH) was purchased from Alfa Aesar and used as received. Methanesulfonyl chloride (MsCl) and *p*-toluenesulfonyl chloride (TsCl) were purchased from Acros Organics and used as received. Column chromatography was performed using silica gel (40 – 64 μm) and thin-layer chromatography (TLC) was carried out using 200 μm thick silica gel plates, which both were purchased from Sorbent

Technologies, Inc. The eluted TLC plates were developed with a molybdenum blue stain followed by heating. Nuclear Magnetic Resonance (NMR) spectra were recorded on a JOEL ECA-500 spectrometer operating at 500 MHz. The data were obtained in chloroform-d ($CDCl_3$) and referenced to δ 7.26 ppm for ^{1}H NMR spectra and 77.00 ppm for ^{13}C NMR spectra.

2.2.3. Synthesis of the Adsorbates

The synthetic strategy used to prepare the targeted single-chain cholesterol-based thiols (**CholCnSH**) is shown in Scheme 2.1. The complete experimental details of each synthetic step are provided in the section that follows.

Scheme 2.1. Preparation of a Series of Cholesterol-based Thiols (**CholCnSH**), where n = 3, 4, 5, 6, 9, and 12.

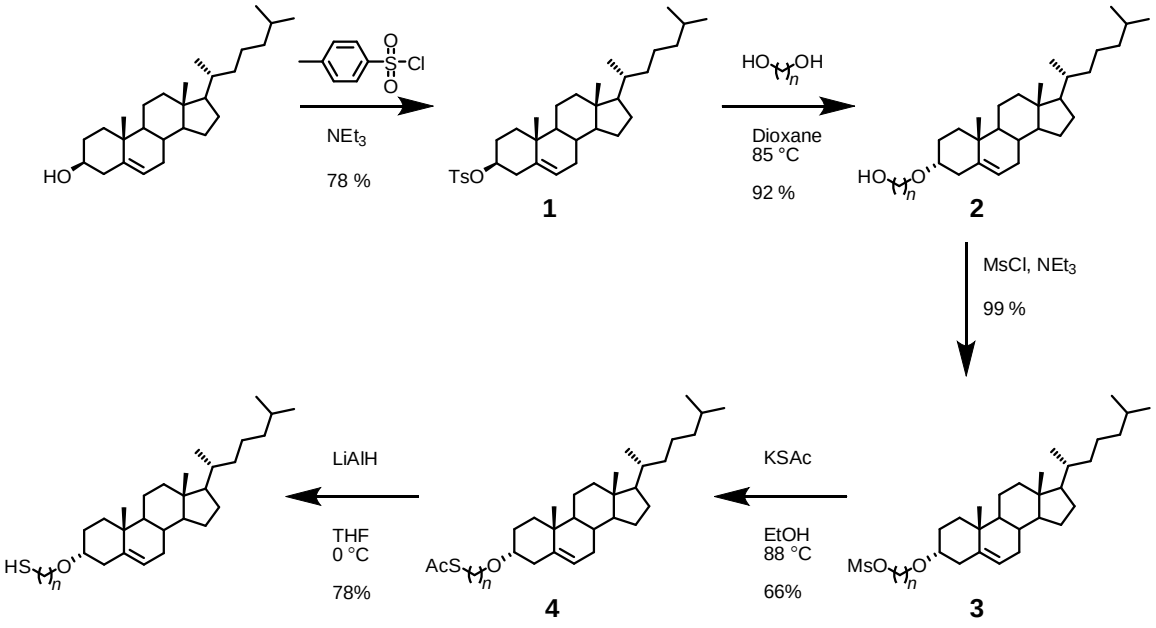

*Cholesterol Tosylate (**1**).* Cholesterol tosylate was synthesized by combining 18.09 g of cholesterol (46.78 mmol) and 37.71 g *p*-toluenesulfonyl chloride (197.8 mmol) in 60.0 mL of triethylamine (430 mmol). After purging with nitrogen, the reaction was allowed to stir overnight at room temperature. TLC confirmed that a reaction occurred. The reaction was worked up by the addition of 150 mL of dichloromethane and 150 mL water. The organic layer was washed with 2 × 100 mL of each of the following solutions: 1N hydrochloric acid, water, and brine. The organic layer was dried with anhydrous sodium sulfate and the solvent was reduced under vacuum to yield a yellow liquid. The product was precipitated by the addition of methanol and filtered to collect a white solid. Yield: 19.76 g (36.54 mmol, 78 %). TLC (80 % hexane: 20 % ethyl

acetate): R_f = 0.62. Crude ^{1}H NMR (500 MHz, $CDCl_3$): δ 0.61 (s, 3 H), 0.86 – 1.58 (m, 34 H), 1.69 (m, 1 H), 1.81 (m, 3 H), 2.00 (m, 2 H), 2.25 (m, 1 H), 2.43 (m, 4 H), 4.31 (m, 1 H), 5.29 (m, 1 H), 7.32 (d, *J* = 7.90 Hz, 2 H), 7.79 (d, *J* = 8.25 Hz, 2 H).

C*holest-5-en-3β-oxypropan-3-ol (**2**).* Cholest-5-en-3β-oxypropan-3-ol was synthesized by combining 1.115 g of tosylate **1** (2.061 mmol) and 5.00 mL of 1,3-propanediol (69.2 mmol) in 24.0 mL of anhydrous dioxane. The reaction was heated to 85 ºC for 4 hours under nitrogen. TLC confirmed that a reaction occurred. The reaction was worked up by the addition of 50 mL of dichloromethane and 50 mL water. The organic layer was washed with 2 × 100 mL of each of the following solutions: water, 1N hydrochloric acid, and brine. The organic layer was dried with anhydrous sodium sulfate, filtered, and the solvent was removed under vacuum to yield a yellow solid. The crude compound was purified by column chromatography (99% hexane: 1% ethyl acetate – 70% hexane: 30% ethyl acetate) to provide a white solid. Yield: 0.842 g (1.89 mmol, 92 %). TLC (80 % hexane: 20 % ethyl acetate): R_f = 0.20. ^{1}H NMR (500 MHz, $CDCl_3$): δ 0.67 (s, 3 H), 0.85 – 1.58 (m, 35 H), 1.78 – 2.05 (m, 7 H), 2.15 (m, 1 H), 2.37 (m, 1 H), 2.59 (t, *J* = 5.15 Hz, 1 H), 3.17 (m, 1 H), 3.67 (m, 2 H), 3.87 (q, *J* = 5.50 Hz, 2 H), 5.34 (m, 1 H).

C*holest-5-en-3β-oxypropan-3-mesylate (**3**).* A solution of the alcohol **2** (1.215 g, 2.732 mmol) in triethylamine (6.00 mL, 43.0 mmol) was prepared under nitrogen and allowed to stir for 1 hour. Methanesulfonyl chloride (0.65 mL, 8.4 mmol) was added dropwise over 5 minutes to the stirred mixture. After the addition was completed, stirring was continued for 4 hours at room temperature. The reaction was quenched by the

addition of ice-cold water (200 mL). The mixture was extracted with dichloromethane (3 × 100 mL). The organic phase was washed with water (2 × 100 mL) and 2 × 100 mL of each of the following solutions: 1N hydrochloric acid, water, and brine. The organic layer was dried over anhydrous sodium sulfate, filtered, and the solvent was removed under vacuum to yield a yellow solid. The crude product was used directly in the next step without further purification. Yield: 1.42 g (2.72 mmol, 99 %). TLC (80 % hexane: 20 % ethyl acetate): R_f = 0.25. Crude ^{1}H NMR (500 MHz, $CDCl_3$): δ 0.64 (s, 3 H), 0.85 – 1.62 (m, 37 H), 1.80 – 2.02 (m, 7 H), 2.15 (m, 1 H), 2.34 (m, 1 H), 3.00 (s, 3 H), 3.13 (m, 1 H), 3.57 (m, 2 H), 4.34 (t, *J* = 6.19 Hz, 2 H), 5.34 (m, 1 H).

C*holest-5-en-3β-oxypropan-3-thioacetate (**4**)*. The mesylate **3** (1.416 g, 2.708 mmol) was dissolved in degassed ethanol (24 mL) and added to a reaction flask containing potassium thioacetate (0.983 g, 8.61 mmol). The reaction mixture was heated to 88 °C for 4 hours under nitrogen. The reaction was worked up by addition of cool water (50 mL) and the mixture extracted with dichloromethane (3 × 100 mL). The organic phases were combined and washed with water (3 × 100 mL) and brine (1 × 100 mL), dried over anhydrous sodium sulfate, filtered, and the solvent was removed under vacuum to yield a light yellow solid. The crude product was purified by column chromatography (99% hexane: 1% ethyl acetate) to give a white solid. Yield: 0.900 g (1.79 mmol, 66 %). TLC (80 % hexane: 20 % ethyl acetate): R_f = 0.79. ^{1}H NMR (500 MHz, $CDCl_3$): δ 0.67 (s, 3 H), 0.84 – 1.60 (m, 37 H), 1.78 – 2.02 (m, 7 H), 2.15 (m, 1 H), 2.37 (m, 4 H), 2.96 (t, *J* = 6.87 Hz, 2 H), 3.17 (m, 1 H), 3.51 (m, 2 H), 5.34 (m, 1 H).

C*holest-5-en-3β-oxypropan-3-thiol* (**CholC3SH**). Thioacetate **4** (0.430 g, 0.856 mmol) dissolved in degassed tetrahydrofuran (12 mL) was added into a suspension of lithium aluminum hydride (0.193 g, 4.83 mmol) in degassed tetrahydrofuran (5.0 mL) slowly at 0 ºC. The reaction mixture was allowed to stir for 8 hours at room temperature under an atmosphere of nitrogen and then quenched with degassed water (10 mL). The mixture was acidified to pH ~1 by careful addition of 1.0 M sulfuric acid solution (previously degassed), and then extracted with dichloromethane (3 × 100 mL). The organic layers were combined and washed with a dilute hydrochloric acid solution (1 × 100 mL) and brine (1 × 100 mL). The organic phase was dried over anhydrous sodium sulfate and filtered. After removal of the solvent under vacuum, the crude compound was purified by column chromatography (99% hexane: 1% ethyl acetate), affording a white solid. Yield: 0.309 g (0.671 mmol, 78 %). TLC (80 % hexane: 20 % ethyl acetate): R_f = 0.72. ^{1}H NMR (500 MHz, $CDCl_3$): δ 0.67 (s, 3 H), 0.85 - 1.60 (m, 38 H), 1.78 – 2.05 (m, 7 H), 2.15 (m, 1 H), 2.35 (m, 1 H), 2.64 (q, *J* = 5.15 Hz, 2 H), 3.13 (m, 1 H), 3.56 (m, 2 H), 5.34 (m, 1 H). ^{13}C NMR (500 MHz, $CDCl_3$): δ 11.96, 18.83, 19.48, 21.17, 21.65, 22.69, 22.95, 23.96, 24.39, 28.10, 28.35, 28.53, 31.97, 32.03, 34.33, 35.90, 36.30, 36.96, 37.34, 39.25, 39.62, 39.88, 42.40, 50.27, 56.26, 56.86, 65.77, 79.19, 121.64, 140.95.

C*holest-5-en-3β-oxybutan-4-thiol* (**CholC4SH**). Yield: 0.298 g (0.628 mmol, 76 %). TLC (80 % hexane: 20 % ethyl acetate): R_f = 0.74. ^{1}H NMR (500 MHz, $CDCl_3$): δ 0.67 (s, 3 H), 0.85 – 2.12 (m, 47 H), 2.15 (m, 1 H), 2.35 (m, 1 H), 2.56 (q, *J* = 6.87 Hz, 2 H), 3.13 (m, 1 H), 3.56 (m, 2 H), 5.34 (m, 1 H). ^{13}C NMR (500 MHz, $CDCl_3$): δ 11.96, 18.83, 19.49, 21.17, 22.69, 22.95, 23.96, 24.39, 24.65, 28.10, 28.34, 28.55, 29.05, 31.02,

31.97, 32.05, 35.90, 36.29, 36.97, 37.36, 39.27, 39.62, 39.88, 42.40, 50.28, 56.26, 56.86, 67.41, 79.11, 121.58, 141.05.

C*holest-5-en-3β-oxypentan-5-thiol* (**CholC5SH)**. Yield: 1.11 g (2.27 mmol, 83 %). TLC (80 % hexane: 20 % ethyl acetate): R_f = 0.75. ^{1}H NMR (500 MHz, $CDCl_3$): δ 0.67 (s, 3 H), 0.85 – 2.12 (m, 50 H), 2.15 (m, 1 H), 2.35 (m, 1 H), 2.56 (q, *J* = 7.56 Hz, 2 H), 3.13 (m, 1 H), 3.45 (m, 2 H), 5.34 (m, 1 H). ^{13}C NMR (500 MHz, $CDCl_3$): δ 11.96, 18.85, 19.47, 21.17, 22.71, 22.95, 24.00, 24.02, 24.39, 24.62, 25.19, 28.09, 28.37, 28.55, 29.77, 30.03, 34.03, 35.92, 36.31, 36.93, 37.38, 39.29, 39.61, 39.88, 42.37, 50.26, 56.29, 56.84, 67.82, 79.05, 121.49, 140.96.

C*holest-5-en-3β-oxyhexan-6-thiol* (**CholC6SH)**. Yield: 0.560 g (1.11 mmol, 85 %). TLC (80 % hexane: 20 % ethyl acetate): R_f = 0.77. ^{1}H NMR (500 MHz, $CDCl_3$): δ 0.67 (s, 3 H), 0.85 – 1.65 (m, 46 H), 1.76 – 2.02 (m, 5 H), 2.18 (m, 1 H), 2.35 (m, 1 H), 2.56 (q, *J* = 7.45 Hz, 2 H), 3.13 (m, 1 H), 3.45 (m, 2 H), 5.34 (m, 1 H). ^{13}C NMR (500 MHz, $CDCl_3$): δ 11.96, 18.84, 19.47, 21.17, 22.70, 22.95, 23.99, 24.39, 24.65, 25.84, 28.09, 28.31, 28.36, 28.57, 30.20, 31.97, 32.03, 34.09, 35.91, 36.31, 36.94, 37.39, 39.30, 39.62, 39.89, 42.38, 50.28, 56.28, 56.85, 67.97, 79.04, 121.48, 141.05.

C*holest-5-en-3β-oxynonan-9-thiol* (**CholC9SH)**. Yield: 0.538 g (0.987 mmol, 81 %). TLC (80 % hexane: 20 % ethyl acetate): R_f = 0.81. ^{1}H NMR (500 MHz, $CDCl_3$): δ 0.67 – 1.65 (m, 53 H), 1.74 – 2.02 (m, 5 H), 2.15 (m, 1 H), 2.33 (m, 1 H), 2.49 (q, *J* = 7.46 Hz, 2 H), 3.13 (m, 1 H), 3.45 (m, 2 H), 5.34 (m, 1 H). ^{13}C NMR (500 MHz, $CDCl_3$): δ 11.96, 18.83, 19.48, 21.17, 22.69, 22.94, 23.97, 24.39, 24.72, 26.31, 28.10, 28.35,

28.46, 28.57, 29.13, 29.53, 29.57, 30.32, 31.97, 32.04, 34.16, 35.90, 36.30, 36.97, 37.40, 39.31, 39.61, 39.89, 42.39, 50.28, 56.27, 56.86, 68.17, 79.02, 121.46, 141.13.

C*holest-5-en-3β-oxydodecan-12-thiol* (**CholC12SH**). Yield: 0.188 g (0.320 mmol, 93 %). TLC (80 % hexane: 20 % ethyl acetate): R_f = 0.85. ^{1}H NMR (500 MHz, $CDCl_3$): δ 0.65 – 1.67 (m, 80 H), 1.78 – 2.02 (m, 5 H), 2.18 (m, 1 H), 2.36 (m, 1 H), 2.53 (q, *J* = 7.45 Hz, 2 H), 3.12 (m, 1 H), 3.44 (m, 2 H), 5.34 (m, 1 H). ^{13}C NMR (500 MHz, $CDCl_3$): δ 11.96, 18.82, 19.48, 21.17, 22.68, 22.94, 23.95, 24.39, 24.75, 26.32, 28.10, 28.34, 28.50, 28.58, 29.19, 29.63, 29.68, 30.32, 31.97, 32.05, 34.18, 35.90, 36.29, 36.98, 37.41, 39.31, 39.62, 39.88, 42.40, 50.29, 56.26, 56.87, 68.23, 79.02, 121.48, 141.20.

2.2.4. Preparation of SAMs

The gold substrates were prepared under a vacuum at ~ 1×10^{-5} Torr. A thin layer (100 Å) of nickel-chromium (80 % nickel: 20 % chromium) was first evaporated onto polished Si(100) wafers to assist the adhesion of gold on silicon, followed by the evaporation of 1000 Å of gold. Absolute ethanol was used to rinse the resultant gold-coated wafers, followed by drying under a stream of ultra-pure nitrogen before use. The freshly prepared gold-coated wafers were cut into slides (1 × 3 cm), and then the slides were cleaned by rinsing with absolute ethanol and dried with ultra-pure nitrogen. The slides then were immersed in the following thiol solutions; **C18SH** (1 mM in ethanol), **CholSH** (1 mM in ethanol), **CholC3SH** (1 mM in ethanol), **CholC4SH** (1 mM in ethanol), **CholC5SH** (1 mM in ethanol), **CholC6SH** (1 mM in ethanol), **CholC9SH** (1

mM in ethanol), or **CholC12SH** (1 mM in ethanol). The glass vials containing the thiol solutions were previously cleaned with piranha solution (3:1 mixture of H_2SO_4/H_2O_2) and rinsed thoroughly with deionized water and absolute ethanol. (*Caution: Piranha solution is highly corrosive and should be handled with extreme care*.) All substrates were allowed to equilibrate at room temperature for a period of 48 hours. Then the slides were rinsed with tetrahydrofuran and ethanol, and blown dry with ultra-pure nitrogen before characterization.

2.2.5. Characterization of SAMs

Ellipsometric Thickness Measurements. The thicknesses of the films were measured using a Rudolph Research Auto EL III ellipsometer equipped with a He-Ne laser (632.8 nm) at an angle of incidence of 70°. A refractive index of 1.45 was used for all SAMs studied in this series. For each sample, the data were averaged over the collection from two slides with three spots per slide. The measured thicknesses were always within ± 1 Å of the reported values.

Contact Angle Measurements. A Ramé-Hart model 100 contact angle goniometer was employed to measure the contact angle of the SAMs. The contacting liquids, water (W) and hexadecane (HD), were dispensed (advancing angle, θ_a) and withdrawn (receding angle, θ_r) on the surfaces of SAMs using a Matrix Technologies micro-Electrapette 25 at the slowest possible speed (1 μL/s). The measurements were

performed at room temperature with the pipet tip in contact with the drop. Reported values for each sample were the averages of measurements taken from two slides with three drops per slide using both drop edges and always within ± 2°.

Polarization Modulation Infrared Reflection Absorption Spectroscopy (PM-IRRAS). Surface IR spectra were collected using a Nicolet Nexus 670 Fourier transform spectrometer equipped with a liquid nitrogen-cooled mercury-cadmium-telluride (MCT) detector and a Hinds Instrument PEM-90 photoelastic modulator. The *p*-polarized light was reflected from the sample at an angle of incidence of 80° to the surface normal. The spectra were collected at 512 scans for the C–H stretching region (2750 – 3100 cm^{-1}) with a spectral resolution of 4 cm^{-1}.

X-ray Photoelectron Spectroscopy (XPS). A PHI 5700 X-ray photoelectron spectrometer equipped with a monochromatic Al Kα X-ray source (hν = 1486.7 eV) incident at 90° relative to axis of a hemispherical energy analyzer was employed to obtain XPS spectra of the SAMs at a photoelectron takeoff angle of 45° from the surface and a pass energy of 23.5 eV. The binding energy scales were referenced to the $Au_{4f7/2}$ peak at 84.0 eV.

2.3. Results and Discussion

The new SAMs generated from the targeted cholesterol-based thiols were characterized. For this study, we chose to use ethanol as the developing solvent to generate SAMs owing to the favorable solubility for the adsorbates and to ethanol's use in the majority of similar SAM studies. SAMs generated from a normal alkanethiol, *n*-octadecanethiol, and thiocholesterol were used as reference films for comparison of the data collected from this SAM series to that of previously published materials. We assumed that SAMs derived from the **CholCnSH** adsorbates where n = 3, 4, 5, 6, 9, and 12 would provide instrumental data that correspond to a SAM developed from **CholSH**. This assumption permits a direct comparison of the SAMs in this system in which the number of carbon atoms from the sulfur atom to the oxygen atom increases as n increases and the number of carbon atoms from the oxygen to the terminal group is the same for all the newly synthesized molecules.

2.3.1. Thicknesses of the Films

The thicknesses of each film were measured after the gold substrates were allowed to equilibrate in each thiol solution for 48 hours at room temperature, allowing sufficient time for these adsorbates to order owing to conformational and steric constraints of the novel cholesterol moieties. Additionally, the stereochemistry of these molecules and the α-face and β-face of cholesterol make this series of thiols relatively

bulky, as compared to normal alkanethiols, possibly limiting their access to the 3-fold hollow binding sites on the gold surface. As shown in Figure 2.3, the ellipsometric data for SAMs generated from **C18SH** and **CholSH** are in agreement with previously published data.[26,27,35,36]

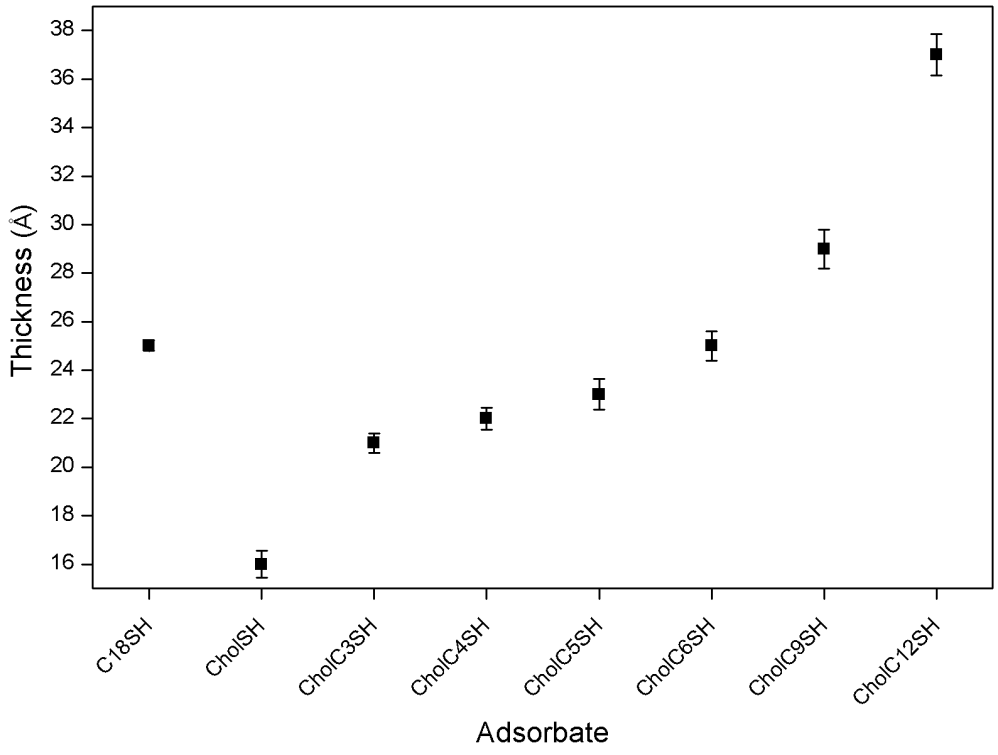

Figure 2.3. The film thicknesses measured at 48 hours equilibration time for each adsorbate.

The film thicknesses for the new series of molecules increases as the methylene chain increases, generally in agreement with previous observations of an average length of 1.2 Å per methylene unit for a trans-extended normal alkanethiolate.[35] After including

the thickness of the SAM formed from **CholSH** and the tilt angle for the new series being similar to that of a SAM developed from **CholSH**,[35] the measured values are within expected values for SAMs generated from the following thiols: **CholC3SH**, **CholC4SH**, **CholC5SH**, **CholC6SH**, and **CholC9SH**. However, the SAM formed from **CholC12SH** is higher than expected based upon these considerations. The thicker film is possibly due to a decrease in the tilt of the molecules in the monolayer formed from **CholC12SH** as compared to the other monolayers in the series, producing a thicker film than predicted. The tilt angle for **CholSH** is calculated to be ~ 37° from the surface normal given that the film thickness is 16 Å yet cholesterol has a calculated length of 20 Å.[26]

For normal alkanethiols, it has been determined that at least 10 carbon atoms are needed to create a film that is crystalline and well packed; films formed from normal alkanethiols having less than 10 carbon atoms are not as crystalline nor well packed.[35,37] This packing efficiency has been accredited to the cumulative van der Waals interactions for the methylene units in the alkyl chain. Given that the SAM generated from **CholC12SH** has a spacer 12 methylene units in length, it is possible that the van der Waals interactions between the methylene spacers has added order to this cholesterol-based film and thus lowered the tilt angle of the molecules below that of a SAM generated from **CholSH**, 37°, creating a thicker film. This reasoning would also explain why the SAMs formed from **CholC9SH**, **CholC6SH**, **CholC5SH**, **CholC4SH**, and **CholC3SH**, which contain fewer methylene units than **CholC12SH**, have thicknesses more in line with that expected for a cholesterol-based SAM. Further analysis of these results will be discussed below to support this conclusion.

2.3.2. Wettabilities of the Films

Advancing and receding contact angle measurements provide information about the organization within a monolayer film (*e.g.,* composition, packing, and structural orientation).[38] The wettabilities of the films from this series of single-chained cholesterol-based thiols are shown in Table 2.1, where the probe liquids used were water and hexadecane. The contact angles for SAMs generated from **C18SH** and **CholSH** are consistent with previously observed values.[26,39] The cholesterol-based films are wetted more by both liquids than the SAM formed from **C18SH**, a result which conforms with expectations since a SAM generated from **C18SH** is well-packed and crystalline. Prior research has shown that SAMs generated from methyl-terminated molecules are less wettable than isopropyl-terminated SAMs.[40] However, the films analyzed in this prior study presented an interface of isopropyl units attached to normal alkanethiolate chains, whereas the cholesterol-based SAMs contain an isopropyl group as part of the isooctyl tailgroup of cholesterol. The overall increase in advancing contact angles, Figure 2.4, for both liquids in this series shows an increase in packing density of the films as the hydrocarbon chain spacer is increased.[41]

The rigid polycyclic region and isooctane tailgroup of cholesterol are known to be hydrophobic. As expected, the advancing contact angles for water for this series of films are above 90° and therefore hydrophobic. It is notable that the advancing contact angles for water for the films formed from **C18SH**, **CholC9SH**, **CholC12SH** are similar suggesting similar interfacial packing, even though the composition and molecular

Table 2.1. Advancing (θ_a, °) and Receding Contact Angles (θ_r, °) Measured on SAMs Formed from **C18SH**, **CholSH**, **CholC3SH**, **CholC4SH**, **CholC5SH**, **CholC6SH**, **CholC9SH**, and **CholC12SH**, with Values of Hysteresis ($\Delta\theta = \theta_a - \theta_r$).

Adsorbate	**Probe Liquid** [a]					
	W			**HD**		
	θ_a	θ_r	$\Delta\theta$	θ_a	θ_r	$\Delta\theta$
C18SH	116	105	11	50	40	10
CholSH	108	92	16	16	0	- [b]
CholC3SH	108	88	20	18	0	- [b]
CholC4SH	113	94	19	23	0	- [b]
CholC5SH	110	91	19	17	0	- [b]
CholC6SH	114	92	22	22	0	- [b]
CholC9SH	116	92	24	23	0	- [b]
CholC12SH	117	91	26	24	0	- [b]

[a] Probe liquids used in this experiment are W = water and HD = hexadecane.

[b] When a receding contact angle could not be obtained, the hysteresis value could not be calculated.

ordering are very different for a normal alkanethiolate and cholesterol-based SAM. Additionally, the films formed from **CholC9SH** and **CholC12SH** apparently present surfaces that are more efficiently packed than the other cholesterol-based films. The general increase in advancing contact angles for the newly synthesized series of films, as compared to the SAM generated from **CholSH**, reflects the higher integrity, less defects as a result of better packing, of the cholesterol-based films.[42] The advancing contact angle suggests an increase in the interfacial packing of the monolayers which also would indicate an increase in ordering of the molecules in the monolayer. Due to cholesterol's lipophilic property, hexadecane has a much lower advancing contact angle than water and this contacting liquid apparently intercalates within the surface chains of these cholesterol-based films, preventing the measurement of a receding contact angle for all of the new cholesterol-based SAMs in this study.

The hysteresis of the contacts angles, $\Delta\theta = \theta_a - \theta_r$, can provide insight into the homogeneity of the interface of the film. The hysteresis values for the SAMs generated from **C18SH** and **CholSH** are comparable to values previously obtained for these SAMs, as shown in Table 2.1.[26,37,41] The large hysteresis of the SAM generated from **CholSH** with water is as expected due to defects in the SAM caused by packing misalignments and the bulkiness of the adsorbate. The hysteresis values for water for all cholesterol-based SAMs increase as the methylene chain increases in length, suggesting that the film interface is becoming more heterogeneous. As the adsorbates become longer, the SAMs become thicker and more ordered yet the surface interface interacts more with the water, the contacting liquid, as determined by the increasing hysteresis values. The packing and

ordering of the molecules for these cholesterol-based SAMs must be controlled by the rigid polycyclic ring region which allows for the isooctyl tailgroups to be disordered at the surface interface thus producing a more fluid surface interface. The disorder of the isooctyl tailgroups of cholesterol allows for more interactions between the probe liquid and methylene and methyl units thus producing a larger hysteresis value for the cholesterol-based SAMs.

It is also notable from the advancing contact angle data in Figure 2.4 that the interaction with the contacting liquids at the surface of the films is different based on the length of the hydrocarbon chain linker.[43,44] The films containing methylene spacers where n = 3, 4, 5, and 6 present a phenomenon where the SAMs generated from the cholesterol-based thiols with an even numbered methylene units are less wet than the SAMs generated from the cholesterol-based thiols with an odd number of methylene units.[45] The films with an odd number of hydrocarbons, where n = 3 and 5, have lower advancing contact angles than the films containing an even number of hydrocarbons, where n = 4 and 6, for both water and hexadecane. A surface-exposed methylene group is more wettable, with a lower contact angle, than an interfacial terminal methyl group, with a higher contact angle.[43,46,47] Since this parity phenomenon is seen with both water and hexadecane for the SAMs formed from **CholC3SH**, **CholC4SH**, **CholC5SH**, and **CholC6SH**, a change in the orientation of the bulky cholesterol moiety near the interface is believed to be contributing to this effect, however an exact determination of this orientational change has not been determined at this time. It is possible that the systematic increase in methylene units in the spacer region below the cholesterol moiety

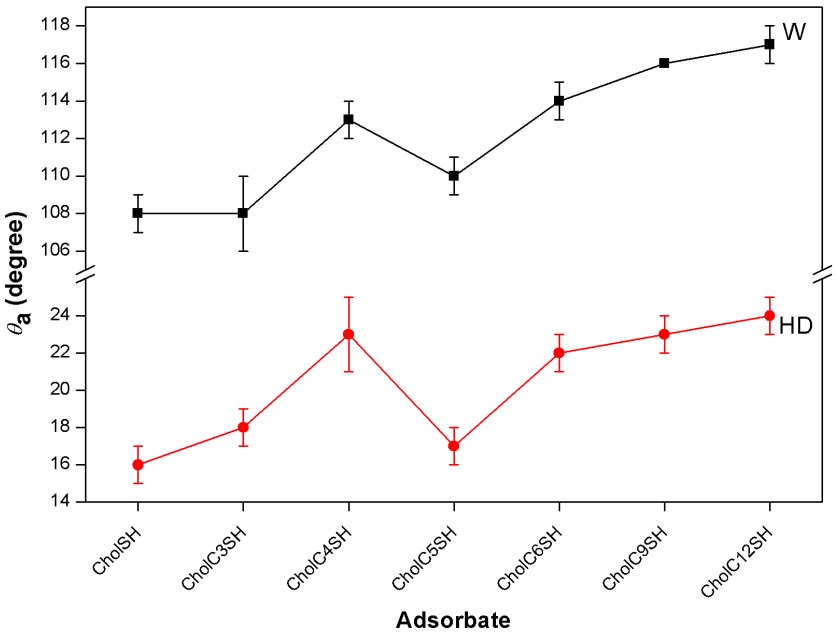

Figure 2.4. Comparison of the advancing contact angles for SAMs generated from **CholSH**, **CholC3SH**, **CholC4SH**, **CholC5SH**, **CholC6SH**, **CholC9SH**, and **CholC12SH** using various probe liquids: W = water (■) and HD = hexadecane (●). The lines connecting data points are provided to emphasize trends.

is influencing the alignment and packing of the overlying cholesterol as shown in Figure 2.5. The drawings in Figure 2.5 reflect a typical Au–S–C bond angle for SAMs; however, the actual angle may vary if the monolayer film is subject to stress due to packing interactions (*e.g.*, steric repulsion and/or van der Waals attraction) of the molecules within the film.[48] Further, these stresses might give rise to an alternative geometry about the sulfur, leading to an change in the Au–S–C bond angle from that shown in Figure 2.5. Importantly, the contact angle values can plausible vary systematically with changes in the packing structure, but we see no clear evidence of any

systematic changes in packing density based on the data obtained by ellipsometry, PM-IRRAS, and XPS reported here.

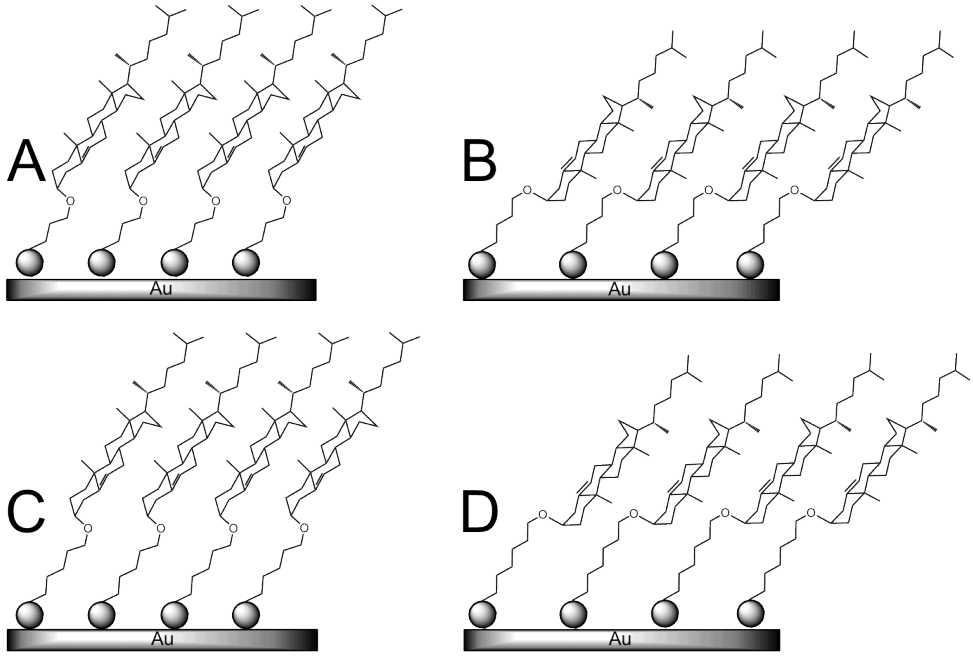

Figure 2.5. Illustration representing the change in orientation of the molecules used to form SAMs as the number of methylene units in the spacer region is systematically increased for SAMs generated from (A) **CholC3SH**, (B) **CholC4SH**, (C) **CholC5SH**, and (D) **CholC6SH**. Molecular sizes and dimensions are not drawn to scale.

2.3.3. PM-IRRAS Studies

The infrared-reflectance spectra in the C–H stretching region of the cholesterol-based SAMs are shown in Figure 2.6, with the peak assignments shown in Table 2.2. The degree of crystallinity and packing density for alkyl chains in a SAM can be

interpreted through PM-IRRAS.[35] A well-packed crystalline SAM will have an antisymmetric methylene peak located at 2919 cm^{-1}, based on films formed from crystalline polyethylene, which is sensitive to the degree of conformational order.[49,50] A higher value for the $\nu_a^{CH_2}$ of about 2928 cm^{-1} is the result of a less crystalline, more liquid-like polyethylene film.[49-51]

The surface IR for a SAM generated from **CholSH** versus a crystalline SAM generated from **C18SH** is very different, revealing noticeable differences in peak intensity and frequency, reflecting the differences in the structural and chemical environments of the C–H bonds. For cholesterol-based films, the most intense peak is the antisymmetric methyl stretch, 2963 cm^{-1} for a SAM generated from **CholSH**, where as SAMs generated from a normal alkanethiols typically show the antisymmetric methylene peak as the most intense peak, at ~ 2919 cm^{-1}. This difference between the two types of structures can be explained by the orientation of the bonds to the surface, the number of bonds invovled, and the structure and ordering of the two types of molecules.[52,53] Normal alkanethiols have a majority of methylene units where the transition dipole moments are more perpendicular to the surface and therefore they produce an intense antisymmetric methylene stretch signal in surface IR. A higher number of signals associated with the number of methylene units, along with an increased crystallinity, positioning these stretches more perpendicular to the surface, lead to an intense peak in PM-IRRAS. The strength of the adsorption of the perpendicular vibrations can be explained by the surface selection rule associated with surface IR.[54] The same principal applies to the cholesterol-based SAMs that have a strong $\nu_a^{CH_3}$ peak. The cholesterol moiety contains five methyl

groups, four of which are predicted to have transition dipole moments that aligns with the surface normal, thus producing an intense signal and providing a molecular axis that is parallel or nearly parallel to the surface normal.[26]

For this series of SAMs, the frequencies of the $\nu_a^{CH_2}$ peaks do not shift as the number of methylene units is increased, with the exception of the spectra from the SAM generated from **CholC9SH** and **CholC12SH**. Part of the reason for the shape of the peak for $\nu_a^{CH_2}$ is that the cholesterol structure is present in all the SAMs, thus the underlying alkyl chain only adds to the IR for the SAM generated from **CholSH**. The $\nu_a^{CH_2}$ peak for the SAM formed from **CholC9SH** has a shoulder, located at 2927 cm^{-1}, associated with an increase in the signal from the methylene units as compared to the SAM formed from **CholC6SH**. The spectra for the SAM formed from **CholC12SH** has a signal from the antisymmetric methylene stretch located at 2924 cm^{-1}, confirming an increase in order as determined by the advancing contact angles and an increase in the number of methylene units as confirmed by the ellipsometric data. The $\nu_a^{CH_2}$ peak for the SAMs generated from **CholC9SH** and **CholC12SH** indicate a greater influence of the underlying alkyl chain upon the packing and ordering in the film. The greater influence of the underlying methylene units of the spacer region is also seen in the symmetric methylene stretch in that the relative intensity compared to the other peaks in each spectra is increasing as n increases, most notably in the spectra of SAMs generated from **CholC9SH** and **CholC12SH**.

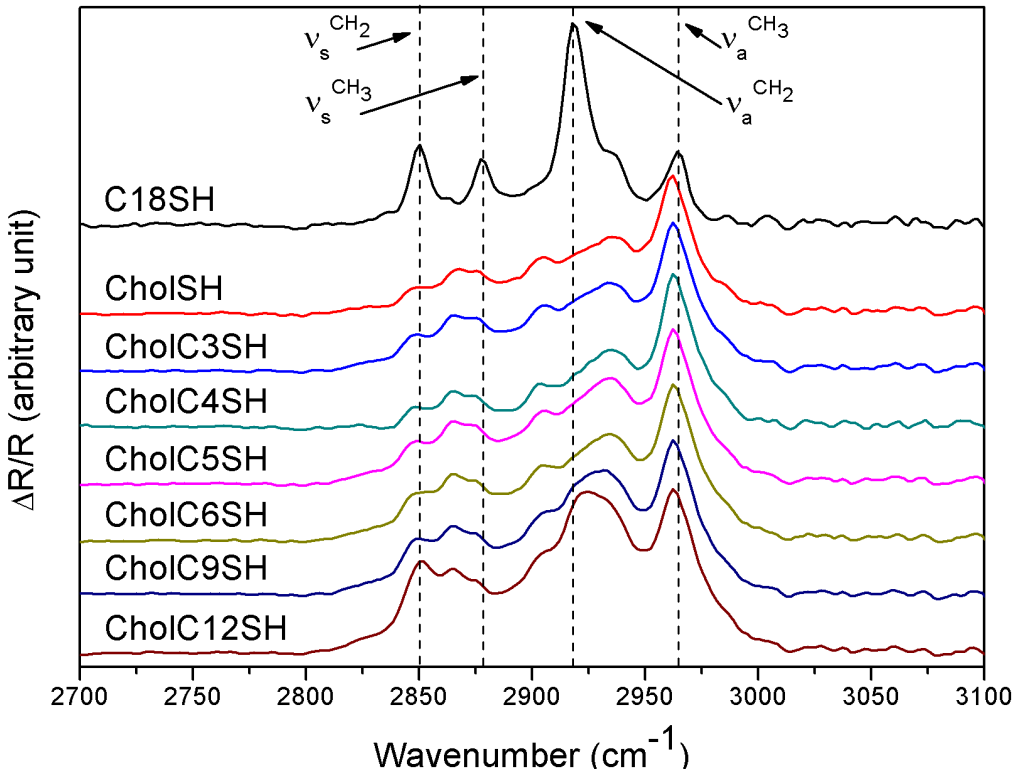

Figure 2.6. PM-IRRAS spectra in C–H stretching region of SAMs generated by the adsorption of **C18SH**, **CholSH**, **CholC3SH**, **CholC4SH**, **CholC5SH**, **CholC6SH**, **CholC9SH**, and **CholC12SH** onto evaporated gold substrates. The dashed vertical lines provide the positions of four key C–H stretches, are provided as a guide for the eye, and are assigned according to their respective position for the SAM generated from **C18SH**.

The change in relative intensities is very noticeable in the spectra from the SAM generated from **CholC12SH** as the $\nu_a^{CH_3}$ and $\nu_a^{CH_2}$ are almost the same intensity. The width at half height for the peaks identified in all spectra for the cholesterol-containing SAMs could not be calculated or compared as the peaks are broad and overlapping. A comparison of this value would have provided more structural information about the

position of the cholesterol moiety in the monolayer as n increases from 3 to 6 methylene units as observed in the advancing contact angle data.

Table 2.2. Peak Assignments for the PM-IRRA Spectra of SAMs Generated from **CholSH**, **CholC3SH**, **CholC4SH**, **CholC5SH**, **CholC6SH**, **CholC9SH**, **CholC12SH**, and **C18SH**.

Adsorbates	**Peak Assignments**			
	$\nu_a^{CH_2}$	$\nu_a^{CH_3}$	$\nu_s^{CH_3}$	$\nu_s^{CH_2}$
CholSH	2935	2962	2868, 2875	2850
CholC3SH	2934	2962	2866, 2875	2849
CholC4SH	2935	2963	2865, 2873	2849
CholC5SH	2934	2962	2865, 2876	2849
CholC6SH	2934	2963	2865, 2876	2853
CholC9SH	2932	2962	2865, 2876	2850
CholC12SH	2924	2962	2865, 2876	2851
C18SH	2918	2964	2878	2850

2.3.4. XPS Studies

XPS spectra obtained from SAMs can be used to reveal the chemical composition of the films and the nature of the chemical bond between the adsorbate headgroup and the substrate.[37] The XPS spectra of the C_{1s}, O_{1s}, and S_{2p} regions are shown in Figure 2.7 for SAMs generated from **CholSH**, **CholC3SH**, **CholC4SH**, **CholC5SH**, **CholC6SH**,

CholC9SH, and **CholC12SH**. These spectral regions confirm the presence of intact cholesterol-based thiolates on a gold surface. Several studies have shown that the binding energy of the C_{1s} peak can be utilized to roughly determine the relative coverage (i.e., packing density) of the adsorbates on the metal substrate.[41,55-58] Well-packed alkanethiolate SAMs have the ability to resist the emission of photoelectrons from the surface during X-ray irradiation,[57] while loosely packed surfaces act like a poor insulator, making the emission more facile and causing the C_{1s} peak to shift to a lower binding energy.[56,59] For the C_{1s} peak position, the peak obtained from the SAM generated from **C18SH** appears at 285.0 eV, while the binding energy of the C_{1s} peak for the cholesterol-based SAMs shifts to a slightly lower energy, as seen in Figure 2.7 (A). The shift of the C_{1s} peaks for the cholesterol-based films to a lower binding energy suggests a lower hydrocarbon chain density relative to **C18SH**. However, the structural differences between the extended alkyl chain and the cholesterol moiety might also play a role in this shift. Utilizing the XPS spectra from both the loosely packed SAM formed from **CholSH** and the efficiently packed SAM formed from **C18SH** provides a clearer picture of how the blend of the two structural components influences the C_{1s} peak position in the balance of the cholesterol-based SAMs. The C_{1s} peak of the SAM generated from **CholC12SH** is in between the peak for the SAMs generated from **C18SH** and **CholSH**, indicating a higher density SAM than the remaining cholesterol-based films yet the SAM generated from **C18SH** is a denser monolayer. This interpretation regarding the shift in the C_{1s} peak is in agreement with previously published data suggesting that the SAM

generated from **CholSH** has a 65 % coverage compared to the SAM formed from **C18SH**.[26,27]

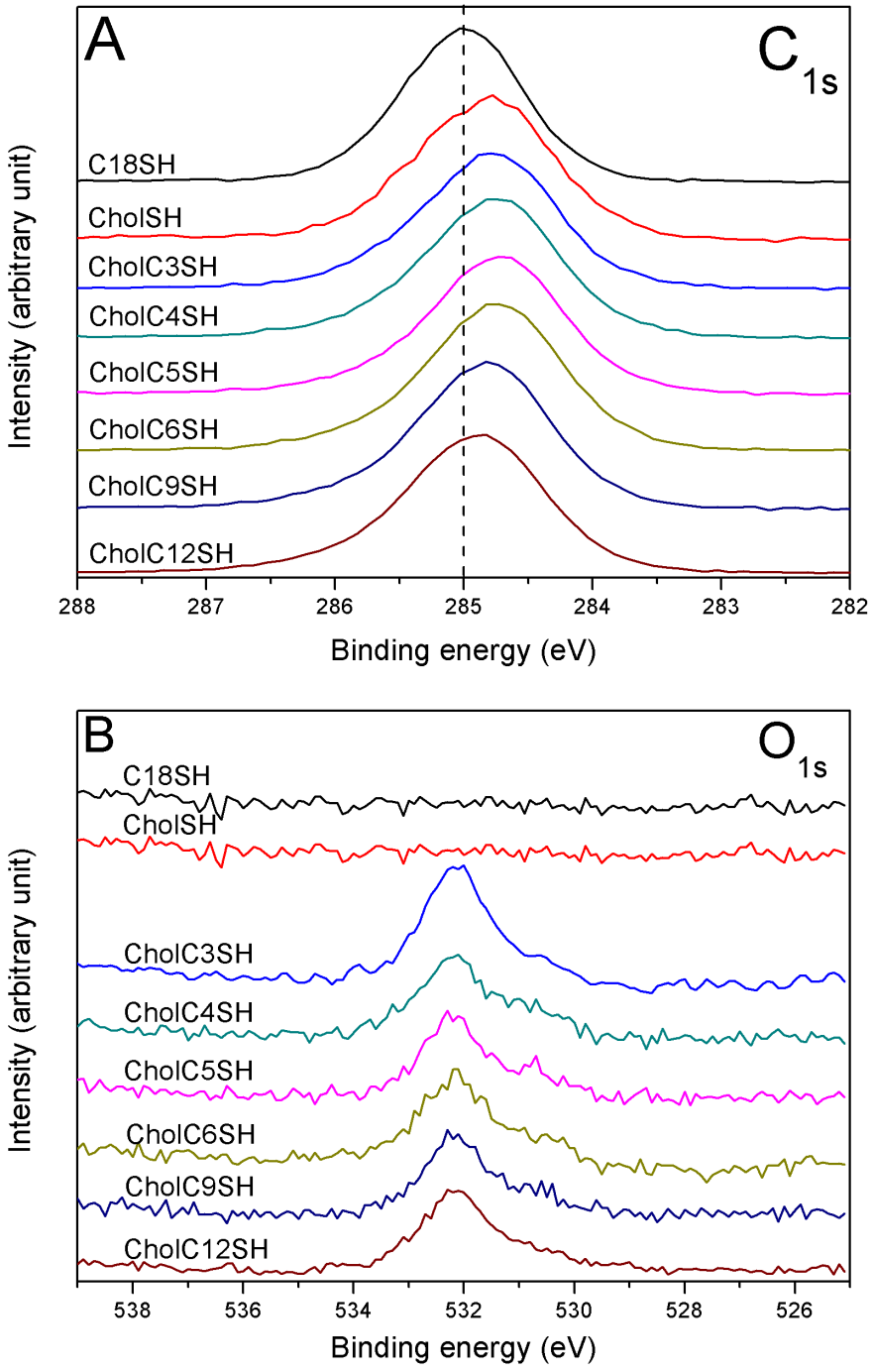

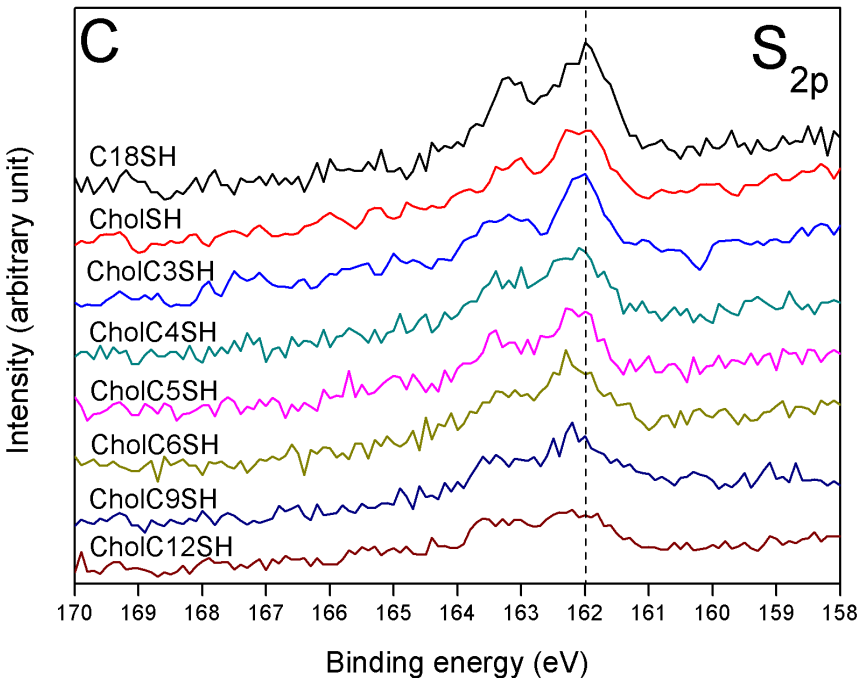

Figure 2.7. XPS spectra of the (A) C_{1s}, (B) O_{1s}, and (C) S_{2p} regions for the series of cholesterol-based SAMs, along with that formed from **C18SH**. The dashed lines in the spectra for the C_{1s} and S_{2p} region are aligned with the peak position for the SAM generated from **C18SH**.

For thiol adsorbates on gold surfaces, the binding energies of the $S_{2p3/2}$ orbitals are used to evaluate the S–Au bond formation. The $S_{2p3/2}$ binding energy for bound thiolate is assigned to 162 eV, while that for unbound thiol or disulfide is shown roughly around 164 eV and for oxidized sulfur at 166 to 168 eV.[60,61] Figure 2.7 (C) shows the XPS spectra in the S_{2p} region for the SAMs derived from cholesterol-based thiols and **C18SH**. While the S_{2p} signal is weak and attenuated, and the signal-to-noise ratio is not optimum, the spectra still show the presence of bound thiol and the absence of oxidized adsorbates.

Comparing the relative intensities of the individual elemental peaks provides insight into the relative film density and composition of the monolayer, Figure 2.8.[55,62] In this series of SAMs, the ratio of the C_{1s} and Au_{4f} signals (the C:Au ratio) increases as the methylene spacer is increased. However, the signal for the carbons underneath the cholesterol moiety is attenuated by the overlying structure. A thicker monolayer also relates to an increase in the C_{1s} signal, as there are more carbons in the monolayer therefore the ratio of the integrated area under the peaks for carbon as compared to those for gold, Au_{4f}, will provide some insight into the film density. The ratios of the intensities of the carbon signal to the gold signal are normalized to the shortest of the new cholesterol-based films, the SAM formed from **CholC3SH**, for comparison purposes. The large increase in the ratio for the larger n values validates the ellipsometry data, as the methylene spacer unit is increased, the ratio disproportionately increases. The **CholC12SH** film has a larger C:Au ratio than expected, which can be interpreted as an indication of greater film density.

The ratio of sulfur-to-gold provides packing information about the monolayer since the sulfur atom is located in the same relative position as the gold interface. The ratios of the integrated peak areas for the binding energies associated with the S_{2p} and Au_{4f} signals (the S:Au ratio) have been normalized to the ratio for the SAM generated from **CholC3SH** for purposes of comparison. A decrease in the ratio of sulfur-to-gold is expected as the films are become more packed, based on PM-IRRAS and contact angle data, and thus the sulfur signal should be attenuated more for the thicker films. For the SAMs with a low n value, a trend appears to be present that leads to a S:Au ratio of

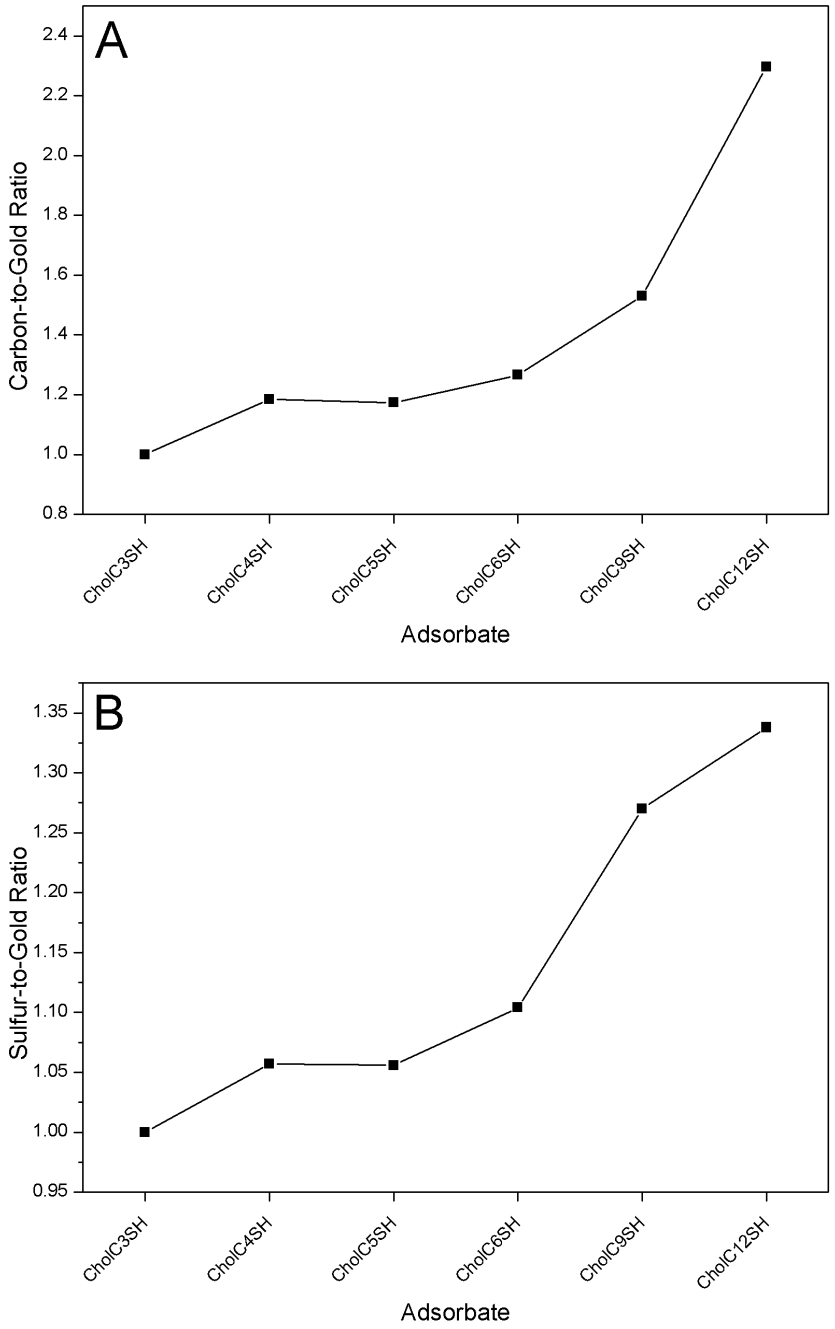

Figure 2.8. Normalized integrated peak ratios calculated from the XPS data for the peaks associated with (A) the C_{1s} and Au_{4f} binding energies (C:Au ratio) and (B) the S_{2p} and Au_{4f} binding energies (S:Au ratio), for the series of cholesterol-based SAMs. The lines connecting data points are provided as a guide for the eye to emphasize trends.

~ 1.10 for the SAM generated from **CholC6SH**. However for the thicker monolayers, SAMs generated from **CholC9SH** and **CholC12SH**, the S_{2p} signal has been subject to more attenuation by the overlying monolayer and thus the ratio is higher than the ratio for the shorter films.

2.4. Conclusions

A series of cholesterol-based adsorbates were successfully synthesized and used to form single-component SAMs on gold. Characterization of all the monolayers in the series revealed that these molecules can be used to generate SAMs at room temperature that are more efficiently packed than films formed from **CholSH**. The SAMs generated from **CholC9SH** and **CholC12SH** have a decreased molecular tilt, increased density, and increased order than the other cholesterol-based SAMs, yet are not as dense or crystalline as a SAM generated from **C18SH**. The addition of the methylene spacer to cholesterol allows for a better formation of a SAM than thiocholesterol. These molecules show potential for use in studying the cholesterol condensing effect as compared to thiocholesterol.

2.5. References

(1) Lipowsky, R.; Sackmann, E. *Structure and Dynamics of the Membranes*; North–Holland: Amsterdam, 1995.

(2) Yeagle, P. L. *Biochim. Biophys. Acta* **1985**, *822*, 267–287.

(3) Leathes, J. B. *Lancet* **1925**, *208*, 853–856.

(4) Demel, R. A.; Deenen, L. L. M. V.; Pethica, B. A. *Biochim. Biophys. Acta* **1967**, *135*, 11–19.

(5) Pillips, M. C. *Progress in Surface and Membranes Science* **1972**, *5*, 139–222.

(6) Hung, W. C.; Lee, M. T.; Chen, F. Y.; Huang, H. W. *Biophys. J.* **2007**, *92*, 3960–3967.

(7) Alonso, C.; Kuzmenko, I.; Jensen, T. R.; Kjaer, K.; Lahav, M.; Leiserowitz, L. *J. Phys. Chem. B* **2001**, *105*, 8563–8568.

(8) Alwarawrah, M.; Dai, J.; Huang, J. *J. Phys. Chem. B* **2010**, *114*, 7516–7523.

(9) McIntosh, T. *Biochim. Biophys. Acta* **1978**, *513*, 43–58.

(10) Mattjus, P.; Bittman, R.; Slotte, J. P. *Langmuir* **1996**, *12*, 1284–1290.

(11) Wydro, P.; Knapczyk, S.; Lapczynska, M. *Langmuir* **2011**, *27*, 5433–5444.

(12) Bonn, M.; Roke, S.; Berg, O.; Juurlink, L. B. F.; Stamouli, A.; Muller, M. *J. Phys. Chem. B* **2004**, *108*, 19083–19085.

(13) Martinez-Seara, H.; Rog, T.; Karttunen, M.; Vattulainen, I.; Reigada, R. *J. Phys. Chem. B* **2009**, *113*, 8347–8356.

(14) Li, L. K.; So, L.; Spector, A. *J. Lipid Res.* **1985**, *26*, 600–609.

(15) Somerharju, P.; Virtanen, J. A.; Cheng, K. H. *BBA - Mol. Cell Biol. L.* **1999**, *1440*, 32–48.

(16) McConnell, H. M.; Radhakrishnan, A. *BBA - Biomembr.* **2003**, *1610*, 159–173.

(17) Huang, J.; Feigenson, G. W. *Biophys. J.* **1999**, *76*, 2142–2157.

(18) Ivankin, A.; Kuzmenko, I.; Gidalevitz, D. *Phys. Rev. Lett.* **2010**, *104*, 108101–108104.

(19) Kusumi, A.; Subczynski, W. K.; Pasenkiewicz-Gierula, M.; Hyde, J. S.; Merkle, H. *BBA - Biomembr.* **1986**, *854*, 307–317.

(20) McMullen, T. P. W.; Lewis, R. N. A. H.; McElhaney, R. N. *Biochemistry* **1993**, *32*, 516–522.

(21) Presti, F. T.; Chan, S. I. *Biochemistry* **1982**, *21*, 3821–3830.

(22) Cadenhead, D. A.; Phillips, M. C. *J. Colloid Interface Sci.* **1967**, *24*, 491–499.

(23) Parker, A.; Miles, K.; Cheng, K. H.; Huang, J. *Biophys. J.* **2004**, *86*, 1532–1544.

(24) Gupta, R. K.; Suresh, K. A. *Colloid Surface A* **2008**, *320*, 233–239.

(25) Segura, A.; Batina, N. *NSTI Nanotechnology* **2006**, *1*, 261–264.

(26) Yang, Z. P.; Engquist, I.; Kauffmann, J. M.; Liedberg, B. *Langmuir* **1996**, *12*, 1704–1707.

(27) Yang, Z.; Engquist, I.; Wirde, M.; Kauffmann, J. M.; Gelius, U.; Liedberg, B. *Langmuir* **1997**, *13*, 3210–3218.

(28) Yang, Z.; Engquist, I.; Liedberg, B.; Kauffmann, J. M. *J. Electroanal. Chem.* **1997**, *430*, 189–195.

(29) Bittoun, E.; Marmur, A.; Ostblom, M.; Ederth, T.; Liedberg, B. *Langmuir* **2009**, *25*, 12374–12379.

(30) Andersson, O.; Ulrich, C.; Bjorefors, F.; Liedberg, B. *Sensor. Actuat. B - Chem.* **2008**, *134*, 545–550.

(31) Indrieri, M.; Suardi, M.; Podesta, A.; Ranucci, E.; Ferruti, P.; Milani, P. *Langmuir* **2008**, *24*, 7830–7841.

(32) Trevor, J. L.; Lykke, K. R.; Pellin, M. J.; Hanley, L. *Langmuir* **1998**, *14*, 1664–1673.

(33) Blasi, L.; Pisignano, D.; Di Benedetto, F.; Maruccio, G.; Ciccarella, G.; Maffei, A.; Vasapollo, G.; Cingolani, R.; Rinaldi, R. *BBA - Biomembr.* **2005**, *1714*, 93–102.

(34) Boden, N.; Bushby, R. J.; Clarkson, S.; Evans, S. D.; Knowles, P. F.; Marsh, A. *Tetrahedron* **1997**, *53*, 10939–10952.

(35) Porter, M. D.; Bright, T. B.; Allara, D. L.; Chidsey, C. E. D. *J. Am. Chem. Soc.* **1987**, *109*, 3559–3568.

(36) Shon, Y. S.; Lee, T. R. *Langmuir* **1999**, *15*, 1136–1140.

(37) Laibinis, P. E.; Whitesides, G. M.; Allara, D. L.; Tao, Y. T.; Parikh, A. N.; Nuzzo, R. G. *J. Am. Chem. Soc.* **1991**, *113*, 7152–7167.

(38) Shon, Y. S.; Lee, S.; Colorado, R., Jr.; Perry, S. S.; Lee, T. R. *J. Am. Chem. Soc.* **2000**, *122*, 7556–7563.

(39) Tamada, K.; Nagasawa, J.; Nakanishi, F.; Abe, K.; Hara, M.; Knoll, W.; Ishida, T.; Fukushima, H.; Miyashita, S.; Usui, T.; Koini, T.; Lee, T. R. *Thin Solid Films* **1998**, *327–329*, 150–155.

(40) Barriet, D.; Chinwangso, P.; Lee, T. R. *ACS Appl. Mater. Interfaces* **2010**, *2*, 1254–1265.

(41) Bain, C. D.; Troughton, E. B.; Tao, Y. T.; Evall, J.; Whitesides, G. M.; Nuzzo, R. G. *J. Am. Chem. Soc.* **1989**, *111*, 321–335.

(42) Miller, W. J.; Abbott, N. L. *Langmuir* **1997**, *13*, 7106–7114.

(43) Sellers, H.; Ulman, A.; Shnidman, Y.; Eilers, J. E. *J. Am. Chem. Soc.* **1993**, *115*, 9389–9401.

(44) Bain, C. D.; Whitesides, G. M. *Angew. Chem.* **1989**, *101*, 522–528.

(45) Colorado, R., Jr.; Villazana, R. J.; Lee, T. R. *Langmuir* **1998**, *14*, 6337–6340.

(46) Tao, F.; Bernasek, S. L. *Chem. Rev. (Washington, DC, U. S.)* **2007**, *107*, 1408–1453.

(47) Bain, C. D.; Whitesides, G. M. *J. Am. Chem. Soc.* **1989**, *111*, 7164–7175.

(48) Rong, H. T.; Frey, S.; Yang, Y. J.; Zharnikov, M.; Buck, M.; Wuhn, M.; Woll, C.; Helmchen, G. *Langmuir* **2001**, *17*, 1582–1593.

(49) Nuzzo, R. G.; Fusco, F. A.; Allara, D. L. *J. Am. Chem. Soc.* **1987**, *109*, 2358–2368.

(50) Nuzzo, R. G.; Dubois, L. H.; Allara, D. L. *J. Am. Chem. Soc.* **1990**, *112*, 558–569.

(51) Snyder, R. G.; Strauss, H. L.; Elliger, C. A. *J. Phys. Chem.* **1982**, *86*, 5145–5150.

(52) Bradshaw, A. M.; Richardson, N. V. *Pure Appl. Chem.* **1996**, *68*, 457–467.

(53) Lummerstorfer, T.; Hoffmann, H. *Langmuir* **2004**, *20*, 6542–6545.

(54) Greenler, R. G. *J. Chem. Phys.* **1966**, *44*, 310–315.

(55) Frey, S.; Heister, K.; Zharnikov, M.; Grunze, M.; Tamada, K.; Colorado, R., Jr.; Graupe, M.; Shmakova, O. E.; Lee, T. R. *Isr. J. Chem.* **2000**, *40*, 81–97.

(56) Biebuyck, H. A.; Bain, C. D.; Whitesides, G. M. *Langmuir* **1994**, *10*, 1825–1831.

(57) Ishida, T.; Hara, M.; Kojima, I.; Tsuneda, S.; Nishida, N.; Sasabe, H.; Knoll, W. *Langmuir* **1998**, *14*, 2092–2096.

(58) Tamada, K.; Ishida, T.; Knoll, W.; Fukushima, H.; Colorado, R., Jr.; Graupe, M.; Shmakova, O. E.; Lee, T. R. *Langmuir* **2001**, *17*, 1913–1921.

(59) Park, J. S.; Smith, A. C.; Lee, T. R. *Langmuir* **2004**, *20*, 5829–5836.

(60) Castner, D. G.; Hinds, K.; Grainger, D. W. *Langmuir* **1996**, *12*, 5083–5086.

(61) Sun, F.; Grainger, D. W.; Castner, D. G.; Leach-Scampavia, D. K. *Macromolecules* **1994**, *27*, 3053–3062.

(62) Zhang, S.; Jamison, A. C.; Schwartz, D. K.; Lee, T. R. *Langmuir* **2008**, *24*, 10204-10208.

Chapter 3. Self-assembled Monolayers Generated from Unsymmetrical Double-chained Cholesterol-based Thiols on Gold

3.1. Introduction

The self-assembly of molecules to form monolayers has been of interest over the past two decades and has applications in anticorrosion,[1] surface patterning,[2,3] biomaterials,[4,5] and fabrication of mico and nanoelectronic devices.[6,7] Self-assembled monolayers (SAMs) form by the spontaneous chemisorption of organic molecules onto a metal surface. Since the first description of well-packed monolayers in 1983 by Nuzzo and Allara, this area of research has become a leading field in nano-sized films.[8] Monolayer films can provide a protective barrier and be easily manipulated for a desired surface property (*e.g.,* wetting,[9,10] friction,[11-13] molecular sensing,[14] adhesion,[15-17] and patterning[14,18]). The most investigated type of SAM involve thiols on gold due to many factors including the ease of use of gold, which does not form a stable oxide surface under atmospheric conditions and the strong chemical interaction between gold and sulfur.[14,18-21] Normal alkanethiols are known to form dense well-packed monolayers adopting a trans-extended conformation with ~ 30° tilt from the surface normal.[14,20] Pure SAMs are known to produce films with and without defects, however mixed SAMs, containing more than one component, show phase separation.[22-26]

Mixed SAMs have a tendency to phase separate due to molecular interactions of the two, or more, components. Phase separation has been seen in mixed monolayers with

molecular mismatches (*e.g.*, aliphatic vs. aromatic hydrocarbons,[22,24,27-31] polycyclic vs. aliphatic hydrcarbons,[32-34] saturated vs. unsaturated (or branched) alkyl chains,[35-38] long vs. short aliphatic chains,[27,33] hydrogenated vs. fluorinated chains,[25,26,28-31,35,39-41] and others[23,42-47]). The ability to manipulate phase separations has potential in advanced SAM systems as seen in interactions with nanoparticles,[48] nanoelectronics,[49,50] nanocircuits,[51] and biosensors.[52]

Phase manipulation, on a three-dimensional scale, is achieved with the use of surfactants. Micelles form when surfactants are introduced into a two component, phase-separated liquid due to the reduction of interfacial tension between the two phases. Mimicking surfactants on a three-dimensional scale, specifically designed molecules should act as surfactants on a two-dimensional scale in a monolayer. These two-dimensional surfactants should possess a headgroup that is compatible with all components of the monolayer and a tailgroup(s) that provides a phase preference compatibility with each of the components of the monolayer, independent of the other component. Schwartz *et al.* have studied molecules on the air-water interface using Langmuir monolayers and have demonstrated the ability to utilize specially designed surfactants to manipulate the phase boundary between hydrocarbon and fluorocarbon phases.[53-57]

Of particular interest are double tailgroup molecules for the manipulation of phase separation. Double tailgroup molecules form SAMs that are less crystalline, contain more defects, and are less ordered than normal alkanethiols (Figure 3.1). Despite these downfalls, these molecules are still of interest for their two-dimensional homogeneity

within the monolayer. We propose the use of cholesterol as one tailgroup and an alkyl hydrocarbon chain as the other tailgroup. Utilizing the cholesterol condensing effect, these molecules should form a homogenously mixed single-component SAM with physical properties resembling a two-component SAM (Figure 3.1 B). The phenomenon of the condensing effect on a hydrocarbon monolayer by cholesterol is not well understood. First described in 1925 by Leathes, the cholesterol condensing effect is a phenomenon seen in monolayers and bilayers of lipids containing cholesterol.[58] The condensing effect is described as a decrease in surface area of a mixed monolayer containing cholesterol and lipids.[59] The mechanism by which cholesterol condenses a lipid monolayer is debatable and tends to follow one of three mechanistic models.[60-62]

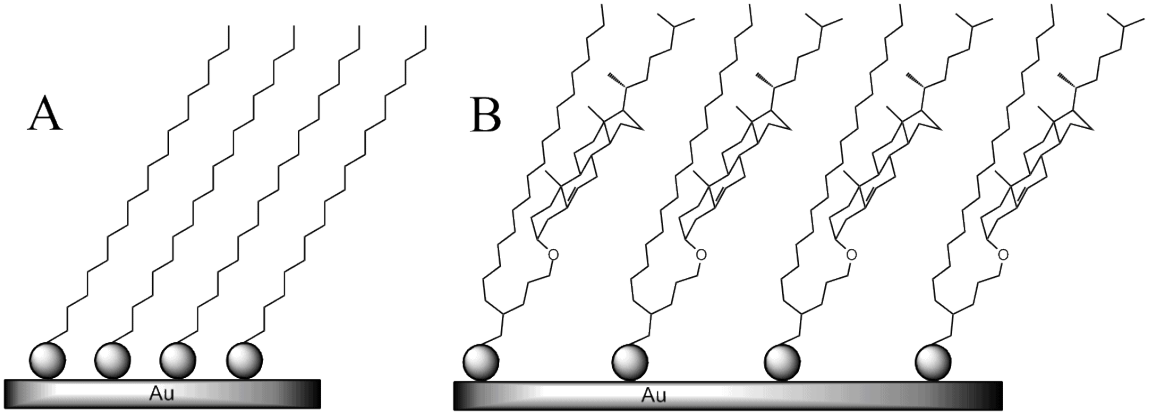

Figure 3.1. Illustration of the structures of SAMs examined in this study generated from (A) $CH_3(CH_2)_{17}SH$ (**C18SH**) with trans-extended conformation and (B) the cholesterol-based double-chain moieties (**C18CnCholSH**). The image shows **C18CholC3SH** as an example of the cholesterol-based, double-chained thiols. Molecular sizes and dimensions are not drawn to scale.

We hope to provide some insight into this condensing phenomenon with our novel, specifically designed molecules for use in SAMs.

Within, we describe the synthesis and characterization of the double-chained thiols: 2-(cholest-5-en-3β-oxypropyl)-eicosan-1-thiol, 2-(cholest-5-en-3β-oxyhexyl)-eicosan-1-thiol, and 2-(cholest-5-en-3β-oxynonyl)-eicosan-1-thiol (denoted as **C18C3CholSH**, **C18C6CholSH**, **C18C9CholSH**, Figure 3.2). The compounds were used to form monolayers on flat gold and analyzed by ellipsometry, contact angle goniometry, polarization modulation infrared-reflection adsorption spectroscopy (PM-IRRAS), and X-ray photoelectron spectroscopy (XPS). These results were compared with those of monolayers generated on flat gold from the adsorption of *n*-octadecanethiol (**C18SH**).

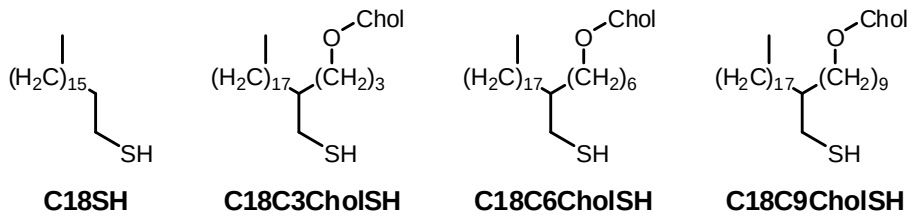

C18SH **C18C3CholSH** **C18C6CholSH** **C18C9CholSH**

Figure 3.2. Structures of *n*-octadecanethiol (**C18SH**) and the corresponding double-chained cholesterol-containing thiols (**C18C3CholSH**, **C18C6CholSH**, and **C18C9CholSH**).

3.2. Experimental Section

3.2.1 Nomenclature

We denote the names of the thiol adsorbates used in this study as follows: *n*-octadecanethiol ($CH_3(CH_2)_{17}SH$), **C18SH**; 2-(cholest-5-en-3β-oxypropyl)-eicosan-1-thiol, **C18C3CholSH**; 2-(cholest-5-en-3β-oxyhexyl)-eicosan-1-thiol, **C18C6CholSH**; 2-(cholest-5-en-3β-oxynonyl)-eicosan-1-thiol, **C18C9CholSH**. The letters indicates the chemical composition of the adsorbate: **Chol** denotes a cholesterol moiety, **C** denotes methyl and methylene units (CH_3 and CH_2) within the hydrocarbon chain, and **SH** denotes thiol structure. The number following each letter indicates the number of each unit along the chain backbone.

3.2.2. Materials

Gold shot (99.99 %) was purchased from Kamis Inc. Nickle-chromium canes (80 % nickel and 20 % chromium) were purchased from Kurt J. Lesker Company. Polished single-crystal Si(100) wafers were purchased from Silicon Sense, Inc. and rinsed with absolute ethanol (EtOH, Aaper Alcohol and Chemical Co.) before use. The contacting liquids used for wettability measurements were of the highest purity available from the following sources and were used as received: water generated from Milli Q Water System with resistance of 18.2 MΩ, Millipore Corporation; and hexadecane from Aldrich

Chemical Co.. *n*-Octadecanethiol (**C18SH**) was purchased from TCI America Co. and used without further purification. Tetrahydrofuran (THF) was purchased from Mallinckrodt Baker, Inc, distilled over calcium hydride, and stored under argon. Anhydrous dioxane, anhydrous *N*,*N*-dimethylformamide (DMF), methanol, cholesterol, sodium hydride (NaH, 60 % dispersion in mineral oil), 1,3-propanediol, 1,6-hexanediol, 1,9-nonanediol, triethylamine (NEt_3), sodium iodide, and potassium thioacetate (KSAc) were purchased from Aldrich Chemical Co. and used as received. Lithium aluminum hydride (LiAlH) was purchased from Alfa Aesar and used as received. Methanesulfonyl chloride (MsCl) and *p*-toluenesulfonyl chloride (TsCl) were purchased from Acros Organics and used as received. Column chromatography was performed using silica gel (40 – 64 μm) and thin-layer chromatography (TLC) was carried out using 200 μm-thick silica gel plates, which both were purchased from Sorbent Technologies, Inc. The eluted TLC plates were developed with a molybdenum blue stain followed by heating. Nuclear Magnetic Resonance (NMR) spectra were recorded on a JOEL ECA-500 spectrometer operating at 500 MHz. The data were obtained in $CDCl_3$ and referenced to δ 7.26 ppm for ^{1}H NMR spectra and 77.00 ppm for ^{13}C NMR spectra.

3.2.3. Synthesis of the Adsorbates

The synthetic strategy used to prepare the targeted double-chain cholesterol-based thiols (**C18CnCholSH**) is shown in Scheme 3.2. The complete experimental details of each synthetic step are provided in the section that follows.

Scheme 3.1. Preparation of a Series of Double-chained Cholesterol-based Thiols (**C18CnCholCSH**), where n = 3, 6, and 9.

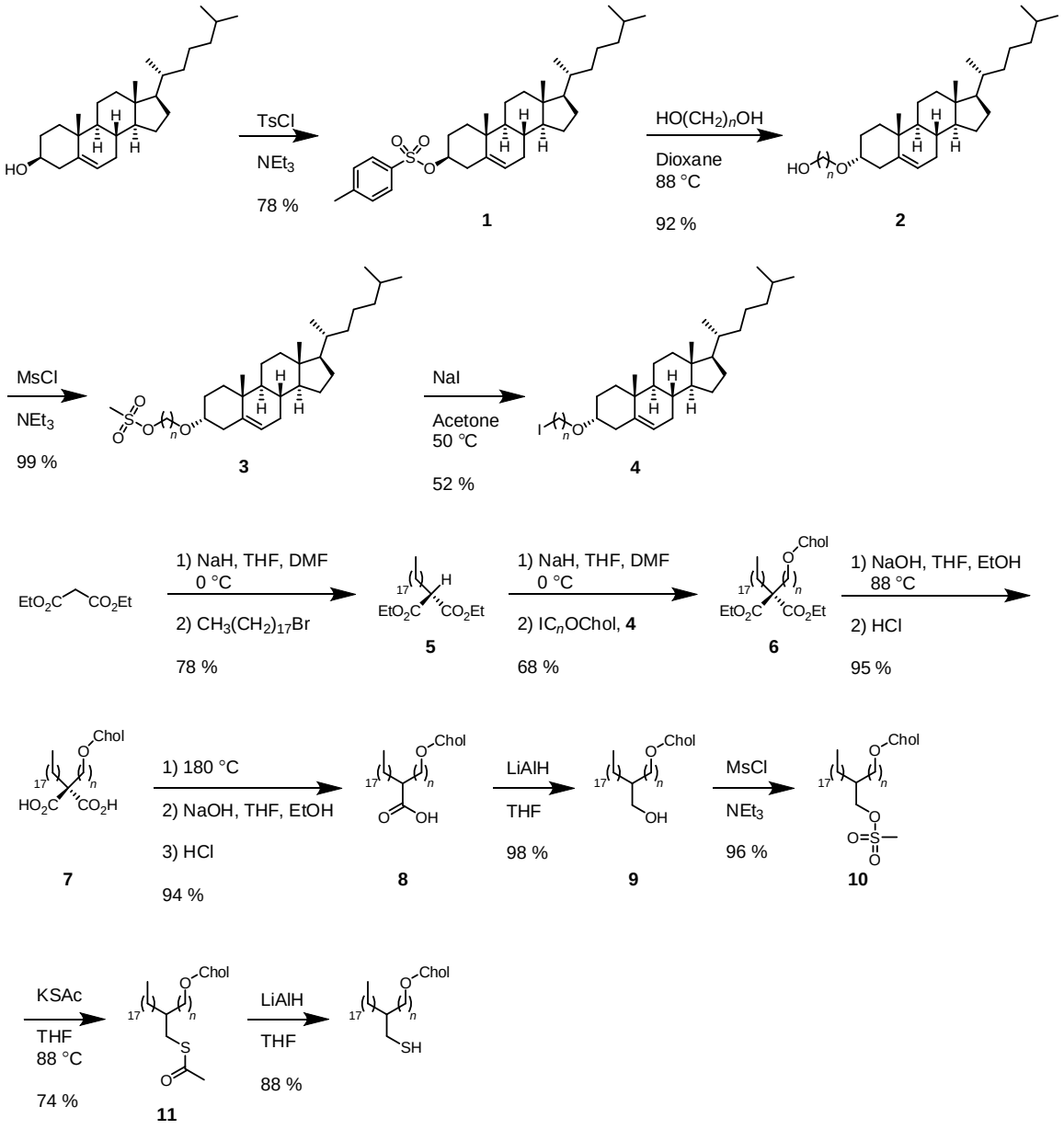

*Cholesterol Tosylate (**1**).* Cholesterol tosylate was synthesized by combining 18.09 g of cholesterol (46.78 mmol) and 37.71 g *p*-toluenesulfonyl chloride (197.8 mmol) in

60.0 mL of triethylamine (430 mmol). After purging with nitrogen, the reaction was allowed to stir overnight at room temperature. TLC confirmed that a reaction occurred. The reaction was worked up by the addition of 150 mL of dichloromethane and 150 mL water. The organic layer was washed with 2 × 100 mL of each of the following solutions: 1N hydrochloric acid, water, and brine. The organic layer was dried with anhydrous sodium sulfate, and the solvent was evaporated under vacuum to yield a yellow liquid. The product was precipitate by the addition of methanol and filtered to collect a white solid. Yield: 19.76 g (36.54 mmol, 78 %). TLC (80 % hexane: 20 % ethyl acetate): R_f = 0.62. Crude ^{1}H NMR (500 MHz, $CDCl_3$): δ 0.61 (s, 3 H), 0.86 – 1.58 (m, 34 H), 1.69 (m, 1 H), 1.81 (m, 3 H), 2.00 (m, 2 H), 2.25 (m, 1 H), 2.43 (m, 4 H), 4.31 (m, 1 H), 5.29 (m, 1 H), 7.32 (d, *J* = 7.90 Hz, 2 H), 7.79 (d, *J* = 8.25 Hz, 2 H).

C*holest-5-en-3β-oxypropan-3-ol* ***(2)***. Cholest-5-en-3β-oxypropan-3-ol was synthesized by combining 1.115 g of tosylate **1** (2.061 mmol) and 5.00 mL of 1,3-propanediol (69.2 mmol) in 24.0 mL of anhydrous dioxane. The reaction was heated to 85 ºC for 4 hours under nitrogen. TLC confirmed that a reaction occurred. The reaction was worked up by the addition of 50 mL of dichloromethane and 50 mL water. The organic layer was washed with 2 × 100 mL of each of the following solutions: water, 1N hydrochloric acid, and brine. The organic layer was dried with anhydrous sodium sulfate, filtered, and the solvent was removed under vacuum to yield a yellow solid. The crude compound was purified by column chromatography (99 % hexane: 1 % ethyl acetate – 70 % hexane: 30 % ethyl acetate) to provide a white solid. Yield: 0.842 g (1.89 mmol, 92 %). TLC (80 % hexane: 20 % ethyl acetate): R_f = 0.20. ^{1}H NMR (500 MHz, $CDCl_3$): δ

0.67 (s, 3 H), 0.85 – 1.58 (m, 35 H), 1.78 – 2.05 (m, 7 H), 2.15 (m, 1 H), 2.37 (m, 1 H), 2.59 (t, *J* = 5.15 Hz, 1 H), 3.17 (m, 1 H), 3.67 (m, 2 H), 3.87 (q, *J* = 5.50 Hz, 2 H), 5.34 (m, 1 H).

C*holest-5-en-3β-oxypropan-3-mesylate (**3**)*. A solution of the alcohol **2** (1.215 g, 2.732 mmol) in triethylamine (6.00 mL, 43.0 mmol) was prepared under nitrogen and allowed to stir for 1 hour. Methanesulfonyl chloride (0.65 mL, 8.4 mmol) was added dropwise over 5 minutes to the stirred mixture. After the addition was completed, stirring was continued for 4 hours at room temperature. The reaction was quenched by the addition of ice-cold water (200 mL). The mixture was extracted with dichloromethane (3 × 100 mL). The organic phase was washed with water (2 × 100 mL) and 2 × 100 mL of each of the following solutions: 1N hydrochloric acid, water, and brine. The organic layer was dried over anhydrous sodium sulfate, filtered, and the solvent was removed under vacuum to yield a yellow solid. The crude product was used directly in the next step without further purification. Yield: 1.42 g (2.72 mmol, 99 %). TLC (80 % hexane: 20 % ethyl acetate): R_f = 0.25. Crude ^{1}H NMR (500 MHz, $CDCl_3$): δ 0.64 (s, 3 H), 0.85 – 1.62 (m, 37 H), 1.80 – 2.02 (m, 7 H), 2.15 (m, 1 H), 2.34 (m, 1 H), 3.00 (s, 3 H), 3.13 (m, 1 H), 3.57 (m, 2 H), 4.34 (t, *J* = 6.19 Hz, 2 H), 5.34 (m, 1 H).

C*holest-5-en-3β-oxypropan-3-iodide (**4**)*. The mesylate **3** (1.416 g, 2.708 mmol) was dissolved in degassed ethanol (24 mL) and added to a reaction flask containing sodium iodide (0.983 g, 8.61 mmol). The reaction mixture was heated to 88 °C for 4 hours under nitrogen. The reaction was worked up by addition of cool water (50 mL) and the mixture extracted with dichloromethane (3 × 100 mL). The organic phases were

combined and washed with water (3 × 100 mL) and brine (1 × 100 mL), dried over anhydrous sodium sulfate, filtered, and the solvent was removed under vacuum to yield a light yellow solid. The crude product was purified by column chromatography (99 % hexane: 1 % ethyl acetate) to give a white solid. Yield: 0.900 g (1.62 mmol, 66 %). TLC (80 % hexane: 20 % ethyl acetate): R_f = 0.79. ^{1}H NMR (500 MHz, $CDCl_3$): δ 0.67 (s, 3 H), 0.84 – 1.60 (m, 37 H), 1.78 – 2.02 (m, 7 H), 2.15 (m, 1 H), 2.37 (m, 4 H), 2.96 (t, *J* = 6.87 Hz, 2 H), 3.17 (m, 1 H), 3.51 (m, 2 H), 5.34 (m, 1 H).

Diethyl 2-octadecylmalonate (**5**). A solution of sodium hydride (5.246 g, 131.1 mmol; 60 % dispersion in mineral oil) in tetrahydrofuran (50 mL) and N,N-dimethylformamide (24 mL) was prepared at 0 °C under an atmosphere of nitrogen. To this stirred solution maintained at 0 °C, diethyl malonate (18.50 mL, 121.9 mmol) was added slowly. Stirring was continued for 15 minutes at room temperature, and then bromooctadecane (20.09 g, 60.25 mmol) was added. The reaction mixture was stirred at room temperature overnight and then concentrated under reduced pressure. The resultant oil was suspended in water (100 mL), and extracted with ethyl acetate (2 × 150 mL). The organic layer was washed with water (2 × 100 mL) and brine (1 × 100 mL). The organic layer was dried over anhydrous sodium sulfate, filtered, and concentrated under reduced pressure to provide brown oil. The crude compound was purified by column chromatography (95 % hexane: 5 % ethyl acetate) to give a white solid. Yield: 39.37 g (95.41 mmol, 78 %). TLC (80 % hexane: 20 % ethyl acetate): R_f = 0.74. ^{1}H NMR (500 MHz, $CDCl_3$): δ 0.88 (t, *J* = 6.87 Hz, 3 H), 1.22 – 1.32 (m, 40 H), 1.88 (m, 2 H), 3.31 (t, *J* = 7.56 Hz, 1 H), 4.19 (m, 4 H).

Diethyl 2-(cholest-5-en-3β-oxypropane)-2-octadecylmalonate (**6**). A solution of sodium hydride (0.790 g, 19.8 mmol) in tetrahydrofuran (16 mL) and N,N-dimethylformamide (2 mL) was prepared at 0 °C under an atmosphere of nitrogen. To this solution, diester **5** (5.035 g, 12.20 mmol) was added slowly. The mixture was allowed to stir at room temperature for 15 minutes, and then iodide **4** (6.796 g, 12.25 mmol) was transferred into the mixture via syringe. The reaction mixture was allowed to stir at room temperature overnight and then concentrated under vacuum. The resultant oil was suspended in water (100 mL), and extracted with ethyl acetate (2 × 100 mL). The organic layer was washed with water (2 × 50 mL) and brine (1 × 100 mL), dried over anhydrous sodium sulfate, filtered, and concentrated under reduced pressure. The yellow oil was purified by column chromatography (95 % hexane: 5 % dichloromethane) to give a colorless oil. Yield: 6.98 g (8.32 mmol, 68 %). TLC (80 % hexane: 20 % ethyl acetate): $R_f = 0.77$. ^{1}H NMR (500 MHz, $CDCl_3$): δ 0.63 (s, 3 H), 0.78 – 1.70 (m, 84 H), 1.75 – 2.01 (m, 10 H), 2.12 (m, 1 H), 2.29 (m, 1 H), 3.07 (m, 1 H), 3.39 (t, J = 6.30 Hz, 2 H), 4.13 (q, J = 6.87 Hz, 4 H), 5.27 (m, 1 H).

2-(Cholest-5-en-3β-oxypropane)-2-octadecylmalonic acid (**7**). Malonate **6** (6.984 g, 8.321 mmol) and sodium hydroxide (7.545 g, 188.6 mmol) were dissolved in ethanol (100 mL) with dry tetrahydrofuran (15 mL). After purging with nitrogen, the reaction mixture was refluxed for 12 hours at 88 °C. The reaction mixture was then cooled in an ice bath and concentrated hydrochloric acid was added until the mixture was acidic. The product was extracted into ethyl acetate (3 × 50 mL), washed with water (2 × 50 mL) and once with brine (50 mL). The organic phase was dried over anhydrous sodium sulfate,

filtered, and the solvent was evaporated under vacuum to yield a white solid. The crude product was used directly in the next step without any purification. Yield: 6.17 g (7.88 mmol, 95 %). TLC (80 % hexane: 20 % ethyl acetate): R_f = 0.05. Crude ^{1}H NMR (500 MHz, $CDCl_3$): δ 0.66 (s, 3 H), 0.80 – 1.73 (m, 72 H), 1.77 – 2.07 (m, 9 H), 2.22 (m, 1 H), 2.36 (m, 1 H), 3.30 (m, 1 H), 3.62 (t, *J* = 5.73 Hz, 2 H), 5.34 (m, 1 H).

2-(C*holest-5-en-3β-oxypropane)-2-eicosanoic acid* (**8**). Crude malonic acid **7** (6.171 g, 7.879 mmol) was placed in a flask fitted with a reflux condenser and purged with argon for 10 minutes. The starting material was then heated to 180 °C until gasses were no longer evolving through an oil bubbler. The flask was then cooled to room temperature, and sodium hydroxide (5.617 g, 140.4 mmol) along with tetrahydrofuran (11 mL) and ethanol (100 mL) were added to the flask. The mixture was refluxed for 12 hours at 88 °C. The mixture was then cooled to room temperature, and concentrated hydrochloric acid was added until the mixture was acidic. The product was extracted into ethyl acetate (3 × 50 mL), washed with water (2 × 50 mL) and once with brine (50 mL). The organic phase was dried over anhydrous sodium sulfate, filtered, and the solvent was evaporated under vacuum to yield a yellow solid. The crude compound was purified by column chromatography (90 % hexane: 10 % ethyl acetate – 60 % hexane: 40 % ethyl acetate) to provide a white solid. Yield: 5.45 g (7.37 mmol, 94 %). TLC (80 % hexane: 20 % ethyl acetate): R_f = 0.48. ^{1}H NMR (500 MHz, $CDCl_3$): δ 0.66 (s, 3 H), 0.80 – 1.73 (m, 76 H), 1.76 – 2.05 (m, 5 H), 2.17 (m, 1 H), 2.33 (m, 1 H), 3.11 (m, 1 H), 3.45 (t, *J* = 4.58 Hz, 2 H), 5.31 (m, 1 H).

2-(C*holest-5-en-3β-oxypropane)-2-eicosan-1-ol* (**9**). The carboxylic acid **8** (4.541 g, 6.143 mmol) was dissolved in degassed tetrahydrofuran (30 mL) was added into a slurry of lithium aluminum hydride (6.128 g, 153.4 mmol) in degassed tetrahydrofuran (50 mL) slowly at 0 ºC. The reaction mixture was allowed to stir for 8 hours at room temperature under an atmosphere of nitrogen and then quenched with degassed water (20 mL). The mixture was acidified to pH ~1 by careful addition of 6.0 M sulfuric acid solution (previously degassed), and then extracted with dichloromethane (3 × 100 mL). The organic layers were combined and washed with a dilute hydrochloric acid solution (1 × 100 mL) and brine (1 × 100 mL). The organic phase was dried over anhydrous sodium sulfate, filtered, and the solvent evaporated under vacuum to yield a light yellow solid. The crude compound was used directly in the next step without further purification. Yield: 4.36 g (6.01 mmol, 98 %). TLC (80 % hexane: 20 % ethyl acetate): R_f = 0.46. Crude ^{1}H NMR (500 MHz, $CDCl_3$): δ 0.66 (s, 3 H), 0.80 – 1.75 (m, 76 H), 1.76 – 2.06 (m, 5 H), 2.17 (m, 1 H), 2.35 (m, 1 H), 3.13 (m, 1 H), 3.45 (m, 2 H) , 3.55 (ABX, *J* = 10.88, 5.15 Hz, 2 H), 5.33 (m, 1 H).

2-(C*holest-5-en-3β-oxypropane)-2-eicosan-1-mesylate* (**10**). Alcohol **9** (4.357 g, 6.008 mmol) was dissolved in triethylamine (60.0 mL, 430 mmol) and allowed to stir for 1 hour under nitrogen. Methanesulfonyl chloride (1.40 mL, 18.1 mmol) was added dropwise over 5 minutes to the stirred mixture and the reaction was allowed to stir for 6 hours at room temperature. The reaction was worked up by the addition of ice-cold water (200 mL). The mixture was extracted with dichloromethane (2 × 100 mL). The organic layer was washed with 2 × 100 mL of each of the following solutions: water, 1N

hydrochloric acid, and brine. The organic layer was dried over anhydrous sodium sulfate, and the solvent was evaporated under vacuum to yield a yellow solid. The crude product was used directly in the next step without any purification. Yield: 4.65 g (5.79 mmol, 96 %). TLC (80 % hexane: 20 % ethyl acetate): R_f = 0.50. Crude ^{1}H NMR (500 MHz, $CDCl_3$): δ 0.66 (s, 3 H), 0.78 – 1.61 (m, 83 H), 1.65 – 2.03 (m, 9 H), 2.16 (m, 1 H), 2.33 (m, 1 H), 2.99 (s, 3 H), 3.12 (m, 2 H), 3.44 (m, 2 H), 4.13 (ABX, *J* = 9.74, 5.73 Hz, 2 H), 5.33 (m, 1 H).

2-(Cholest-5-en-3β-oxypropane)-2-eicosan-1-thioacetate (**11**). The mesylate **10** (4.653 g, 5.792 mmol) was dissolved in degassed ethanol (100 mL) and added to a reaction flask containing potassium thioacetate (2.005 g, 17.56 mmol). The reaction mixture was heated to 88 °C for 4 hours under nitrogen. The reaction was worked up by addition of cool water (50 mL) and the mixture extracted with dichloromethane (2 × 100 mL). The organic phases were combined and washed with water (3 × 100 mL) and brine (1 × 100 mL), dried over anhydrous sodium sulfate, filtered, and the solvent evaporated under vacuum to yield an orange solid. The crude product was purified by column chromatography (90 % hexane: 10 % dichloromethane) to give a white solid. Yield: 3.44 g (4.30 mmol, 74 %). TLC (80 % hexane: 20 % ethyl acetate): R_f = 0.85. ^{1}H NMR (500 MHz, $CDCl_3$): δ 0.67 (s, 3 H), 0.79 – 1.75 (m, 79 H), 1.77 – 2.04 (m, 5 H), 2.17 (m, 1 H), 2.28 – 2.37 (m, 4 H), 2.90 (ABX, *J* = 13.75, 6.30 Hz, 2 H), 3.12 (m, 1 H), 3.43 (m, 2 H), 5.33 (m, 1 H).

2-(C*holest-5-en-3β-oxypropane)-2-eicosan-1-thiol* (**C18C3CholSH).** The thioacetate **11** (3.437 g, 4.300 mmol) was dissolved in degassed tetrahydrofuran (30 mL)

was added into a slurry of lithium aluminum hydride (2.712 g, 67.88 mmol) in degassed tetrahydrofuran (70 mL) slowly at 0 ºC. The reaction mixture was allowed to stir for 8 hours at room temperature under an atmosphere of nitrogen and then quenched with degassed water (50 mL). The mixture was acidified to pH ~1 by careful addition of 1.0 M sulfuric acid solution (previously degassed), and then extracted with dichloromethane (2 × 100 mL). The organic layers were combined and washed with a dilute hydrochloric acid solution (1 × 100 mL) and brine (1 × 100 mL). The organic phase was dried over anhydrous sodium sulfate, filtered, and the solvent evaporated under vacuum to yield a yellow solid. The crude compound was purified by column chromatography (90 % hexane: 10 % dichloromethane), affording a white solid. Yield: 2.82 g (3.80 mmol, 88 %). TLC (80 % hexane: 20 % ethyl acetate): R_f = 0.90. ^{1}H NMR (500 MHz, $CDCl_3$): δ 0.67 (s, 3 H), 0.79 – 1.74 (m, 78 H), 1.78 – 2.04 (m, 5 H), 2.18 (m, 1 H), 2.36 (m, 1 H), 2.54 (dd, *J* = 5.73 Hz, 2 H), 3.12 (m, 1 H), 3.43 (m, 2 H), 5.34 (m, 1 H). ^{13}C NMR (500 MHz, $CDCl_3$): δ 11.96, 14.28, 18.84, 19.47, 21.19, 22.70, 22.84, 22.95, 24.00, 24.40, 26.73, 27.33, 28.11, 28.36, 28.51, 28.59, 28.75, 29.55, 29.81, 29.84, 29.86, 29.88, 29.90, 30.05, 31.98, 32.05, 32.08, 32.35, 35.93, 36.32, 36.96, 37.41, 39.32, 39.63, 39.90, 40.00, 42.39, 50.30, 56.29, 56.87, 68.24, 79.10, 121.51, 141.01.

2-(C*holest-5-en-3β-oxyhexane)-2-eicosan-1-thiol* (**C18C6CholSH**). Yield: 2.71 g (3.46 mmol, 85 %). TLC (80 % hexane: 20 % ethyl acetate): R_f = 0.87. ^{1}H NMR (500 MHz, $CDCl_3$): δ 0.67 (s, 3 H), 0.78 – 1.67 (m, 84 H), 1.76 – 2.03 (m, 5 H), 2.18 (m, 1 H), 2.35 (m, 1 H), 2.52 (dd, *J* = 5.73 Hz, 2 H), 3.12 (m, 1 H), 3.44 (m, 2 H), 5.34 (m, 1 H). ^{13}C NMR (500 MHz, $CDCl_3$): δ 11.96, 14.28, 18.84, 19.47, 21.19, 22.70, 22.84, 22.95,

24.00, 24.40, 26.34, 26.66, 26.75, 28.11, 28.36, 28.56, 28.59, 29.55, 29.82, 29.84, 29.86, 29.90, 30.10, 30.34, 31.98, 32.05, 32.09, 32.35, 32.41, 35.93, 36.32, 36.96, 37.42, 39.34, 39.63, 39.91, 40.12, 42.39, 50.31, 56.29, 56.87, 68.14, 79.04, 121.46, 141.09.

2-(C*holest-5-en-3β-oxynonane)-2-eicosan-1-thiol* (**C18C9CholSH**). Yield: 1.46 g (1.77 mmol, 75 %). TLC (80 % hexane: 20 % ethyl acetate): R_f = 0.86. ^{1}H NMR (500 MHz, $CDCl_3$): δ 0.67 (s, 3 H), 0.78 – 1.67 (m, 94 H), 1.76 – 2.03 (m, 5 H), 2.17 (m, 1 H), 2.35 (m, 1 H), 2.53 (dd, *J* = 5.73 Hz, 2 H), 3.12 (m, 1 H), 3.44 (m, 2 H), 5.34 (m, 1 H). ^{13}C NMR (500 MHz, $CDCl_3$): δ 11.96, 14.28, 18.84, 19.47, 21.19, 22.70, 22.84, 22.95, 24.01, 24.40, 26.37, 26.73, 26.76, 28.11, 28.37, 28.56, 28.59, 29.55,29.66, 29.72, 29.74, 29.82, 29.85, 29.87, 29.90, 30.11, 30.37, 31.98, 32.05, 32.09, 32.43, 35.94, 36.32, 36.96, 37.43, 39.34, 39.64, 39.91, 40.15, 42.39, 50.31, 56.30, 56.87, 68.20, 79.04, 121.44, 141.09.

3.2.4. Preparation of SAMs

The gold substrates were prepared under a vacuum at ~1×10^{-5} Torr. A thin layer (100 Å) of nickel-chromium (80 % nickel: 20 % chromium) was first evaporated onto polished Si(100) wafers to assist the adhesion of gold on silicon, followed by the evaporation of 1000 Å of gold. Absolute ethanol was used to rinse the resultant gold-coated wafers, followed by drying under a stream of ultra-pure nitrogen before use. The freshly prepared gold-coated wafers were cut into slides (1 × 3 cm), and then the slides were cleaned by rinsing with absolute ethanol and dried with ultra-pure nitrogen. The

slides then were immersed in the following thiol solutions; **C18SH** (1 mM in ethanol), **CholSH** (1 mM in ethanol), **C18C3CholSH** (1 mM in ethanol), **C18C6CholSH** (1 mM in ethanol), and **C18C9CholSH** (1 mM in ethanol). The glass vials containing the thiol solutions were previously cleaned with piranha solution (3:1 mixture of H_2SO_4/H_2O_2) and rinsed thoroughly with deionized water and absolute ethanol. (*Caution: Piranha solution is highly corrosive and should be handled with extreme care*.) All substrates were allowed to equilibrate at room temperature for a period of 48 hours. Then the slides were rinsed with tetrahydrofuran and ethanol, and blown dry with ultra-pure nitrogen before characterization.

3.2.5. Characterization of SAMs

Ellipsometric Thickness Measurements. The thicknesses of the films were measured using a Rudolph Research Auto EL III ellipsometer equipped with a He-Ne laser (632.8 nm) at an angle of incidence of 70°. To measure the thickness, a refractive index of 1.45 is used for all SAMs in this study. For each sample, the data were averaged over the collection from two separate slides with three spots per slide. The measured thicknesses were always within ± 1 Å of the reported values.

Contact Angle Measurements. A Ramé-Hart model 100 contact angle goniometer was employed to measure the contact angle of the SAMs. The contacting liquids, water (W) and hexadecane (HD), were dispensed (advancing angle, θ_a) and

withdrawn (receding angle, θ_r) on the surfaces of SAMs using a Matrix Technologies micro-Electrapette 25 at the slowest possible speed (1 μL/s). The measurements were performed at room temperature with the pipet tip in contact with the drop. Reported values for each sample were the averages of measurements taken from two separate slides with three drops per slide using both drop edges and were always within ± 2°.

Polarization Modulation Infrared Reflection Absorption Spectroscopy (PM-IRRAS). Surface IR spectra were collected using a Nicolet Nexus 670 Fourier transform spectrometer equipped with a liquid nitrogen-cooled mercury-cadmium-telluride (MCT) detector and a Hinds Instrument PEM-90 photoelastic modulator. The *p*-polarized light was reflected from the sample at an angle of incidence of 80° to the surface normal. The spectra were collected at 512 scans for the C-H stretching region (2750 – 3100 cm^{-1}) with a spectral resolution of 4 cm^{-1}.

X-ray Photoelectron Spectroscopy (XPS). A PHI 5700 X-ray photoelectron spectrometer equipped with a monochromatic Al Kα X-ray source (hν = 1486.7 eV) incident at 90° relative to axis of a hemispherical energy analyzer was employed to obtain XPS spectra of the SAMs at a photoelectron takeoff angle of 45° from the surface and a pass energy of 23.5 eV. The binding energy scales were referenced to the $Au_{4f7/2}$ peak at 84.0 eV.

3.3. Results and Discussion

The new SAMs generated from the targeted cholesterol-based thiols were characterized. Here, we chose to use ethanol as the equilibrating solvent to generate SAMs due to the ease of dissolving the adsorbates and to ethanol's use in the majority of SAM studies. SAMs generated from normal alkanethiol and thiocholesterol were used as references in order to compare the data collected from this new series of SAMs to previously published materials. We assume that SAMs derived from the double tailgroup series **C18CnCholSH** where n = 3, 6, and 9 will produce data similar to that of SAMs generated from **CholSH** and **C18SH**. This assumption permits a direct comparison of the SAMs in this system in which the double tailgroup molecules contain one alkyl chain and one cholesterol-containing chain.

3.3.1. Thicknesses of the Films

The thicknesses were measured by ellipsometry after 48 hours to allow for full equilibration as the molecules are bulky and hindered by two chiral centers, the stereochemistry of the cholesterol moiety, and the potential for phase separation based on the two tailgroups. As seen in Figure 3.3, the thicknesses of SAMs generated from **C18SH** and **CholSH** are comparable to literature values and the thicknesses of the new double tailgroup series SAMs increase as the hydrocarbon linker increases.[19,57,63] The thickness of the SAM generated from **C18C3CholSH** is more than the SAM generate

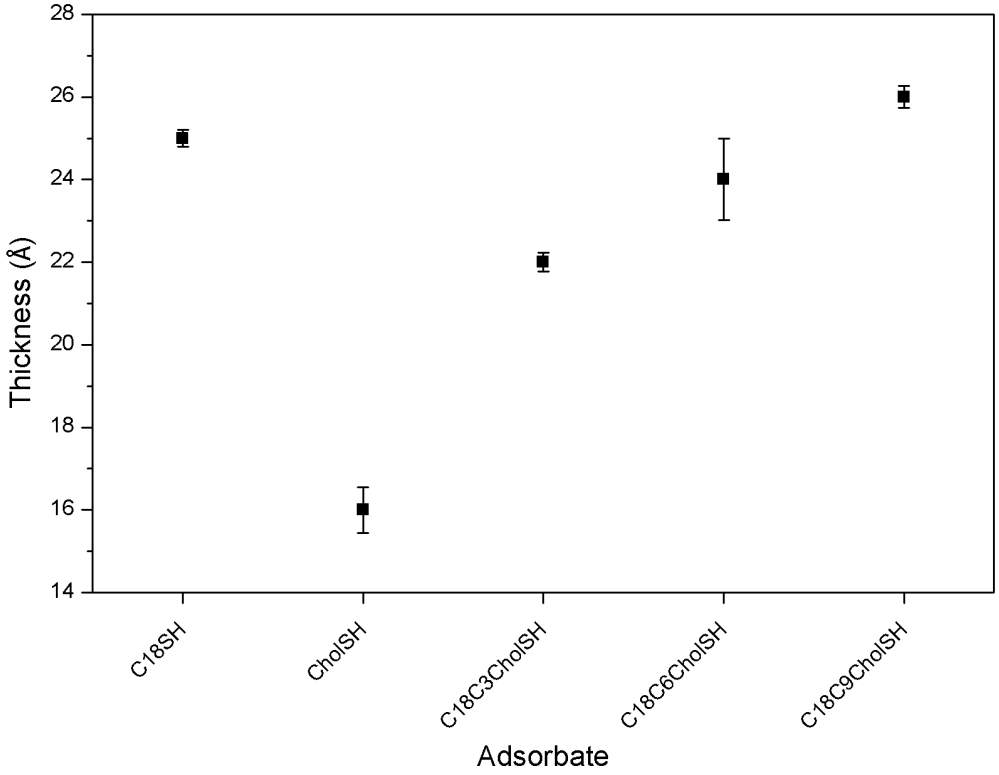

Figure 3.3. The thicknesses for SAMs generated from each adsorbate measured at 48 hours equilibration time.

CholSH, as expected, due to the added hydrocarbon chain linker of the cholesterol-based tailgroup. The differences in the thicknesses of the SAMs generated from **C18C3CholSH**, **C18C6CholSH**, and **C18C9CholSH** are consistent with a ~ 4 Å increase in thickness which correlates with an increase of 3 methylene units, consistent with literature values for a normal alkanethiolate SAM having an average increase in thickness of 1.2 Å per methylene unit.[19] It is worth noting that the thicknesses of the SAMs generated from **C18C3CholSH**, **C18C6CholSH**, and **C18C9CholSH** are

comparable, and within the experimental error of the instrument, with the thicknesses of corresponding SAMs formed from single tailgroup, cholesterol-based thiols (data not shown, refer to Chapter 2, Section 2.3.1.). For the data in the paper by Zhang *et al.*, their double tailgroup SAMs are approximately the same thickness as the average of the thickness of SAMs formed from the corresponding single tailgroup molecules, however, the current data fail to meet this expectation.[57]

3.3.2. Wettabilities of the Films

The advancing (θ_a, °) and receding (θ_r, °) contact angle measurements serve as a sensitive probe for the surface interface of the SAM, providing detail about the composition, orientation, and packing of the film.[10] The contact angle hysteresis ($\Delta\theta = \theta_a - \theta_r$) provides information about the roughness of the surface interface.[18] Low values of hysteresis generally correlate to a homogeneous, smooth surface while high values relate to a heterogeneous and/or rough surface. For this wettability study, water and hexadecane were used as probe liquids. Both hydrocarbons and cholesterol are known to be hydrophobic and lipophilic and the data in Table 3.1 support these expectations for this series of SAMs generated from double tailgroup molecules. The advancing contact angles for SAMs developed from **C18SH** and **CholSH** are consistent with previously published work.[64,65] The hysteresis values for SAMs generated from **C18SH** and **CholSH** are also comparable to previously published values.[20,64,65] Normal alkanethiols are well known for their ability to create a well-packed, dense monolayer while

cholesterol is known to create a rough surface as expected from this moiety's rigid structure and the dissimilarities of the α-face and β-face.

The advancing contact angles for the double tailgroup series of SAMs are consistent with the data for single tailgroup cholesterol-based SAMs with the exception of the SAM generated from **C18C3CholSH**. The SAM formed from the single tailgroup molecule with a hydrocarbon spacer of 3 methylene units, Cholest-5-en-3β-oxypropan-3-thiol, has advancing/receding contact angles of 108/88 and 18/0 for water and hexadecane, respectively (Chapter 2, Section 2.3.2.). The SAM generated from **C18C3CholSH** has a higher than expected advancing contact angle for water, when comparing it to the SAM formed from the single tailgroup molecule, and an advancing contact angle for hexadecane between that of the two single-component SAMs developed from a normal alkanethiol and the cholesterol-based single tailgroup molecule. This result for hexadecane is consistent with an interface uniformly composed of a mixture of the two components.[57] It is also worth noting that the SAM generated from **C18C3CholSH** has a receding contact angle for hexadecane of 18 when most of the cholesterol-based SAMs associated with this research project do not exhibit a receding contact angle. Having a hysteresis of 15, the SAM generated from **C18C3CholSH** has a similar surface interface as the SAM formed from **CholSH**, yet both SAMs have a surface interface that is rougher than the SAM formed from **C18SH**. The SAMs formed from **C18C6CholSH** and **C18C9CholSH** did not produce a receding contact angle for hexadecane. Such a strong interaction with the surface of these films indicates either an

increased presence of cholesterol on the surface interface and/or larger defects in which hexadecane can intercalate.

Table 3.1. Advancing Contact Angles (θ_a, °) and Receding Contact Angles (θ_r, °) Measured on SAMs Generated from **C18SH**, **CholSH**, **C18C3CholSH**, **C18C6CholSH**, and **C18C9CholSH**, with Values of Hysteresis ($\Delta\theta = \theta_a - \theta_r$).

Adsorbate	**Probe Liquid** [a]					
	W			**HD**		
	θ_a	θ_r	$\Delta\theta$	θ_a	θ_r	$\Delta\theta$
C18SH	116	106	10	50	40	10
CholSH	108	92	16	16	0	16
C18C3CholSH	122	92	30	33	18	15
C18C6CholSH	117	92	25	23	0	- [b]
C18C9CholSH	117	92	25	20	0	- [b]

[a] Probe liquids used in this experiment are W = water and HD = hexadecane.

[b] When a receding contact angle could not be obtained, the hysteresis value could not be calculated.

3.3.3. PM-IRRAS Studies

The infrared-reflectance spectra for this series of SAMs on gold for the C–H stretching region are shown in Figure 3.4. The position for specific C–H stretching peaks

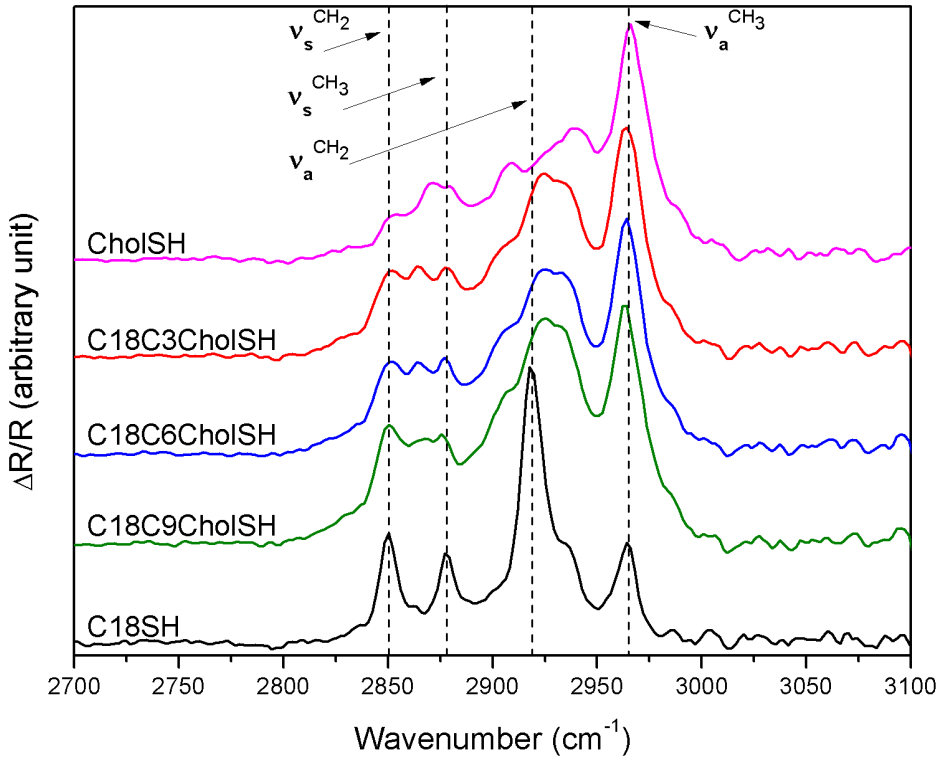

Figure 3.4. PM-IRRAS spectra for the C–H stretching region for SAMs generated by the adsorption of **CholSH**, **C18C3CholSH**, **C18C6CholSH**, and **C18C9CholSH** onto evaporated gold substrates. The PM-IRRAS spectra for a SAM generated from **C18SH** is shown at the bottom for purposes of comparison. The dashed vertical lines provide the positions of four key C–H stretches, are provided as a guide for the eye and assigned according to their respective position for the SAM generated from **C18SH**.

in the IR spectrum is known to be a sensitive indicator of the conformational order of the alkyl chains and the environment of the chains.[66] The degree of conformational order can be determined from the shift in frequency of the antisymmetric methylene peak as it has been determined for crystalline polyethylene to be located at 2919 cm^{-1} and at 2928 cm^{-1} for liquid polyethylene.[19,66] Due to the surface selection rule, the transition dipole moment for a bond must contain a measurable component that is perpendicular to the surface in order to be detected and the more perpendicular the vibration, the stronger the intensity of the detected signal. The quantity of the bonds involved in the motion also affects the strength of the signal in that as more perpendicular vibrations are detected (*e.g.*, an increase in methylene units), the peak will have a stronger intensity.

The peak assignments for the PM-IRRAS spectra are provided in Table 3.2. For SAMs generated from **CholSH**, the strongest band is the antisymmetric methyl vibration located at 2963 cm^{-1}. Such an intense signal indicates that the orientation of the C–H antisymmetric vibration has a transition dipole more perpendicular to the surface and that the associated bonds are present in sufficient number to produce a large signal. For SAMs generated from **C18SH**, the strongest band is the antisymmetric methylene stretch which orients the transition dipole of the C–H bond nearly perpendicular to the surface. For this series of SAMs, the PM-IRRAS spectra resemble a mixture of cholesterol and alkyl chains. There is an increase in the intensity of the symmetric and antisymmetric methylene stretches for the SAMs generated from double tailgroup molecules as compared to SAMs generated from **CholSH**.

Table 3.2. Peak Assignments for the PM-IRRA Spectra of SAMs Generated from **CholSH**, **C18C3CholSH**, **C18C6CholSH**, **C18C9CholSH**, and **C18SH**.

Adsorbates	**Peak Assignments**				
	$\nu_a^{CH_3}$	$\nu_a^{CH_2}$ [a]	$\nu_a^{CH_2}$ [b]	$\nu_s^{CH_3}$	$\nu_s^{CH_2}$
CholSH	2962	-	2935	2868, 2875	2850
C18C3CholSH	2964	2926	2930	2864, 2877	2852
C18C6CholSH	2964	2926	2933	2864, 2877	2852
C18C9CholSH	2963	2926	2932	2868, 2875	2851
C18SH	2964	2918	-	2878	2850

[a] Associated with the alkyl tailgroup

[b] Associated with the cholesterol-based tailgroup

For the SAMs generated from **C18C3CholSH**, **C18C6CholSH**, and **C18C9CholSH**, the $\nu_a^{CH_2}$ band exhibits a broad increase and reduces the cholesterol peak to a shoulder. The shift of the peak position of the most intense $\nu_a^{CH_2}$ stretch for these SAMs is indicative of the added hydrocarbon tailgroup. The $\nu_a^{CH_2}$ stretch produced from the added alkyl tailgroup is located at 2926 cm^{-1} thus a SAM formed from these double tailgroup molecules is less crystalline than the SAM generated from **C18SH,** indicative of the alkyl tailgroup of the double-chain molecules being less conformationaly ordered than the alkyl chains from a SAM generated from **C18SH**. The shoulder of the $\nu_a^{CH_2}$ peak is a result of an overlap of the antisymmetric methylene stretch from the cholesterol-

region of the molecule that is less intense than the cumulative antisymmetric stretches from the alkyl chain. The change in intensity of the $\nu_a^{CH_2}$ signal, from the added alkyl tailgroup of the molecules and the cholesterol region of the molecules, to the $\nu_a^{CH_3}$ peak shows a change in the quantity of the methylene groups as n increases and with the added alkyl chain tailgroup as compared to SAMs generated from **CholSH**. A comparison of the antisymmetric methylene stretches for the SAMs generated from these double tailgroup molecules and the related single tailgroup molecules is unachievable due to the overlap of the signal from the added alkyl tailgroup of the double tailgroup molecules.

3.3.4. XPS Studies

The C_{1s}, O_{1s}, and S_{2p} XPS spectra for this series of double tailgroup SAMs are shown in Figure 3.5. These peaks in the XPS spectra confirm the presence of intact cholesterol-based thiolates on a gold surface. The binding energy of an electron in XPS is a function of the environment and the type of atom from which the electron is ejected.[67] The C_{1s} binding energy has been reported to shift to a lower value as the packing density decreases, appearing at 285.0 eV for a SAM generated from normal alkanethiols.[20,68] Additionally, the relative intensity of the C_{1s} binding energy peaks for a series of normal alkanethiolate SAMs has been used as a means of determining the relative thickness of a SAM of similarly structured adsorbates.[20,68] Therefore the binding energy of the C_{1s} peak can be used as a measure of the thickness and packing density of the SAM. Figure 3.5 (A) shows the shift in the C_{1s} peak where the SAM formed from

CholSH has a lower value, 284.6 eV, as indicated by the dashed line in Figure 3.5 (A), than the SAMs generated from the double tailgroup molecules. The C_{1s} peak is located at 284.9 eV for all three double tailgroup SAMs, indicating an increase in packing density for these monolayers over the **CholSH** SAM. The shift in the C_{1s} peak might also be explained by the structural differences between the single-component SAMs formed from extended alkyl chain and a single-component SAM formed from the cholesterol moiety. However, it is worth noting that the C_{1s} bands for the SAMs generated from **C18C3CholSH**, **C18C6CholSH**, and **C18C9CholSH** are the same, do not exhibit any broadening or skewing towards the **CholSH** peak position, and are only slightly lower in energy than the C_{1s} peak for the SAM generated form **C18SH**.

The increase in the signal-to-noise ratio for the O_{1s} spectra, Figure 3.5 (B), as compared to the C_{1s} spectra, is as expected since the oxygen atom is buried in the film and the signal is attenuated by the hydrocarbon structure above the oxygen atom. The absence of a measurable oxygen signal in the SAM formed from **CholSH** indicates the effectiveness of the ultra high vacuum conditions at removing residual ethanol from the cholesterol-containing monolayer film, however the integration of the area under the oxygen peak cannot be used for comparison purposes due to the potential for oxygen contamination. While the SAM formed from **C18SH** and **CholSH** do not have an oxygen signal, it is possible that the SAMs generated from the cholesterol-based molecules have some unknown amount of oxygen from trapped solvent or residual atmospheric molecules in the vacuum chamber.

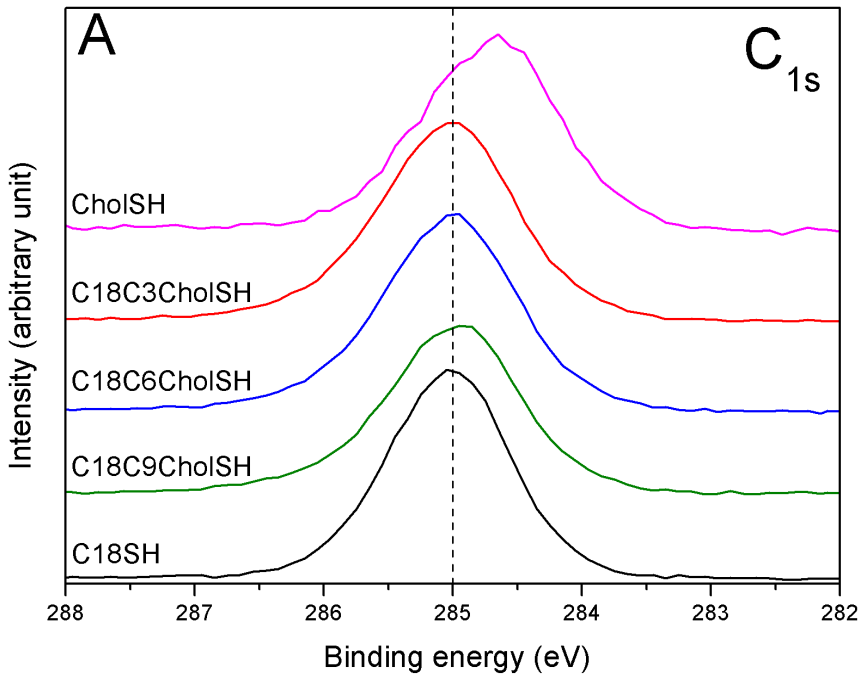
A
C1s
CholSH
C18C3CholSH
C18C6CholSH
C18C9CholSH
C18SH
Intensity (arbitrary unit)
288
287
286
285
284
283
282
Binding energy (eV)

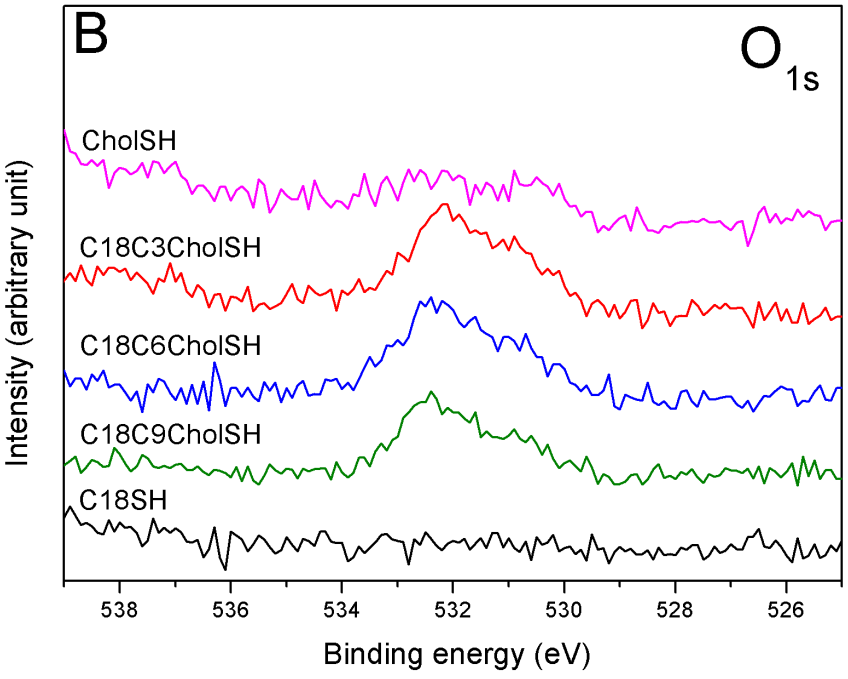
B
O1s
CholSH
C18C3CholSH
C18C6CholSH
C18C9CholSH
C18SH
Intensity (arbitrary unit)
538
536
534
532
530
528
526
Binding energy (eV)

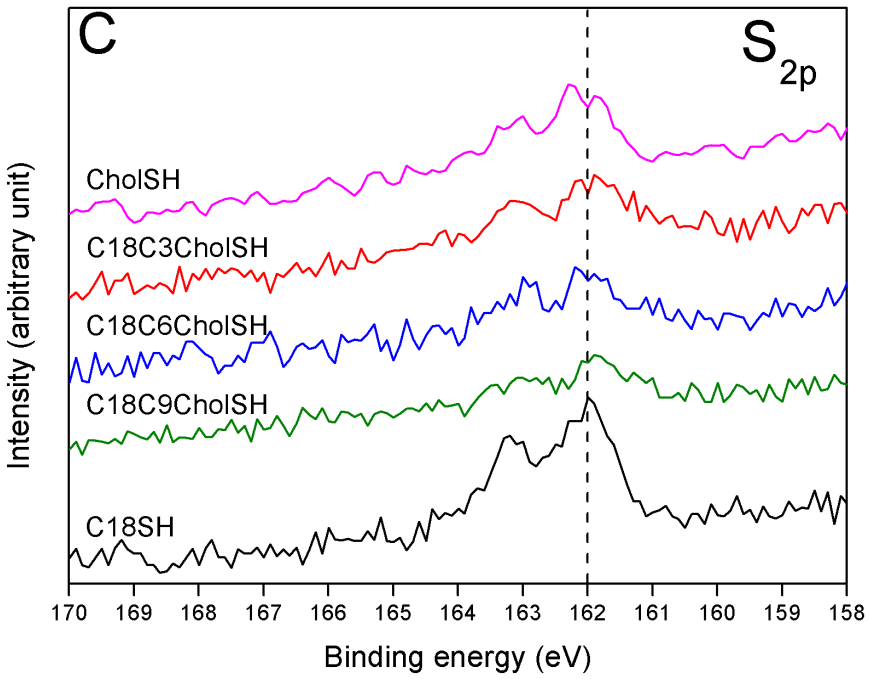

Figure 3.5. The XPS spectra of (A) C_{1s}, (B) O_{1s}, and (C) S_{2p} regions for the series of cholesterol-based SAMs, along with that formed from **C18SH**. The dashed line in the spectra for the C_{1s} and S_{2p} regions are aligned with the peak position for the SAM generated from **C18SH** and are intended to serve as a guide for the eye.

The increase in the signal-to-noise ratio in the S_{2p} spectra is expected for these films owing to the attenuation of signal associated with the distance of the element from the surface of the film. The doublet signal located at 162.0 eV ($S_{2p3/2}$) is indicative of bound sulfur on the gold substrate as compared to unbound thiol, which is found at 164 eV and oxidized sulfur at 166 to 168 eV.[69,70] Therefore, only one species of sulfur is present for this series of films. The weak S_{2p} signal, has a signal-to-noise ratio that is not optimum despite best efforts to attain a better ratio, yet still provides discernible peaks from which integrated peak data has been obtained.

Comparison of the relative intensities of the individual elemental signals in the form of ratios with gold, such as the ratio of carbon-to-gold (C:Au ratio), is a method of determining relative packing density for a series of films. The C:Au ratio for this series is shown in Figure 3.6 (A). For SAMs generated from double tailgroup molecules, the C_{1s} signal should slightly increase as n increases given there are more carbons present in the monolayer to produce a stronger signal. The gold signal is only minimally impacted by the overlaying monolayer, but is subject to variation related to changes in the intensity of the X-ray beam. And the carbon signal not only responds to changes in beam intensity by also increases as n increases, so a comparison of the ratio of carbon-to-gold, normalized to the SAM generated from **C18C3CholSH**, should provide comparative information about this series of cholesterol-based SAMs. In agreement with the ellipsometric data, the ratio increases as n increases.

The assessment of the relative intensities of the sulfur-to-gold signals (S:Au ratio) for the SAMs generated from double tailgroup molecules is shown in Figure 3.6 (B). The comparison of the S_{2p} and Au_{4f} signals provides insight into the relative packing density of the monolayers. The sulfur-to-gold ratios have been normalized to the SAM with the shortest molecule, the SAM generated from **C18C3CholSH** for purposes of comparison. The decrease in the S:Au ratio is a consequence of the increase in the attenuation of the S_{2p} signal as n increases.

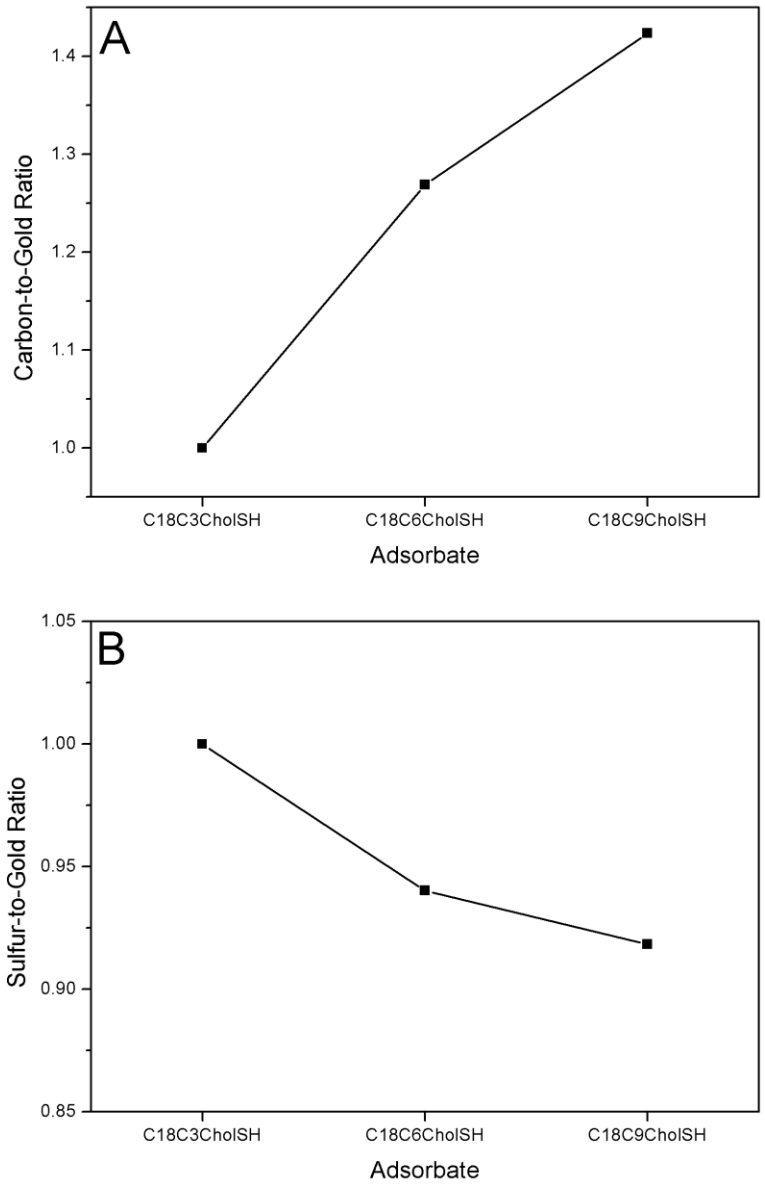

Figure 3.6. Normalized integrated peak ratios calculated from the XPS data for the peaks associated with (A) the C_{1s} and Au_{4f} binding energies (C:Au ratio) and (B) the S_{2p} and Au_{4f} binding energies (S:Au ratio), for the series of cholesterol-based SAMs. The lines connecting data points are provided as a guide for the eye.

3.4. Conclusions

A series of cholesterol-based, double tailgroup adsorbates were successfully synthesized and used to form single-component SAMs on gold, where the sulfur headgroup is bound to the gold substrate and the double tailgroups extend away from the surface in a well-organized array. Monolayers of these molecules were successfully formed as determined by the ellipsometric and XPS data. For the SAM generated from **C18C3CholSH**, the resulting film exhibits a surface interface that is a mixture of the two tailgroups, an extended alkyl chain and a chain terminated by a cholesterol-based moiety. This SAM produced contact angle data that fell between that of the single-component SAMs generated from the two individual tailgroups, respectively. The SAMs generated from **C18C3CholSH**, **C18C6CholSH**, and **C18C9CholSH** produce spectra that show the presence of both tailgroups as seen in the PM-IRRAS data. A definite overlap of signals from the extended alkyl chains and the cholesterol-based moieties are observed. The XPS data show that the SAMs formed from **C18C3CholSH**, **C18C6CholSH**, and **C18C9CholSH** are denser monolayers compared to the SAM formed from **CholSH** and almost as dense as the SAM formed from **C18SH**. Overall, the new double tailgroup series of molecules are capable of producing a well-structured single-component SAM. Further examination of these thiols within a mixed SAM format, along with similarly structured cholesterol-based molecules, will provide insight into the cholesterol condensing effect utilizing self-assembled monolayer films.

3.5. References

(1) Jennings, G. K.; Laibinis, P. E. *J. Am. Chem. Soc.* **1997**, *119*, 5208–5214.

(2) Lee, T. C.; Chen, P. C.; Lai, T. Y.; Tuntiwechapikul, W.; Kim, J. H.; Lee, T. R. *Appl. Surf. Sci.* **2008**, *254*, 7064–7068.

(3) Miller, J. S.; Bethencourt, M. I.; Hahn, M.; Lee, T. R.; West, J. L. *Biotechnol. Bioeng.* **2006**, *93*, 1060–1068.

(4) Katz, E.; Heleg-Shabtai, V.; Willne, I.; Rau, H. K.; Haehnel, W. *Angew. Chem. Int. Ed.* **1998**, *37*, 3253–3256.

(5) Ariga, K.; Nakanishi, T.; Michinobu, T. *J. Nanosci. Nanotechnol.* **2006**, *6*, 2278–2301.

(6) Fozdar, D. Y.; Lu, Y.; Shao, D.; Chen, S. *Handbook of Organic Electronics and Photonics* **2008**, *1*, 113–137.

(7) Xia, Y.; Zhao, X. M.; Whitesides, G. M. *Microelectron. Eng.* **1996**, *32*, 255–268.

(8) Nuzzo, R. G.; Allara, D. L. *J. Am. Chem. Soc.* **1983**, *105*, 4481–4483.

(9) Dubois, L. H.; Zegarski, B. R.; Nuzzo, R. G. *J. Am. Chem. Soc.* **1990**, *112*, 570–579.

(10) Shon, Y. S.; Lee, S.; Colorado, R., Jr.; Perry, S. S.; Lee, T. R. *J. Am. Chem. Soc.* **2000**, *122*, 7556–7563.

(11) Lee, S.; Shon, Y. S.; Colorado, R., Jr.; Guenard, R. L.; Lee, T. R.; Perry, S. S. *Langmuir* **2000**, *16*, 2220–2224.

(12) Kim, H. I.; Graupe, M.; Oloba, O.; Koini, T.; Imaduddin, S.; Lee, T. R.; Perry, S. S. *Langmuir* **1999**, *15*, 3179–3185.

(13) Lee, S.; Shon, Y. S.; Randall Lee, T.; Perry, S. S. *Thin Solid Films* **2000**, *358*, 152–158.

(14) Ulman, A. *An Introduction to Ultrathin Organic Films: From Langmuir-Blodgett to Self-Assembly*; Academic Press: San Diego, 1991.

(15) Lopez, G. P.; Albers, M. W.; Schreiber, S. L.; Carroll, R.; Peralta, E.; Whitesides, G. M. *J. Am. Chem. Soc.* **1993**, *115*, 5877–5878.

(16) Chaudhury, M. K.; Whitesides, G. M. *Science* **1992**, *255*, 1230–1232.

(17) Lopez, G. P.; Biebuyck, H. A.; Harter, R.; Kumar, A.; Whitesides, G. M. *J. Am. Chem. Soc.* **1993**, *115*, 10774–10781.

(18) Ulman, A. *Chem. Rev.* **1996**, *96*, 1533–1554.

(19) Porter, M. D.; Bright, T. B.; Allara, D. L.; Chidsey, C. E. D. *J. Am. Chem. Soc.* **1987**, *109*, 3559–3568.

(20) Bain, C. D.; Troughton, E. B.; Tao, Y. T.; Evall, J.; Whitesides, G. M.; Nuzzo, R. G. *J. Am. Chem. Soc.* **1989**, *111*, 321–335.

(21) Bain, C. D.; Whitesides, G. M. *Angew. Chem.* **1989**, *101*, 522–528.

(22) Mathauer, K.; Frank, C. W. *Langmuir* **1993**, *9*, 3446–3451.

(23) Stranick, S. J.; Atre, S. V.; Parikh, A. N.; Wood, M. C.; Allara, D. L.; Winograd, N.; Weiss, P. S. *Nanotechnology* **1996**, *7*, 438–442.

(24) Hayes, W. A.; Kim, H.; Yue, X.; Perry, S. S.; Shannon, C. *Langmuir* **1997**, *13*, 2511–2518.

(25) Ishida, T.; Mizutani, W.; Tokumoto, H.; Hokari, H.; Azehara, H.; Fujihira, M. *Appl. Surf. Sci.* **1998**, *130–132*, 786–791.

(26) Ishida, T.; Mizutani, W.; Choi, N.; Ogiso, H.; Azehara, H.; Hokari, H.; Akiba, U.; Fujihira, M.; Kojima, I.; Tokumoto, H. *Colloid Surface A* **1999**, *154*, 219–225.

(27) Sparr, E.; Ekelund, K.; Engblom, J.; Engstroem, S.; Wennerstroem, H. *Langmuir* **1999**, *15*, 6950–6955.

(28) Shibata, O.; Yamamoto, S. K.; Lee, S.; Sugihara, G. *J. Colloid Interface Sci.* **1996**, *184*, 201–208.

(29) Dupres, V.; Cantin, S.; Benhabib, F.; Perrot, F. *Europhys. Lett.* **1999**, *48*, 86–92.

(30) Imae, T.; Takeshita, T.; Kato, M. *Langmuir* **2000**, *16*, 612–621.

(31) Monobe, H.; Koike, A.; Muramatsu, H.; Chiba, N.; Yamamoto, N.; Ataka, T.; Fujihira, M. *Ultramicroscopy* **1998**, *71*, 287–293.

(32) Anderson, T. G.; McConnell, H. M. *J. Phys. Chem. B* **2000**, *104*, 9918–9928.

(33) Ekelund, K.; Sparr, E.; Engblom, J.; Wennerstroem, H.; Engstroem, S. *Langmuir* **1999**, *15*, 6946–6949.

(34) Silvius, J. R.; Giudice, D. d.; Lafleur, M. *Biochemistry* **1996**, *35*, 15198–15208.

(35) Solletti, J. M.; Botreau, M.; Sommer, F.; Brunat, W. L.; Kasas, S.; Duc, T. M.; Celio, M. R. *Langmuir* **1996**, *12*, 5379–5386.

(36) Solletti, J. M.; Botreau, M.; Sommer, F.; Tran Minh, d.; Celio, M. R. *J. Vac. Sci. Technol., B* **1996**, *14*, 1492–1497.

(37) Leporatti, S.; Bringezu, F.; Brezesinski, G.; Moehwald, H. *Langmuir* **1998**, *14*, 7503–7510.

(38) Nag, K.; Keough, K. M. W. *Biophys. J.* **1993**, *65*, 1019–1026.

(39) Meyer, E.; Overney, R.; Luethi, R.; Brodbeck, D.; Howald, L.; Frommer, J.; Guentherodt, H. J.; Wolter, O.; Fujihara, M.; Takano, H.; Gotoh, Y. *Thin Solid Films* **1992**, *220*, 132–137.

(40) Overney, R. M.; Meyer, E.; Frommer, J.; Guentherodt, H. J.; Fujihira, M.; Takano, H.; Gotoh, Y. *Langmuir* **1994**, *10*, 1281–1286.

(41) Lehmler, H. J.; Jay, M.; Bummer, P. M. *Langmuir* **2000**, *16*, 10161–10166.

(42) Lee, T. R.; Carey, R. I.; Biebuyck, H. A.; Whitesides, G. M. *Langmuir* **1994**, *10*, 741–749.

(43) Kakiuchi, T.; Sato, K.; Iida, M.; Hobara, D.; Imabayashi, S.; Niki, K. *Langmuir* **2000**, *16*, 7238–7244.

(44) Stranick, S. J.; Parikh, A. N.; Tao, Y. T.; Allara, D. L.; Weiss, P. S. *J. Phys. Chem.* **1994**, *98*, 7636–7646.

(45) Atre, S. V.; Liedberg, B.; Allara, D. L. *Langmuir* **1995**, *11*, 3882–3893.

(46) Brewer, N. J.; Leggett, G. J. *Langmuir* **2004**, *20*, 4109–4115.

(47) Rowe, G. K.; Creager, S. E. *Langmuir* **1994**, *10*, 1186–1192.

(48) DeVries, G. A.; Brunnbauer, M.; Hu, Y.; Jackson, A. M.; Long, B.; Neltner, B. T.; Uzun, O.; Wunsch, B. H.; Stellacci, F. *Science* **2007**, *315*, 358–361.

(49) Reed, M. A.; Chen, J.; Rawlett, A. M.; Price, D. W.; Tour, J. M. *Appl. Phys. Lett.* **2001**, *78*, 3735–3737.

(50) Majumdar, N.; Gergel-Hackett, N.; Bean, J.; Harriott, L.; Pattanaik, G.; Zangari, G.; Yao, Y.; Tour, J. *J. Electron. Mater.* **2006**, *35*, 140–146.

(51) Ma, H.; Zin, M. T.; Zareie, M. H.; Kang, M. S.; Kang, S. H.; Kim, K. S.; Reed, B. W.; Behar, C. T.; Sarikaya, M.; Jen, A. K. Y. *J. Nanosci. Nanotechnol.* **2007**, *7*, 2549–2566.

(52) Mir, M.; Alvarez, M.; Azzaroni, O.; Knoll, W. *Langmuir* **2008**, *24*, 13001–13006.

(53) Trabelsi, S.; Zhang, S.; Lee, T. R.; Schwartz, D. K. *Phys. Rev. Lett.* **2008**, *100*, 037802/037801–037802/037804.

(54) Trabelsi, S.; Zhang, S.; Lee, T. R.; Schwartz, D. K. *Soft Matter* **2007**, *3*, 1518–1524.

(55) Trabelsi, S.; Zhang, S.; Zhang, Z.; Lee, T. R.; Schwartz, D. K. *Soft Matter* **2009**, *5*, 750–758.

(56) Trabelsi, S.; Zhang, Z.; Zhang, S.; Lee, T. R.; Schwartz, D. K. *Langmuir* **2009**, *25*, 8056–8061.

(57) Zhang, S.; Jamison, A. C.; Schwartz, D. K.; Lee, T. R. *Langmuir* **2008**, *24*, 10204–10208.

(58) Leathes, J. B. *Lancet* **1925**, *208*, 853–856.

(59) Yeagle, P. L. *Biochim. Biophys. Acta* **1985**, *822*, 267–287.

(60) Huang, J.; Feigenson, G. W. *Biophys. J.* **1999**, *76*, 2142–2157.

(61) Finean, J. *Cell. Mol. Life Sci.* **1953**, *9*, 17–19.

(62) Chong, P. L. *Proc. Natl. Acad. Sci. U. S. A.* **1994**, *91*, 10069–10073.

(63) Shon, Y. S.; Lee, T. R. *Langmuir* **1999**, *15*, 1136–1140.

(64) Tamada, K.; Nagasawa, J.; Nakanishi, F.; Abe, K.; Hara, M.; Knoll, W.; Ishida, T.; Fukushima, H.; Miyashita, S.; Usui, T.; Koini, T.; Lee, T. R. *Thin Solid Films* **1998**, *327–329*, 150–155.

(65) Yang, Z. P.; Engquist, I.; Kauffmann, J. M.; Liedberg, B. *Langmuir* **1996**, *12*, 1704–1707.

(66) Snyder, R. G.; Strauss, H. L.; Elliger, C. A. *J. Phys. Chem.* **1982**, *86*, 5145–5150.

(67) Vickerman, J. C., Eds.; *Surface Analysis - the Principal Techniques*; 1 ed.; Wiley: Chichester, 1997.

(68) Biebuyck, H. A.; Bain, C. D.; Whitesides, G. M. *Langmuir* **1994**, *10*, 1825–1831.

(69) Castner, D. G.; Hinds, K.; Grainger, D. W. *Langmuir* **1996**, *12*, 5083–5086.

(70) Sun, F.; Grainger, D. W.; Castner, D. G.; Leach-Scampavia, D. K. *Macromolecules* **1994**, *27*, 3053–3062.

Chapter 4. Two-component Self-assembled Monolayers Generated from Single-chained Cholesterol-based Thiols and *n*-Octadecanethiol on Gold

4.1. Introduction

Recent developments in monolayer analysis have led to an increase in the quantity of studies involving the cholesterol condensing effect within mixed monolayer systems. As evident in the plasma membrane,[1,2] cholesterol condenses the packing of lipid monolayers. Leathes in 1925 first described the phenomenon stating that the surface area of a cholesterol-containing lipid bilayer is less than the sum of areas of the individual bilayer components. [3] Believed to be caused by the molecular mismatch between the rigid cholesterol and the fluid hydrocarbon tailgroups of lipids; the mechanism of the condensing effect is still debated.[4-7] In monolayer studies, the condensing effect is observed over a wide range of cholesterol concentrations, based on the lipid studied; for example, saturated versus unsaturated tailgroups, the chain length of the tailgroups, and the headgroup of the lipid.[8,9]

Mimicking biological membranes, Langmuir and Langmuir-Blodgett (LB) monolayers utilize the air-water interface to form monolayers, bilayers, and multilayers. In 1928, Adams *et al.* first studied the effect of cholesterol on several different carboxylic acid monolayers.[10] These researchers showed the difference in cholesterol's ability to condense different carboxylic acids. Since those initial reports, the majority of condensing effect studies involves mixed, two-component LB monolayers combining

phosphatidylcholine and cholesterol. The condensing effect has been studied with epifluorescence microscopy,[9,11-13] Brewster angle microscopy,[8,13] electrochemical scanning tunneling microscopy,[14] X-ray diffraction,[7,15,16] Monte-Carlo simulations,[6] molecular dynamics simulation,[17] cyclic voltametry,[18] and ellipsometry[16]. These techniques have been used on LB monolayers and bilayers. To the author's knowledge, the condensing effect has been utilized for membrane tethering but has not been directly studied within a self-assembled monolayer (SAM) film.

In 1996, Yang *et al.* performed the first study of thiocholesterol on gold.[19] Thiocholesterol is structurally similar to cholesterol with a thiol moiety at the 3β-position instead of a hydroxyl group. Yang *et al.* showed that thiocholesterol forms a monolayer on gold by self-assembly in a manner similar to cholesterol in a Langmuir monolayer, however defects exist in the monolayer caused by the structural constraints of the rigid polycyclic portion of thiocholesterol. Mixed monolayers with thiocholesterol and 11-mercaptoundecanoic acid have been fully characterized by infrared-reflection adsorption spectroscopy, X-ray photoelectron spectroscopy, ellipsometry, contact angle measurements, and cyclic voltammetry.[20,21] To the author's knowledge, mixed SAMs of thiocholesterol and normal alkanethiols have yet to be studied.

Compared to Langmuir monolayers, the adsorbates that form SAMs on a solid substrate have fewer degrees of freedom during the monolayer formation process, thus providing an alternative route to the monolayer formation for surfactants that fail to assemble at an air-liquid interface. The success of the SAM format for incorporating cholesterol into a monolayer structure has, in the last decade, led to a number of studies

of mixed SAMs involving cholesterol, thiocholesterol, and cholesterol moieties.[22-26] Boden *et al.* synthesized a cholesterol moiety for use as a tether for biomembranes.[26] The molecules studied consisted of a cholesterol tailgroup, an ethylene glycol spacer, and a thiol headgroup. To the author's knowledge, these ethylene glycol and cholesterol-based molecules have never been used to form a pure SAM or to study the cholesterol condensing effect. Molecules with similar structures have been used to study biomembranes yet have not been utilized for the study of the cholesterol condensing effect.[26-29] By generating binary SAMs from a single-chained cholesterol-based thiol and a saturated alkanethiol, we are examining the interfacial properties of mixed films utilizing the cholesterol condensing effect.

Within this work, we generated two-component SAMs on gold from single-chained molecules containing a cholesterol moiety (**CholCnSH**) composed of a thiol headgroup, a hydrocarbon spacer, and cholesterol, in combination with *n*-octadecanethiol (**C18SH**). The specific structure of this series of molecules allows for the study of the cholesterol condensing effect utilizing the hydrocarbon spacer to carry the cholesterol moiety away from the gold substrate. For this series of molecules, **CholCnSH** has a hydrocarbon spacer with n = 3 and 6. Since the hydrocarbon spacer promotes the formation of a well-organized monolayer, the cholesterol moiety should participate in an increased packing density, as compared to thiocholesterol, which does not possess a spacer, as seen in Figure 4.1 and Figure 2.2. The cholesterol-containing molecules will be mixed with *n*-octadecanethiol at five specified concentrations, 10 %, 30 %, 50 %, 70 %, and 90 %. The mixed monolayers will be compared against single-component SAMs

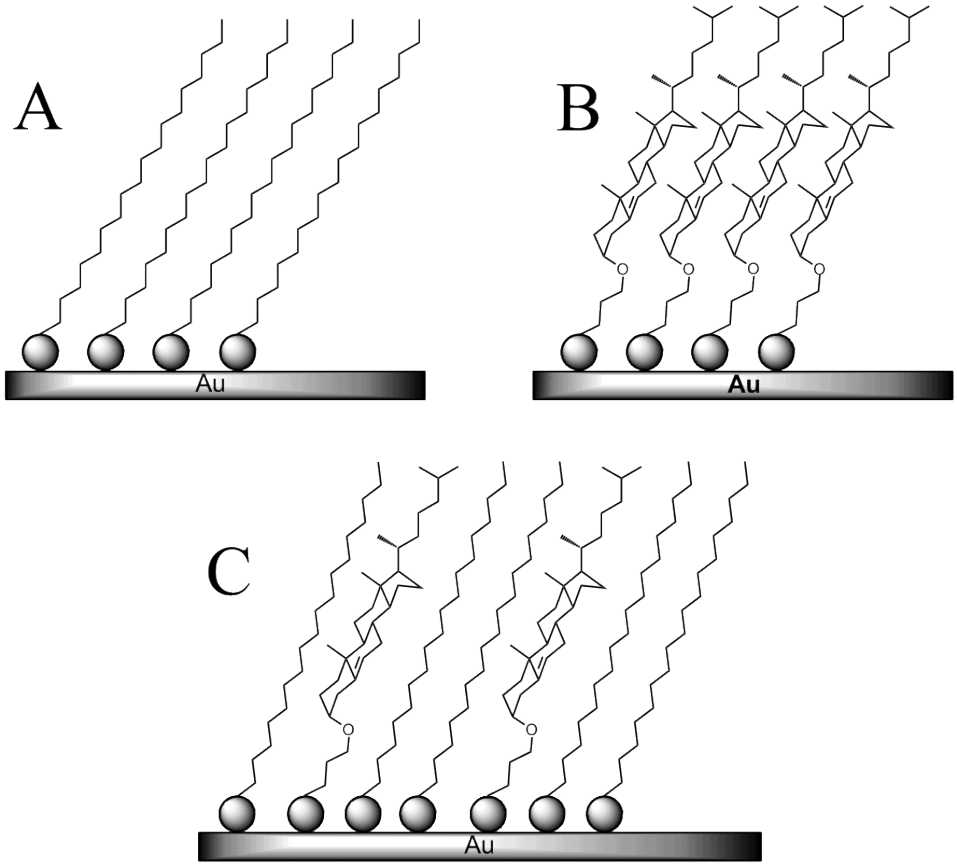

Figure 4.1. Illustration of the structures of SAMs generated from (A) $CH_3(CH_2)_{17}SH$ (**C18SH**) with trans-extended conformation, (B) cholesterol-based moieties (**CholCnSH**) where n = 3, and (C) a mixture of **C18SH** and **CholCnSH** where n = 3. Molecular sizes and dimensions are not drawn to scale.

of each component, *n*-octadecanethiol and the single-chain cholesterol-based thiol used in the series. The structure and interfacial properties of the resultant films were characterized using optical contact angle goniometry, ellipsometry, X-ray photoelectron spectroscopy (XPS), and polarization modulation infrared-reflection absorption spectroscopy (PM-IRRAS). Additionally, we prepared single-component SAMs from

thiocholesterol (5-cholestene-3β-thiol, **CholSH**). The data collected from the cholesterol-based mixed films were compared to those collected from pure SAMs generated from **C18SH**, **CholSH**, and **CholCnSH**, which serve as a basis for determining the effects of mixing.

4.2. Experimental Section

4.2.1 Nomenclature

We denote the names of the thiol adsorbates used in this study as follows: *n*-octadecanethiol ($CH_3(CH_2)_{17}SH$), **C18SH**; thiocholesterol (5-cholestene-3β-thiol), **CholSH**; 5-cholestene-3β-oxypropan-3-thiol, **CholC3SH**; and 5-cholestene-3β-oxyhexan-6-thiol, **CholC6SH**. The letter indicates the chemical composition of the adsorbate: **Chol** denotes a cholesterol moiety, **C** denotes methyl and methylene units (CH_3 and CH_2) within the hydrocarbon chain, and **SH** denotes thiol structure. The number following each letter indicates the number of each unit along the chain backbone.

4.2.2. Materials

Gold shot (99.99 %) was purchased from Kamis Inc. Chromium rods (99.9 %) were purchased from R. D. Mathis Company. Polished single-crystal Si(100) wafers were purchased from Silicon Sense, Inc. and rinsed with absolute ethanol (EtOH, Aaper

Alcohol and Chemical Co.) before use. The contacting liquids used for wettability measurements were of the highest purity available from the following sources and were used as received: water generated from Milli Q Water System with resistance of 18.2 MΩ, Millipore Corporation and hexadecane from Aldrich Chemical Co. *n*-Octadecanethiol (**C18SH**) was also purchased from Aldrich Chemical Co. and used without further purification. Tetrahydrofuran (THF) was purchased from Mallinckrodt Baker, Inc, distilled over calcium hydride, and stored under argon. Anhydrous dioxane, anhydrous *N*,*N*-dimethylformamide (DMF), methanol, cholesterol, sodium hydride (NaH, 60 % dispersion in mineral oil), 1,3-propanediol, 1,6-hexanediol, triethylamine (NEt_3), and potassium thioacetate (KSAc) were purchased from Aldrich Chemical Co. and used as received. Lithium aluminum hydride ($LiAlH_4$) was purchased from Alfa Aesar and used as received. Methanesulfonyl chloride (MsCl) and *p*-toluenesulfonyl chloride (TsCl) were purchased from Acros Organics and used as received. Column chromatography was performed using silica gel (40 – 64 μm) and thin-layer chromatography (TLC) was carried out using 200 μm thick silica gel plates, which both were purchased from Sorbent Technologies, Inc. The eluted TLC plates were developed with a molybdenum blue stain followed by heating. Nuclear Magnetic Resonance (NMR) spectra were recorded on a JOEL ECA-500 spectrometer operating at 500 MHz. The data were obtained in chloroform-d ($CDCl_3$) and referenced to δ 7.26 ppm for ^1H NMR spectra and 77.00 ppm for ^{13}C NMR spectra.

4.2.3. Synthesis of the Adsorbates

The synthetic strategy used to prepare the targeted single-chain cholesterol-based thiols (**CholCnSH**) is shown in Scheme 4.1. The complete experimental details of each synthetic step are provided in Chapter 2, Section 2.2.3.

Scheme 4.1. Preparation of a Series of Cholesterol-based Thiols (**CholCnSH**), where n = 3 and 6.

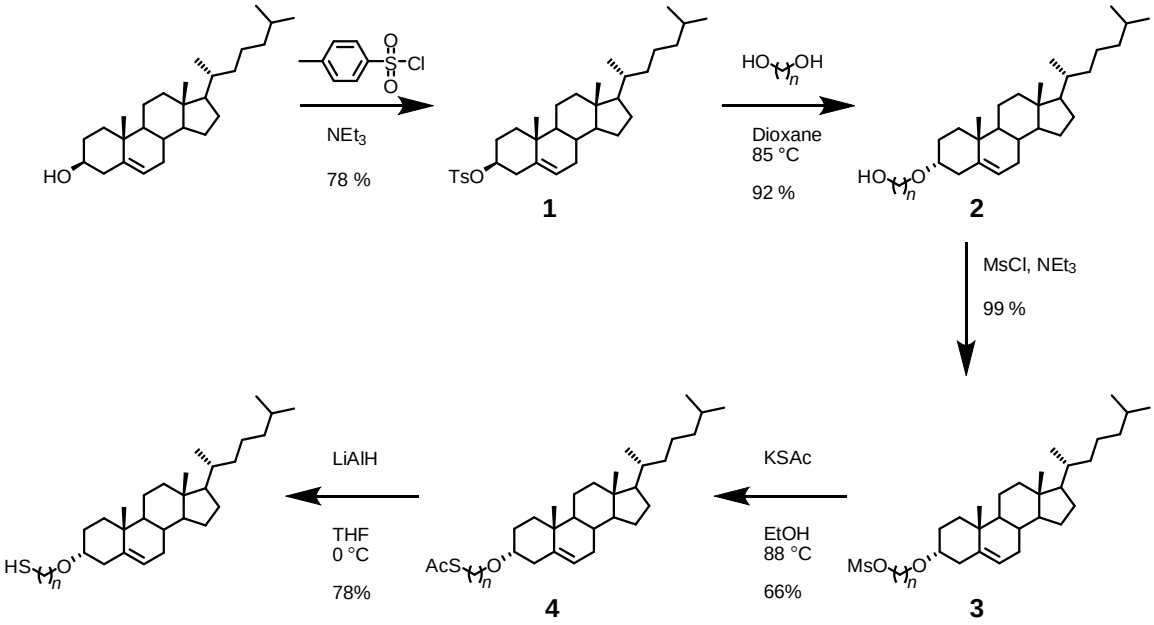

Cholest-5-en-3β-oxypropan-3-thiol (**CholC3SH**). Yield: 0.309 g (0.671 mmol, 78 %). TLC (80 % hexane: 20 % ethyl acetate): R_f = 0.72. ^{1}H NMR (500 MHz, $CDCl_3$): δ 0.67 (s, 3 H), 0.85 - 1.60 (m, 38 H), 1.78 – 2.05 (m, 7 H), 2.15 (m, 1 H), 2.35 (m, 1 H), 2.64 (q, *J* = 5.15 Hz, 2 H), 3.13 (m, 1 H), 3.56 (m, 2 H), 5.34 (m, 1 H). ^{13}C NMR (500

MHz, $CDCl_3$): δ 11.96, 18.83, 19.48, 21.17, 21.65, 22.69, 22.95, 23.96, 24.39, 28.10, 28.35, 28.53, 31.97, 32.03, 34.33, 35.90, 36.30, 36.96, 37.34, 39.25, 39.62, 39.88, 42.40, 50.27, 56.26, 56.86, 65.77, 79.19, 121.64, 140.95.

C*holest-5-en-3β-oxyhexan-6-thiol* (**CholC6SH)**. Yield: 0.560 g (1.11 mmol, 85 %). TLC (80 % hexane: 20 % ethyl acetate): R_f = 0.77. ^{1}H NMR (500 MHz, $CDCl_3$): δ 0.67 (s, 3 H), 0.85 – 1.65 (m, 46 H), 1.76 – 2.02 (m, 5 H), 2.18 (m, 1 H), 2.35 (m, 1 H), 2.56 (q, *J* = 7.45 Hz, 2 H), 3.13 (m, 1 H), 3.45 (m, 2 H), 5.34 (m, 1 H). ^{13}C NMR (500 MHz, $CDCl_3$): δ 11.96, 18.84, 19.47, 21.17, 22.70, 22.95, 23.99, 24.39, 24.65, 25.84, 28.09, 28.31, 28.36, 28.57, 30.20, 31.97, 32.03, 34.09, 35.91, 36.31, 36.94, 37.39, 39.30, 39.62, 39.89, 42.38, 50.28, 56.28, 56.85, 67.97, 79.04, 121.48, 141.05.

4.2.4. Preparation of SAMs

The gold substrates were prepared under a vacuum at ~1 × 10^{-5} Torr. A thin layer (100 Å) of chromium was first evaporated onto polished Si(100) wafers to assist the adhesion of gold on silicon, followed by the evaporation of 1000 Å of gold. Absolute ethanol was used to rinse the resultant gold-coated wafers, followed by drying under a stream of ultra-pure nitrogen before use. The freshly prepared gold-coated wafers were cut into slides (1 × 3 cm), and then the slides were cleaned by rinsing with absolute ethanol and dried with ultra-pure nitrogen. The slides then were immersed in the following thiol solutions; **C18SH** (1 mM in ethanol), **CholSH** (1 mM in ethanol), **CholC3SH** (1 mM in ethanol), **CholC6SH** (1 mM in ethanol), or mixed solutions

(**CholC3SH** and **C18SH** or **CholC6SH** and **C18SH**) where the total thiol concentration was 1 mM in ethanol for all solutions. The glass vials containing the thiol solutions were previously cleaned with piranha solution (3:1 mixture of H_2SO_4/H_2O_2) and rinsed thoroughly with deionized water and absolute ethanol. (*Caution: Piranha solution is highly corrosive and should be handled with extreme care*.) All substrates were allowed to equilibrate at room temperature for a period of 48 hours. Then the slides were rinsed with tetrahydrofuran and ethanol, and blown dry with ultra-pure nitrogen before characterization.

4.2.5. Characterization of SAMs

Ellipsometric Thickness Measurements. The thicknesses of the films were measured using a Rudolph Research Auto EL III ellipsometer equipped with a He-Ne laser (632.8 nm) at an angle of incidence of 70°. A refractive index of 1.45 is used for determining the thickness of the SAM generated from **C18SH** and cholesterol-based thiols. For each sample, the data were averaged over the collection from one slide with four spots per slide. The measured thicknesses were always within ± 2 Å of the reported values.

Contact Angle Measurements. A Ramé-Hart model 100 contact angle goniometer was employed to measure the contact angle of the SAMs. The probe liquids, water (W) and hexadecane (HD), were dispensed (advancing angle, θ_a) and withdrawn

(receding angle, θ_r) on the surfaces of SAMs using a Matrix Technologies micro-Electrapette 25 at the slowest possible speed (1 μL/s). The measurements were performed at room temperature with the pipet tip in contact with the drop. Reported values for each sample were the averages of measurements taken from one slide with four drops per slide using both drop edges and always within ± 2°.

Polarization Modulation Infrared Reflection Absorption Spectroscopy (PM-IRRAS). Surface IR spectra were collected using a Nicolet Nexus 670 Fourier transform spectrometer equipped with a liquid nitrogen-cooled mercury-cadmium-telluride (MCT) detector and a Hinds Instrument PEM-90 photoelastic modulator. The *p*-polarized light was reflected from the sample at an angle of incidence of 80° to the surface normal. The spectra were collected at 512 scans for the C-H stretching region (2750 – 3100 cm^{-1}) with a spectral resolution of 4 cm^{-1}.

X-ray Photoelectron Spectroscopy (XPS). A PHI 5700 X-ray photoelectron spectrometer equipped with a monochromatic Al Kα X-ray source (hν = 1486.7 eV) incident at 90° relative to axis of a hemispherical energy analyzer was employed to obtain XPS spectra of the SAMs at a photoelectron takeoff angle of 45° from the surface and a pass energy of 23.5 eV. The binding energy scales were referenced to the $Au_{4f7/2}$ peak at 84.0 eV.

4.3. Results and Discussion

Self-assembled monolayers generated from mixtures of **C18SH** and **CholC3SH** or **CholC6SH**, with the cholesterol-based thiol having 0, 10, 30, 50, 70, 90, and 100 % solution compositions, were characterized. Ethanol was chosen as the developing solvent to generate SAMs based on the favorable solubility of the adsorbates and to maintain similarity with other SAM studies. The SAMs were allowed to develop for 48 hours and fully characterized within 12 hours beyond the initial incubation period. The concentrations used to develop the SAMs were 10, 30, 50, 70, and 90 % of the cholesterol-based thiol as calculated from the total thiol concentration, which was maintained at 1 mM for each SAM. The data collected from the mixed SAMs were compared to that collected for single-component SAMs generated from each adsorbate used in this study, **C18SH**, **CholC3SH**, and **CholC6SH**.

4.3.1. Thicknesses of the Films

Trends in the characterization of mixed adsorbates for binary SAMs rely upon structural characteristics of single-component SAMs generated from the individual adsorbates. Ellipsometry allows for the detection of trends in the surface profile of our binary SAMs because of the height differences for the components of these adsorbed films.

Assuming systematic mixing of the binary SAMs occurs based on the relative presence of each thiol during development of the monolayer, the anticipated trend for a graph of the ellipsometric measurements for the mixed SAM series would be linear.[30] However, for this series of binary SAMs generated from mixtures of *n*-octadecanethiol and **CholC3SH** or **CholC6SH**, a linear trend is not observed, as shown in Figure 4.2. While the cholesterol and trans-extended alkyl chains are structurally dissimilar and subject to possible phase separation, the cholesterol condensing effect causes a mixing of the two components that leads to an increase in the monolayer thickness. These results are similar to the those presented in the work of McIntosh, who studied mixed Langmuir bilayers, and was the first to attribute the thickness increase to a decrease in chain tilt which causes an increase in order of the lipids.[31] Szoka *et al.* showed the same thickening with lipid Langmuir monolayers as a result of added cholesterol.[32,33] Molecular modeling simulations also conclude that the increase in monolayer and bilayer thickness is a result of the decrease in chain tilt from the surface normal.[34]

The thicknesses for the SAMs generated from a mixture of **C18SH** and **CholC3SH** or **CholC6SH**, peak at a 50 % solution concentration of the cholesterol-based adsorbate. For the SAMs generated from a mixture of **C18SH** and **CholC6SH**, the ellipsometric thickness data exhibits a greater increase at lower concentrations of the cholesterol-bearing thiol than the SAMs generated from a mixture of **C18SH** and **CholC3SH**. This variance might be attributed to competitive adsorption; the favored adsorbate deposited from solution for the SAMs formed from **CholC6SH** and **C18SH** might reflect a different set of dynamics as compared to **CholC3SH** and **C18SH**.

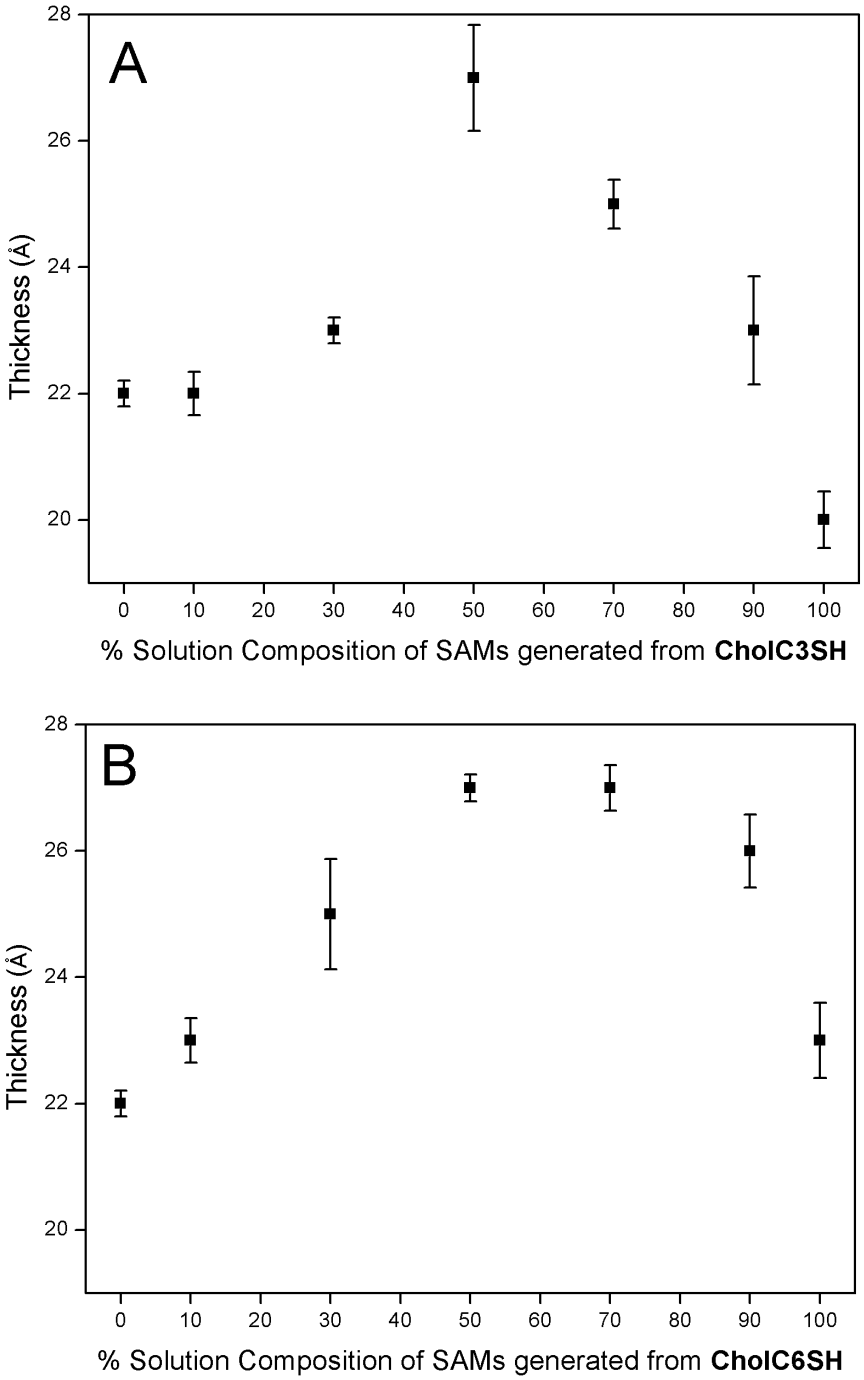

Figure 4.2. The film thicknesses for two-component SAMs generated from (A) **CholC3SH** and **C18SH** and (B) **CholC6SH** and **C18SH**.

Competitive adsorption can be attributed to several factors of which the difference in molecular length of the adsorbates applies to this study.[35-37] A lower solubility in solution of one adsorbate over another can also change the relative rate of adsorption, which is shown to form SAMs with a surface composition favoring that of the least soluble adsorbate in the deposition solution.[37] While all the adsorbates used in this study dissolve in ethanol, the cholesterol-based adsorbates require heat to fully dissolve at a 1 mM concentration; however no difference was noticed between the solubility of **CholC6SH** and **CholC3SH** in ethanol.

The ellipsometric data for these new binary SAMs follow previous reports based on mixed Langmuir monolayer systems, in that the molecules apparently tilt less, producing a thicker monolayer than the single-component SAMs, a result that might be explained by the cholesterol condensing effect.

4.3.2. Wettabilities of the Films

Information about the organization within a monolayer film (*e.g.*, composition, packing, and structural orientation) can be determined from advancing and receding contact angle measurements.[38] The wettabilities of two-component SAMs generated from mixtures of the cholesterol-based thiols and *n*-octadecanethiol are shown in Table 4.1, where the probe liquids used were water and hexadecane. The single-component SAMs generated from **C18SH**, **CholSH**, **CholC3SH**, and **CholC6SH** serve as references for the new two-component SAMs. It is well-known that cholesterol is hydrophobic and

lipophilic, and the advancing contact angles for the SAMs containing cholesterol exhibit data that conform to these physical properties.

The advancing contact angles for water for all binary SAMs in this study indicate similar interfacial packing to that of a SAM generated from normal alkanethiols. The values of the advancing contact angles for water for the binary SAMs indicate a slight increase in hydrophobicity of the SAMs. The minor increase can be associated with fewer interactions between the probe liquid and the surface interface as a result of the decreased tilt of the molecules, as surmised from the ellipsometric data. The decrease in tilt angle of the molecules to the surface normal is associated with tighter packing of the molecules, which is likely generated by the cholesterol condensing effect. The advancing contact angles for hexadecane for the binary SAMs in this study have values similar to a single-component SAM formed from **C18SH**.

The hysteresis values ($\Delta\theta = \theta_a - \theta_r$) for water and hexadecane for the binary SAMs in this study are larger than the values for the pure SAM generated from **C18SH**, indicating a more heterogeneous surface interface similar to that of the pure SAMS generated from the double-chained cholesterol-based adsorbates in Chapter 3. It is notable that the hysteresis values for hexadecane for the binary SAMs containing 90 % cholesterol-based adsorbate in solution have larger values than the other mixed SAMs, possibly indicating a transition in surface composition for this film. With competitive adsorption, it is plausible that the cholesterol-based adsorbates begin to saturate the solution at mole fractions between 70 – 100 % in solution and the resulting SAM contains more cholesterol-based adsorbates on the gold substrate than SAMs at lower

Table 4.1. Advancing Contact Angles (θ_a, °), Receding Contact Angles (θ_r, °), and Calculated Hysteresis Values ($\Delta\theta = \theta_a - \theta_r$) Measured on SAMs Generated from Different Solution Compositions of **C18SH**, **CholSH**, **CholC3SH**, and **CholC6SH** SAMs using Various Probe Liquids[a].

Adsorbate		**Probe Liquids**					
		W			**HD**		
	Solution Composition	θ_a	θ_r	$\Delta\theta$	θ_a	θ_r	$\Delta\theta$
C18SH	100 %	117	104	13	50	39	11
CholSH	100 %	110	92	18	16	0	-[b]
CholC3SH	10 %	120	99	21	50	38	12
	30 %	120	98	22	51	40	11
	50 %	120	102	18	51	39	12
	70 %	120	101	19	49	38	11
	90 %	120	100	20	48	30	18
	100 %	110	91	19	17	0	-[b]
CholC6SH	10 %	120	99	21	48	35	13
	30 %	120	102	18	49	36	13
	50 %	119	101	18	48	36	12
	70 %	119	100	19	49	36	13
	90 %	120	98	22	43	26	17
	100 %	112	92	20	21	0	-[b]

[a] Probe liquids used in this experiment are W = water and HD = hexadecane.

[b] When a receding contact angle could not be obtained, the hysteresis value could not be calculated.

solution concentrations. The same contact angle trend was seen by Liedberg *et al.* during the study of mixed SAMs involving thiocholesterol and 11-mercaptoundecanoic acid, where the greatest change in contact angles occurred as the mole fraction of the cholesterol moiety in solution decreased from 1.0 to 0.8. This was attributed to the difference in the molecular surface area fractions rather than the surface mole fractions .[20]

4.3.3. PM-IRRAS Studies

The infrared-reflectance spectra in the C–H stretching region of the cholesterol-based mixed SAMs are shown in Figure 4.3, with the peak assignments shown in Table 4.2. Through the use of PM-IRRAS, the degree of relative crystallinity and packing density for alkyl chains in a SAM can be determined.[39] A well-packed crystalline SAM will have an antisymmetric methylene peak located at 2919 cm^{-1}, based on films formed from crystalline polyethylene, which is sensitive to the degree of conformational order.[40,41] A less crystalline, liquid-like polyethylene film, will have a higher value for the $\nu_a^{CH_2}$ of about 2928 cm^{-1}.[40-42] However, this interpretation of degrees of relative crystallinity for a film based on the antisymmetric methylene stretch does not necessarily apply to films of a different chemical nature, such as cholesterol-based films that are predominantly a rigid polycyclic structure.

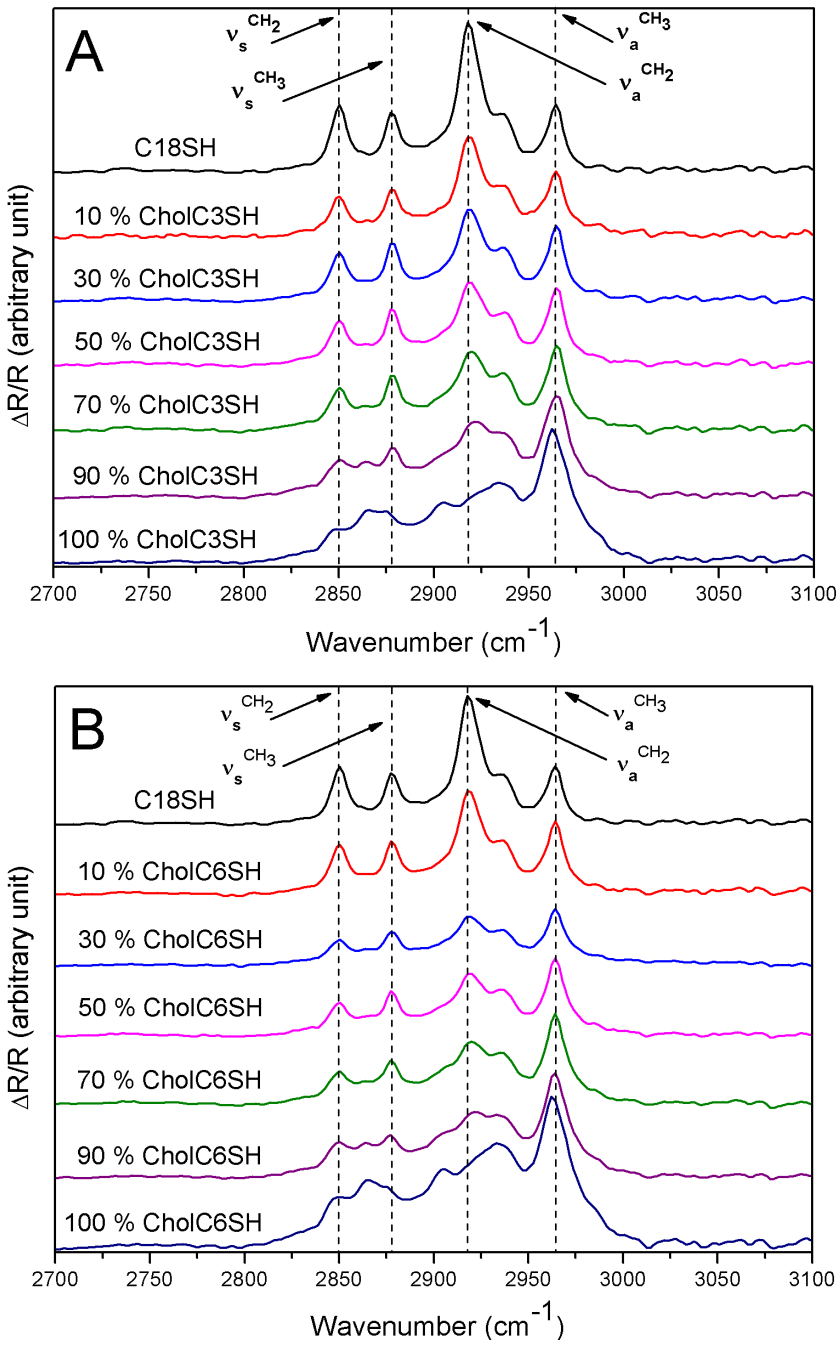

Figure 4.3. PM-IRRAS spectra for the C–H stretching region of binary SAMs generated from a mixture of (A) **C18SH** and **CholC3SH** and (B) **C18SH** and **CholC6SH** with peak assignments according to the SAM generated from **C18SH**.

For a SAM generated from **CholSH**, the surface IR spectra is very different than a spectra from a crystalline SAM generated from **C18SH**, revealing noticeable differences in the peak frequency and intensity. The spectra for these SAMs reflect the differences in the structural and chemical environments of the C–H bonds, as can be seen in Figure 3.4. For SAMs generated from normal alkanethiols, the most intense peak is the antisymmetric methylene stretch at ~ 2919 cm^{-1}, while SAMs generated from **CholSH** show the antisymmetric methyl stretch at 2963 cm^{-1} as the most intense peak. As mentioned previously, the differences in the intensity of the various forms of C–H stretches in these spectra can be explained by the number of bonds involved, the orientation of the bonds to the surface, and the ordering and structure of the two types of molecules.[43,44] For SAMs generated from normal alkanethiols, the majority of methylene units are oriented so that the transition dipole moments are more perpendicular to the surface and therefore they produce an intense antisymmetric methylene stretch signal in surface IR. The strength of the adsorption of the perpendicular vibrations can be explained by the surface selection rule associated with surface IR.[45] The same principal applies for the pronounced $\nu_a^{CH_3}$ peak observed in the spectra for cholesterol-based SAMs. The cholesterol moiety contains five methyl groups, four of which are predicted to have transition dipole moments that align with the surface normal, thus producing an intense signal and providing a molecular axis that is parallel or nearly parallel to the surface normal.[19]

For the PM-IRRAS spectra of the binary SAMs generated from mixtures of **C18SH** and **CholC3SH** or **CholC6SH**, the structural components are similar to that of

the pure SAMs formed from a normal alkanethiol and **CholSH**. As the solution concentration of the cholesterol-based adsorbate increases, the spectrum for the binary SAMs begins to resemble that of the pure cholesterol-based SAMs. The antisymmetric methylene stretch for a SAM generated from normal alkanethiols is seen in these spectra typically around 2919 cm^{-1}, while the antisymmetric methylene stretch for a SAM generated from cholesterol-based moieties, ~ 2936 cm^{-1}, is also observed. The broad band that forms from the many structural placements of this stretching vibration creates difficulties when assigning the peaks for these new binary SAMs. Assigning the antisymmetric methylene stretch for the mixed SAMs containing a large surface population of the cholesterol-based moieties becomes difficult as the peak for the $\nu_a^{CH_2}$ stretch has a predominant peak and shoulder which is determined to be the $\nu_a^{CH_2}$ peak, ~ 2919 cm^{-1}, associated with the alkyl tailgroup overlapping with the $\nu_a^{CH_2}$ peak, ~ 2963 cm^{-1}, associated with the cholesterol-based tailgroup, and is reported as such in Table 4.2.

One of the most noticeable changes in the spectra for the binary SAMs generated from **C18SH** and **CholC3SH** or **CholC6SH** is that as the cholesterol-based solution concentration increases, the relative intensities of the peaks change. The intensity of the antisymmetric methyl stretch becomes larger than all the other peaks as the solution concentration increases for these binary SAMs confirming the adsorption of more cholesterol-based moieties on the metal substrate. Comparing the peak intensity for the antisymmetric methyl stretch from cholesterol-based thiolates, ~ 2963 cm^{-1}, and the antisymmetric methylene stretch from normal alkanethiolates, ~ 2919 cm^{-1}, we are able to determine that the cholesterol-based thiolate is present in the SAMs.

Table 4.2. Peak Assignments for the PM-IRRAS Spectra of Pure SAMs Generated from **C18SH** and **CholSH** and Binary SAMs Generated from **C18SH** and **CholC3SH** or **CholC6SH**.

Adsorbate		**Peak assignments**				
	Solution Composition	$\nu_a^{CH_3}$	$\nu_a^{CH_2}$ [a]	$\nu_a^{CH_2}$ [b]	$\nu_s^{CH_3}$	$\nu_s^{CH_2}$
C18SH	100 %	2965	2919	-	2878	2853
CholSH	100 %	2963	-	2937	2865, 2874	2847
CholC3SH	10 %	2964	2919	2936	2878	2850
	30 %	2964	2918	2936	2878	2850
	50 %	2964	2919	2936	2878	2850
	70 %	2965	2920	2936	2864, 2878	2850
	90 %	2965	2922	2933	2864, 2879	2851
	100 %	2962	-	2934	2866, 2875	2849
CholC6SH	10 %	2964	2918	2936	2878	2850
	30 %	2964	2919	2936	2865, 2878	2850
	50 %	2964	2919	2936	2878	2850
	70 %	2964	2920	2936	2864, 2877	2850
	90 %	2964	2922	2933	2864, 2877	2850
	100 %	2963	-	2934	2865, 2878	2853

[a] $\nu_a^{CH_2}$ peak associated with the alkyl component.

[b] $\nu_a^{CH_2}$ peak associated with the cholesterol component.

At the lowest solution concentration, 10 % cholesterol-based thiol, the difference in these two peak intensities is noticeable. For the binary SAMs developed from

CholC3SH and **C18SH**, the intensities of these two peaks are similar at a 50 % solution composition of the cholesterol-based moiety. For the binary SAMs developed from **CholC6SH** and **C18SH**, the intensities of the two peaks are similar at 30 % solution composition, a trend seen in the ellipsometric data. For the binary SAMs in this study, the PM-IRRAS spectra confirm mixing of the two components, which confirms the thickening of the alkanethiol SAM by cholesterol as predicted by the cholesterol condensing effect.

4.3.4. XPS Studies

XPS spectra obtained from SAMs can be used to reveal the nature of the chemical bond between the adsorbate headgroup and the substrate along with the chemical composition of the films.[46] The XPS spectra of the C_{1s} region for the binary SAMs generated from **C18SH** and **CholC3SH** or **CholC6SH** are shown in Figure 4.4. The XPS spectra of the O_{1s} region for the binary SAMs generated from **C18SH** and **CholC3SH** or **CholC6SH** are shown in Figure 4.5. The XPS spectra of the S_{2p} region for the binary SAMs generated from **C18SH** and **CholC3SH** or **CholC6SH** are shown in Figure 4.6. These spectral regions confirm the presence of intact cholesterol-based thiolates on a gold surface.

Several studies have shown that the binding energy of the C_{1s} peak can be utilized to roughly determine the relative coverage (i.e., packing density) of the adsorbates on the metal substrate.[47-51] Well-packed alkanethiolate SAMs have the ability to resist the

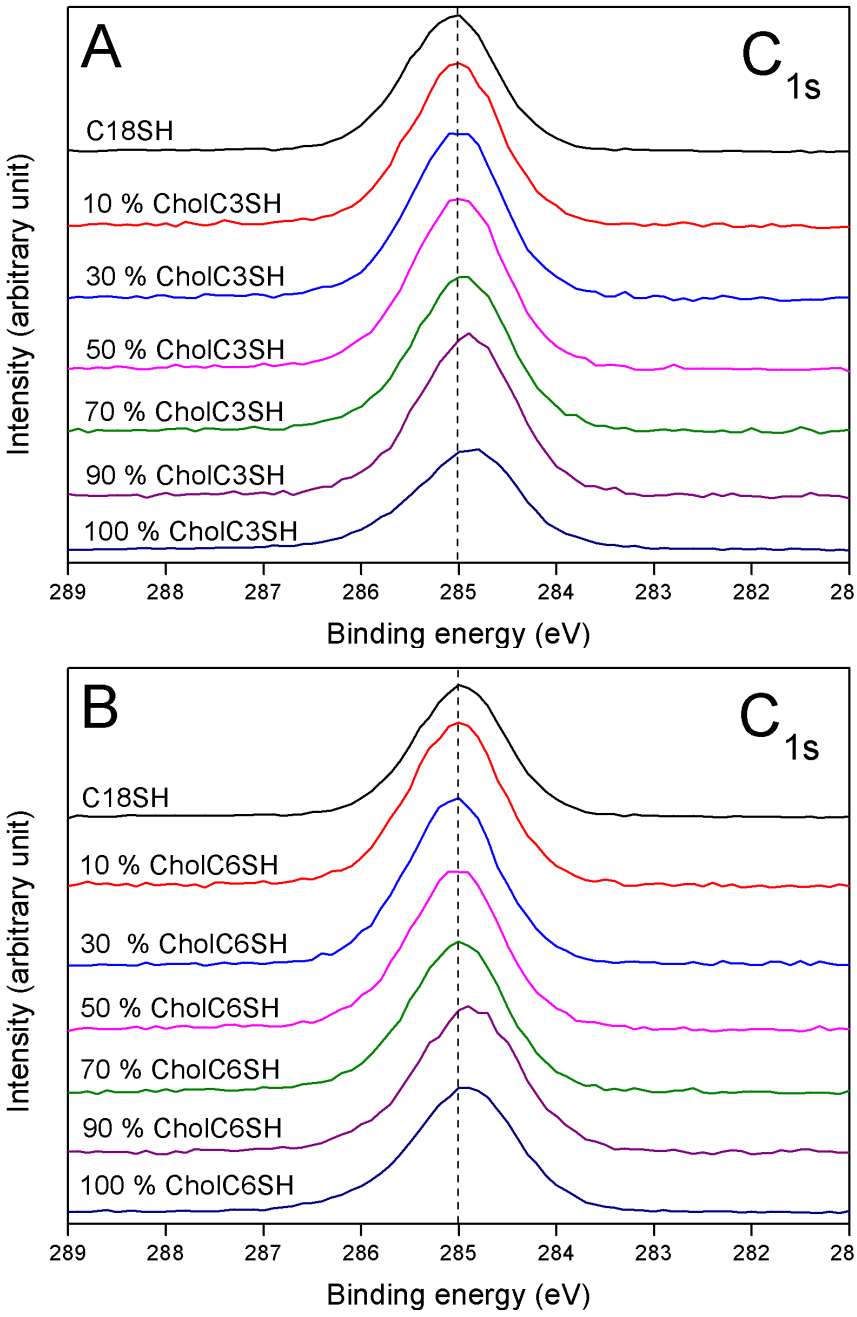

Figure 4.4. XPS spectra of the C_{1s} region for the binary SAMs generated from mixtures of **C18SH** and (A) **CholC3SH** or (B) **CholC6SH**. The dashed lines in the both spectra for the C_{1s} region are aligned with the peak position for the SAM generated from **C18SH** and are intended to serve as a guide for the eye.

emission of photoelectrons from the surface during X-ray irradiation,[49] while loosely packed surfaces act like a poor insulator, making the emission more facile and causing the C_{1s} peak to shift to a lower binding energy.[48,52] For the current research pursued in this report on cholesterol-based SAMs, the data in Chapter 3 helped establish that this methodology was also useful in the examination of these SAMs. For the C_{1s} peak position, the peak obtained from the pure SAM generated from **C18SH** appears at 285.0 eV. The binary SAMs generated from solution mixtures of 10 – 50 % **CholC3SH** and **CholC6SH** have a peak at 285.0 eV, while the binding energy of the C_{1s} peak for the binary SAMs generated from 70 – 100 % **CholC3SH** and **CholC6SH** shifts to a slightly lower energy, as seen in Figure 4.4 (A) and (B). The shift of the C_{1s} peaks for the binary SAMs generated from 70 – 100 % **CholC3SH** and **CholC6SH** to a lower binding energy suggests a lower chain density relative to the SAM generated from **C18SH** and the SAMs generated from solution mixtures of 10 – 50 % **CholC3SH** and **CholC6SH**. However, the structural differences between the extended alkyl chain and the cholesterol moiety and the differences in surface composition of the cholesterol-based adsorbate as the solution composition of this thiol is increased, also impact the C_{1s} peak position.

The increase in the signal-to-noise ratio for the O_{1s} spectra, Figure 4.5, as compared to the C_{1s} spectra, is as expected since the oxygen atom is buried in the film and the signal is attenuated by the hydrocarbon structure above the oxygen atom. Analyzing the data from the O_{1s} spectra must be approached with caution. The absence of a measurable oxygen signal in the SAM formed from **C18SH** indicates the effectiveness of the ultra high vacuum conditions at removing residual ethanol from the

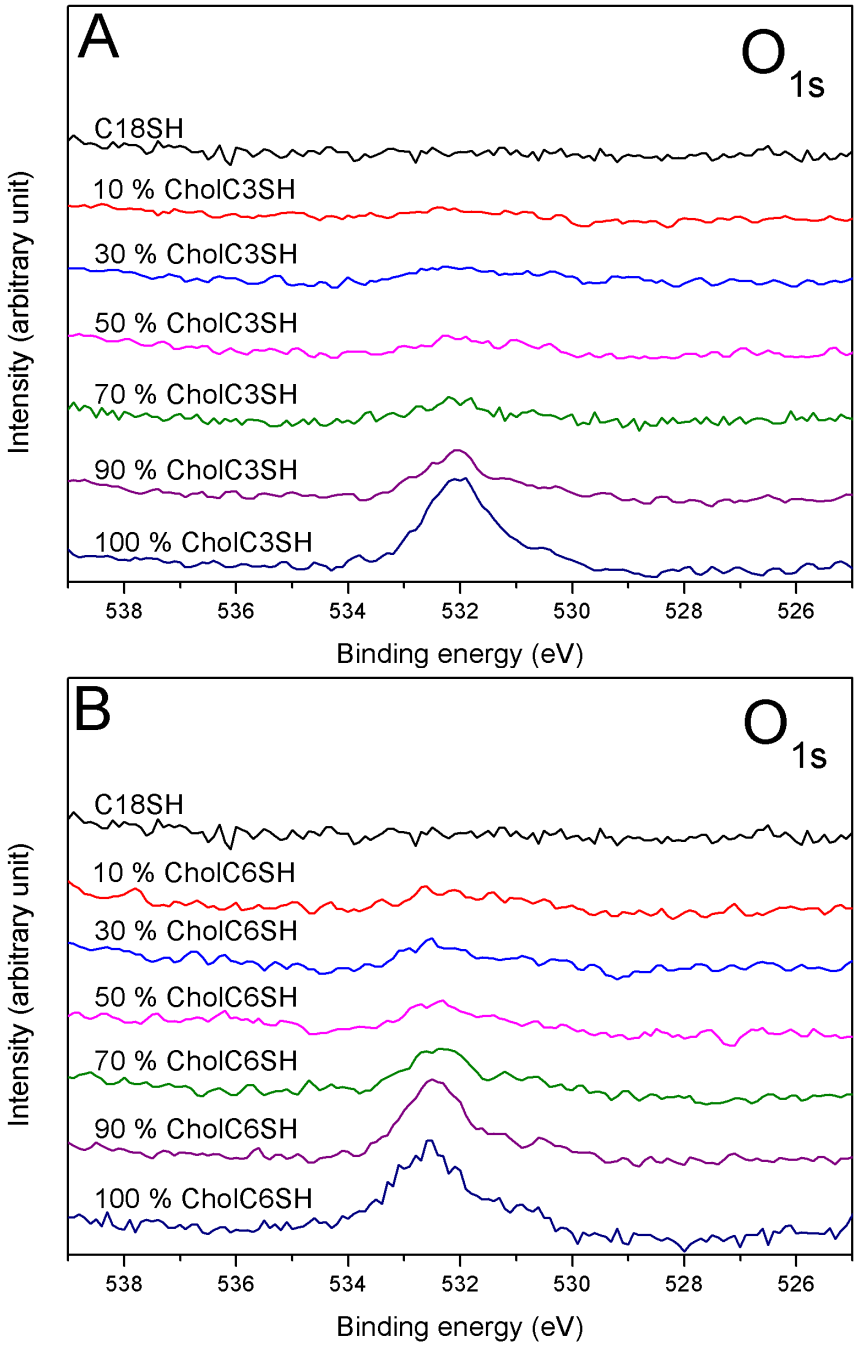

Figure 4.5. XPS spectra of the O_{1s} region for the binary SAMs generated from mixtures of **C18SH** and (A) **CholC3SH** or (B) **CholC6SH**.

cholesterol-containing monolayer film, however, the integration of the area under the oxygen peak should not be relied upon as a sole source for comparison purposes due to the potential for a number of sources of oxygen contamination. With this potential error in mind, the increase in the intensity of the O_{1s} signal for these binary SAMs as the solution concentration increases can be used to roughly estimate the surface composition of the cholesterol-based molecules, *vide infra*. At a solution composition of 90 % cholesterol-based thiol for the binary SAMs developed from **C18SH** and **CholC3SH** or **CholC6SH**, a noticeable O_{1s} peak is observed indicating the presence of the cholesterol-based thiolate on the SAM surface. The binary SAM developed from **C18SH** and **CholC6SH** has a slight O_{1s} peak for the SAM generated from a solution composition of 70 % cholesterol-based thiolate. This O_{1s} peak may indicate a higher surface composition of the cholesterol-based thiolate for the binary SAM generated from **C18SH** and **CholC6SH** as compared to the same solution composition for the binary SAM generated from **C18SH** and **CholC3SH**. In general, the O_{1s} spectra show a delayed adsorption of the cholesterol-based thiolate for both mixed SAM series.

The increase in the signal-to-noise ratio in the S_{2p} spectra is expected for these films owing to the attenuation of signal associated with the distance of the element from the surface of the film, Figure 4.6. The doublet signal located at 162.0 eV ($S_{2p3/2}$) is indicative of bound sulfur on the gold substrate as compared to unbound thiol, which is found at 164 eV and oxidized sulfur at 166 to 168 eV.[53,54] Therefore, only one species of sulfur is present for this series of films. The weak S_{2p} signal has a signal-to-noise ratio that is not optimum, despite best efforts to attain a better ratio, yet still provides

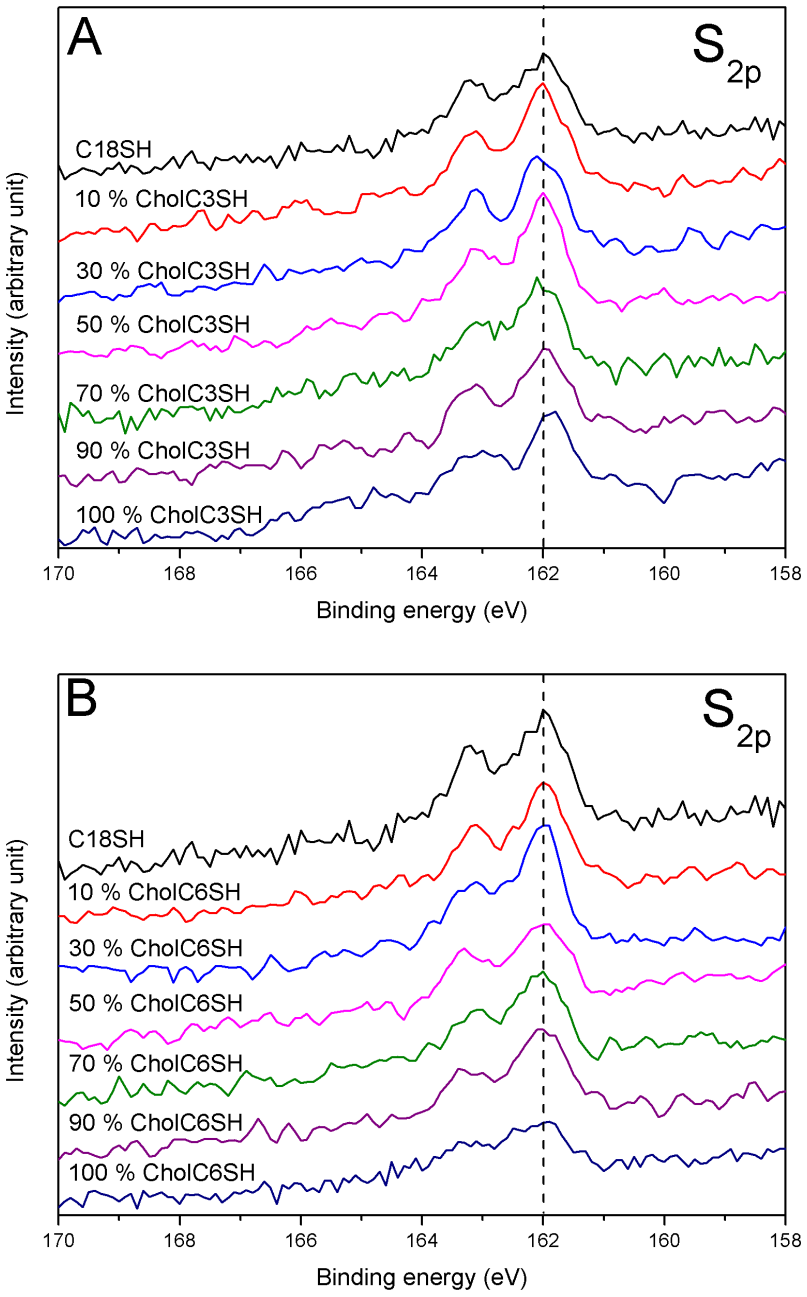

Figure 4.6. XPS spectra of the S_{2p} region for the binary SAMs generated from mixtures of **C18SH** and (A) **CholC3SH** or (B) **CholC6SH**. The dashed lines in the both spectra for the S_{2p} region are aligned with the peak position for the SAM generated from **C18SH** and are intended to serve as a guide for the eye.

discernible peaks from which integrated peak data has been obtained. The S_{2p} signal decreases as the solution concentration increases for these binary SAMs generated from **C18SH** and **CholC3SH** or **CholC6SH**. The chemical environment of the monolayer above the sulfur atom is changing as the surface composition of the cholesterol-based monolayer increases, thus the S_{2p} signal is attenuated more for SAMs with a surface composition predominately cholesterol-based than alkyl-based.

Comparison of the relative integrated peak areas of the individual elemental signals in the form of ratios with gold, such as the ratio of carbon-to-gold (C:Au ratio), is a method of determining relative surface density for a series of films. The C:Au ratio for this series is shown in Figure 4.7 with black squares (■) and are normalized to the pure SAM generated from **CholC3SH** or **CholC6SH**, for purposes of comparison. For binary SAMs generated from a mixture of normal alkanethiols and cholesterol-based thiols, the C_{1s} signal should slightly increase as the surface concentration of the longer cholesterol-based thiolate increases given there are more carbons present in the monolayer to produce a stronger signal. The gold signal is only minimally impacted by the overlaying monolayer, but is subject to variation related to changes in the intensity of the X-ray beam. And the carbon signal not only responds to changes in beam intensity but also increases as n increases, so a comparison of the ratio of carbon-to-gold, normalized to the pure SAM generated from the cholesterol-based thiol, should provide useful information about this series of cholesterol-based SAMs. For both series, the ratios of carbon-to-gold for the mixed SAMs generated from **C18SH** and **CholC3SH** or **CholC6SH** indicate only

minimal change in the surface density of the films as the solution concentration of the cholesterol-based thiol is increased.

The assessment of the relative intensities of the sulfur-to-gold signals (S:Au ratio) for the binary SAMs generated from **C18SH** and **CholC3SH** or **CholC6SH** is shown in Figure 4.7 with red circles (•). The comparison of the S_{2p} and Au_{4f} signals provides insight into the relative packing density of the monolayers. The sulfur-to-gold ratios have been normalized to the pure SAM generated from the cholesterol-based thiol, the SAMs generated from **CholC3SH** or **CholC6SH**, for purposes of comparison. The S:Au ratio has a slight increase for these binary SAMs as the solution composition increases from 0 – 50 % which is consistent with a low surface composition of the cholesterol-based thiolate. For the solution composition 70 – 90 % the S:Au ratio decreases as a consequence of the increase in the attenuation of the S_{2p} signal. The higher attenuation could be a result of an increased packing density and the change in the monolayer as the surface composition resembles that of the pure SAM generated from the cholesterol-based thiols. The increase in the S:Au ratio for the lower solution concentrations of cholesterol-based thiols along with the steady C:Au ratio might be indicative of the cholesterol condensing effect. If the relative presence of sulfur is increasing, despite a measurable increase in film thickness, while the amount of carbon is holding steady, the molecules must be packing more efficiently.

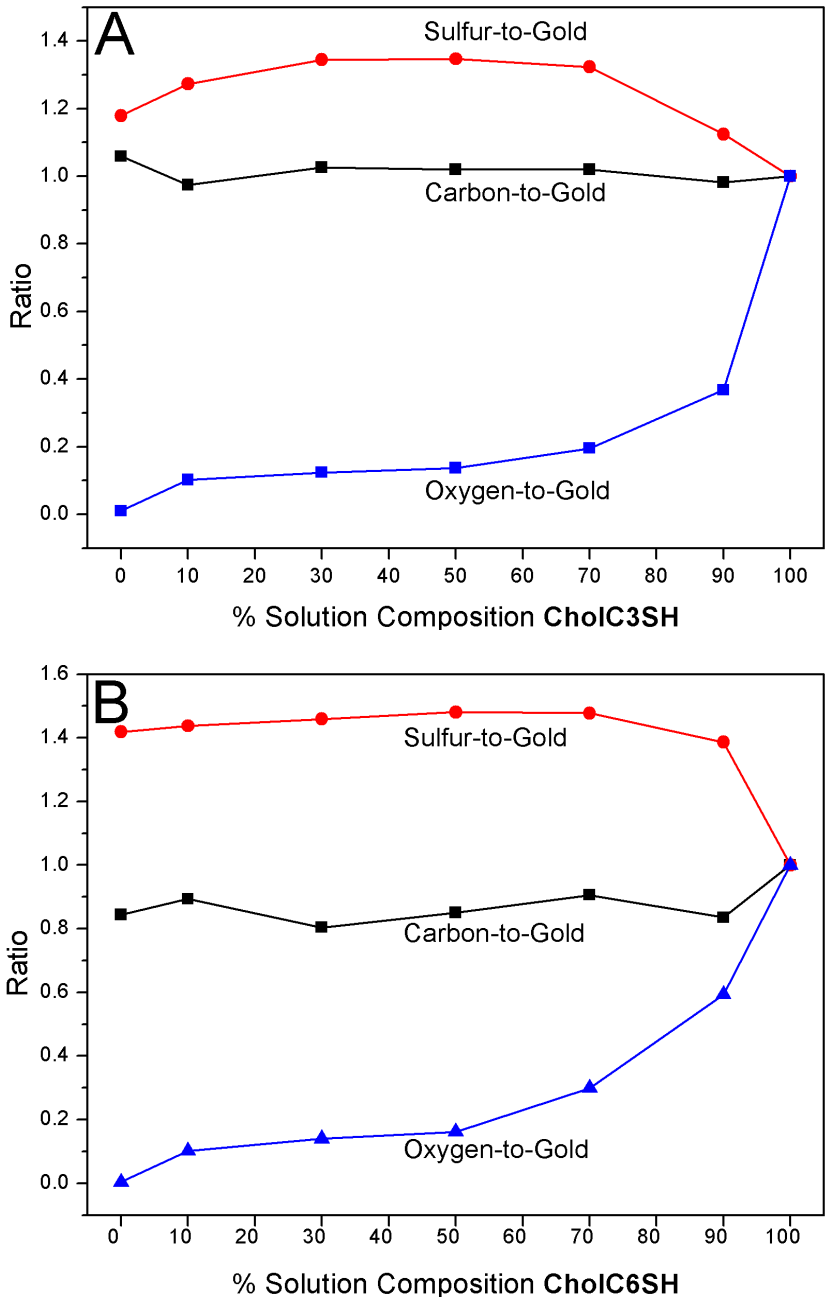

Figure 4.7. The sulfur-to-gold (●), carbon-to-gold (■), and oxygen-to-gold (▲) ratios based on the XPS spectra for the binary SAMs generated from mixtures of **C18SH** and (A) **CholC3SH** or (B) **CholC6SH**. The lines connecting data points are provided as a guide for the eye.

The ratios of the oxygen-to-gold signal for the binary SAMs generated from **C18SH** and **CholC3SH** or **CholC6SH** are shown in Figure 4.7 with blue triangles (▲). As previously mentioned, it cannot be determined if the oxygen signal is from the SAM or a result of contamination, however the comparison of the relative intensities will provide insight into the surface composition, since the cholesterol-based thiolates contain an oxygen atom while the alkylthiolates do not. The oxygen-to-gold ratios have been normalized to the pure SAM generated from the cholesterol-based thiol, the SAM generated from **CholC3SH** or **CholC6SH**, for purposes of comparison. For the binary SAMs with a solution composition 0 – 50 % cholesterol-based thiol, the relative ratios slightly increase. There is a noticeable increase in the O:Au ratios for the SAMs generated from the solution compositions of 70 – 90 % cholesterol-based thiol. This increase in oxygen-to-gold ratio is the result of a higher surface composition of the cholesterol-based thiolate for these binary SAMs. The surface compositions as determined by the O:Au ratios are seen in Figure 4.8 where the red squares (■) show the surface compositions for the binary SAMs generated from **C18SH** and **CholC3SH** and the blue circles (●) show the surface compositions for the binary SAMs generated from **C18SH** and **CholC6SH**. As expected from the IR data, the surface composition of the cholesterol-based thiolates slightly increases as the solution composition increases from 0 – 50 % cholesterol-based thiol and the surface composition greatly increases for the solution compositions 70 – 90 % cholesterol-based thiol. The trends in Figure 4.8 have been interpreted as a clear indication that the bulkier cholesterol-based thiols are the less favored adsorbate for both mixed SAM series.

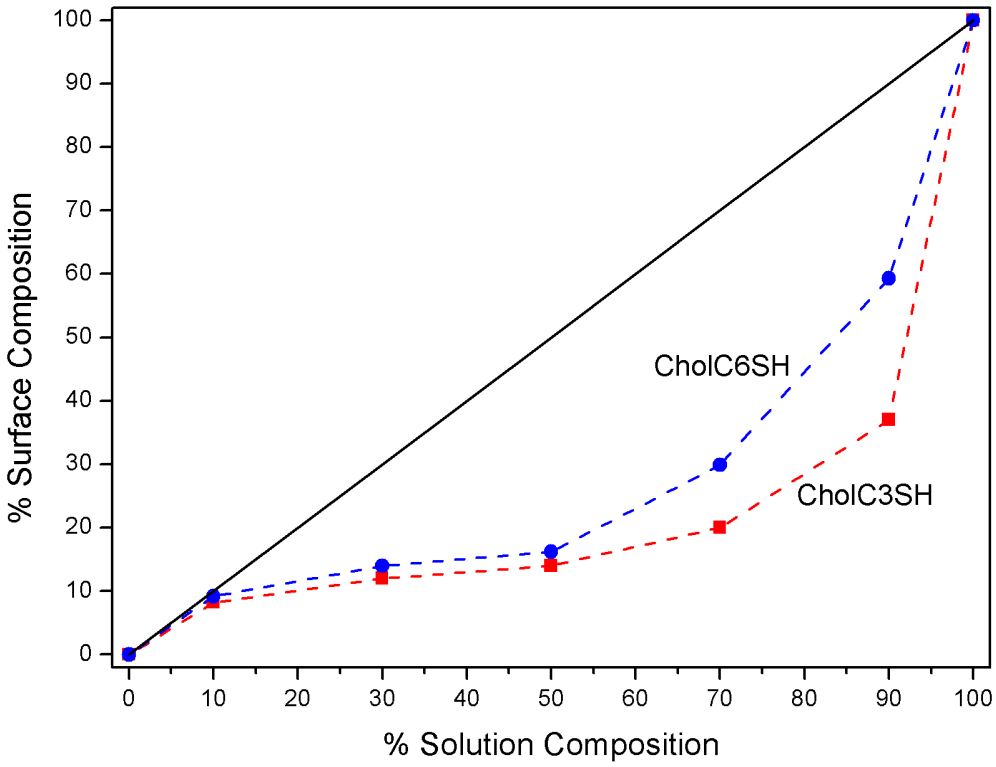

Figure 4.8. The surface composition of SAMs adsorbed from ethanolic mixtures of **C18SH** and **CholC3SH** (■) and **C18SH** and **CholC6SH** (●) based on the composition of the developing solution and the O:Au ratio from XPS data. The solid line indicates where the surface composition and solution composition are equivalent. Dashed lines are provided as guides for the eye.

4.4. Conclusions

A series of cholesterol-based single tailgroup adsorbates were successfully synthesized and used to form double-component SAMs on gold, where the sulfur headgroup is bound to the gold substrate and the cholesterol-based tailgroup extend away from the surface in a well-organized array. The binary SAMs were generated from a series of mixtures of **C18SH** and **CholC3SH** or **CholC6SH**. Monolayers of these mixtures were successfully formed as determined by the ellipsometric and XPS data. For the binary SAMs generated from a solution composition 0 – 70 % cholesterol-based thiol, the resulting film exhibits a surface interface that is similar to that of a pure SAM generated from **C18SH**. These SAMs produced contact angle data that mimic a pure SAM generated from normal alkanethiols. The binary SAMs generated from a solution composition of 90 % cholesterol-based thiol exhibits a surface interface that is a mixture of the two solution components, an extended alkyl chain and a chain terminated by a cholesterol-based moiety. The binary SAMs generated from a 50 % solution composition of **CholC3SH** and a 30 % solution composition of **CholC6SH** show an increase in cholesterol-based thiolates in the surface composition on the PM-IRRAS spectra. A definite overlap of signals from the extended alkyl chains and the cholesterol-based moieties are observed. The XPS data show the binary SAMs formed from mixtures of **C18SH** and **CholC3SH** or **CholC6SH** do not have surface compositions matching that of the developing solution composition, however as the solution composition increases from 70 – 100 % of the cholesterol-based thiol, the surface composition starts to resemble

the solution composition. The elemental ratios show the cholesterol condensing effect for the SAMs generated from solution compositions between 0 and 50 % cholesterol-based thiol. Overall, the new single tailgroup series of molecules are capable of producing a well-structured double-component SAM. Further examination of these thiols within a mixed SAM format, focusing on the solution concentrations between 0 – 50 % cholesterol-based thiol, will provide further insight into the cholesterol condensing effect utilizing self-assembled monolayer films.

4.5. References

(1) Yeagle, P. L. *Biochim. Biophys. Acta* **1985**, *822*, 267–287.

(2) Lipowsky, R.; Sackmann, E. *Structure and Dynamics of the Membranes*; North–Holland: Amsterdam, 1995.

(3) Leathes, J. B. *Lancet* **1925**, *208*, 853–856.

(4) Somerharju, P.; Virtanen, J. A.; Cheng, K. H. *BBA - Mol. Cell Biol. L.* **1999**, *1440*, 32–48.

(5) McConnell, H. M.; Radhakrishnan, A. *BBA - Biomembr.* **2003**, *1610*, 159–173.

(6) Huang, J.; Feigenson, G. W. *Biophys. J.* **1999**, *76*, 2142–2157.

(7) Ivankin, A.; Kuzmenko, I.; Gidalevitz, D. *Phys. Rev. Lett.* **2010**, *104*, 108101–108104.

(8) Wydro, P.; Knapczyk, S.; Lapczynska, M. *Langmuir* **2011**, *27*, 5433–5444.

(9) Mattjus, P.; Bittman, R.; Slotte, J. P. *Langmuir* **1996**, *12*, 1284–1290.

(10) Adam, N. K.; Jessop, G. *Proc. R. Soc. A* **1928**, *120*, 473–482.

(11) Slotte, J. P.; Mattjus, P. *BBA - Lipid Lipid Met.* **1995**, *1254*, 22–29.

(12) Wang, H.; He, G.; Chen, X.; Liu, T.; Ding, L.; Fang, Y. *J. Mater. Chem.* **2012**, *22*, 7529–7536.

(13) Gupta, R. K.; Suresh, K. A. *Colloid Surface A* **2008**, *320*, 233–239.

(14) Sek, S.; Xu, S.; Chen, M.; Szymanski, G.; Lipkowski, J. *J. Am. Chem. Soc.* **2008**, *130*, 5736–5743.

(15) Hung, W. C.; Lee, M. T.; Chen, F. Y.; Huang, H. W. *Biophys. J.* **2007**, *92*, 3960–3967.

(16) Alonso, C.; Kuzmenko, I.; Jensen, T. R.; Kjaer, K.; Lahav, M.; Leiserowitz, L. *J. Phys. Chem. B* **2001**, *105*, 8563–8568.

(17) Dai, J.; Alwarawrah, M.; Huang, J. *J. Phys. Chem. B* **2009**, *114*, 840–848.

(18) Becucci, L.; Scaletti, F.; Guidelli, R. *Biophys. J.* **2011**, *101*, 134–143.

(19) Yang, Z. P.; Engquist, I.; Kauffmann, J. M.; Liedberg, B. *Langmuir* **1996**, *12*, 1704–1707.

(20) Yang, Z.; Engquist, I.; Wirde, M.; Kauffmann, J. M.; Gelius, U.; Liedberg, B. *Langmuir* **1997**, *13*, 3210–3218.

(21) Yang, Z.; Engquist, I.; Liedberg, B.; Kauffmann, J. M. *J. Electroanal. Chem.* **1997**, *430*, 189–195.

(22) Andersson, O.; Ulrich, C.; Bjorefors, F.; Liedberg, B. *Sensor. Actuat. B - Chem.* **2008**, *134*, 545–550.

(23) Indrieri, M.; Suardi, M.; Podesta, A.; Ranucci, E.; Ferruti, P.; Milani, P. *Langmuir* **2008**, *24*, 7830–7841.

(24) Trevor, J. L.; Lykke, K. R.; Pellin, M. J.; Hanley, L. *Langmuir* **1998**, *14*, 1664–1673.

(25) Blasi, L.; Pisignano, D.; Di Benedetto, F.; Maruccio, G.; Ciccarella, G.; Maffei, A.; Vasapollo, G.; Cingolani, R.; Rinaldi, R. *BBA - Biomembr.* **2005**, *1714*, 93–102.

(26) Boden, N.; Bushby, R. J.; Clarkson, S.; Evans, S. D.; Knowles, P. F.; Marsh, A. *Tetrahedron* **1997**, *53*, 10939–10952.

(27) Jeuken, L. J. C.; Connell, S. D.; Nurnabi, M.; O'Reilly, J.; Henderson, P. J. F.; Evans, S. D.; Bushby, R. J. *Langmuir* **2005**, *21*, 1481–1488.

(28) Williams, L. M.; Evans, S. D.; Flynn, T. M.; Marsh, A.; Knowles, P. F.; Bushby, R. J.; Boden, N. *Langmuir* **1997**, *13*, 751–757.

(29) Cheng, Y.; Boden, N.; Bushby, R. J.; Clarkson, S.; Evans, S. D.; Knowles, P. F.; Marsh, A.; Miles, R. E. *Langmuir* **1998**, *14*, 839–844.

(30) Evans, D. F.; Wennerstrom, H. *The Colloidal Domain: Where Physics, Chemistry, Biology, and Technology Meet*; Second ed.; Wiley-VCH: New York, 1999.

(31) McIntosh, T. *Biochim. Biophys. Acta* **1978**, *513*, 43–58.

(32) Bentz, J.; Ellens, H.; Szoka, F. C. *Biochemistry* **1987**, *26*, 2105–2116.

(33) Foglia, F.; Barlow, D. J.; Szoka, F. C.; Huang, Z.; Rogers, S. E.; Lawrence, M. J. *Langmuir* **2011**, *27*, 8275–8281.

(34) Khelashvili, G.; Pabst, G.; Harries, D. *J. Phys. Chem. B* **2010**, *114*, 7524–7534.

(35) Laibinis, P. E.; Nuzzo, R. G.; Whitesides, G. M. *J. Phys. Chem.* **1992**, *96*, 5097–5105.

(36) Folkers, J. P.; Laibinis, P. E.; Whitesides, G. M. *Langmuir* **1992**, *8*, 1330–1341.

(37) Bain, C. D.; Evall, J.; Whitesides, G. M. *J. Am. Chem. Soc.* **1989**, *111*, 7155–7164.

(38) Shon, Y. S.; Lee, S.; Colorado, R., Jr.; Perry, S. S.; Lee, T. R. *J. Am. Chem. Soc.* **2000**, *122*, 7556–7563.

(39) Porter, M. D.; Bright, T. B.; Allara, D. L.; Chidsey, C. E. D. *J. Am. Chem. Soc.* **1987**, *109*, 3559–3568.

(40) Nuzzo, R. G.; Fusco, F. A.; Allara, D. L. *J. Am. Chem. Soc.* **1987**, *109*, 2358–2368.

(41) Nuzzo, R. G.; Dubois, L. H.; Allara, D. L. *J. Am. Chem. Soc.* **1990**, *112*, 558–569.

(42) Snyder, R. G.; Strauss, H. L.; Elliger, C. A. *J. Phys. Chem.* **1982**, *86*, 5145–5150.

(43) Bradshaw, A. M.; Richardson, N. V. *Pure Appl. Chem.* **1996**, *68*, 457–467.

(44) Lummerstorfer, T.; Hoffmann, H. *Langmuir* **2004**, *20*, 6542–6545.

(45) Greenler, R. G. *J. Chem. Phys.* **1966**, *44*, 310–315.

(46) Laibinis, P. E.; Whitesides, G. M.; Allara, D. L.; Tao, Y. T.; Parikh, A. N.; Nuzzo, R. G. *J. Am. Chem. Soc.* **1991**, *113*, 7152–7167.

(47) Frey, S.; Heister, K.; Zharnikov, M.; Grunze, M.; Tamada, K.; Colorado, R., Jr.; Graupe, M.; Shmakova, O. E.; Lee, T. R. *Isr. J. Chem.* **2000**, *40*, 81–97.

(48) Biebuyck, H. A.; Bain, C. D.; Whitesides, G. M. *Langmuir* **1994**, *10*, 1825–1831.

(49) Ishida, T.; Hara, M.; Kojima, I.; Tsuneda, S.; Nishida, N.; Sasabe, H.; Knoll, W. *Langmuir* **1998**, *14*, 2092–2096.

(50) Bain, C. D.; Troughton, E. B.; Tao, Y. T.; Evall, J.; Whitesides, G. M.; Nuzzo, R. G. *J. Am. Chem. Soc.* **1989**, *111*, 321–335.

(51) Tamada, K.; Ishida, T.; Knoll, W.; Fukushima, H.; Colorado, R., Jr.; Graupe, M.; Shmakova, O. E.; Lee, T. R. *Langmuir* **2001**, *17*, 1913–1921.

(52) Park, J. S.; Smith, A. C.; Lee, T. R. *Langmuir* **2004**, *20*, 5829–5836.

(53) Castner, D. G.; Hinds, K.; Grainger, D. W. *Langmuir* **1996**, *12*, 5083–5086.

(54) Sun, F.; Grainger, D. W.; Castner, D. G.; Leach-Scampavia, D. K. *Macromolecules* **1994**, *27*, 3053–3062.

Chapter 5. Conclusions

5.1. Conclusions

The mechanism of the cholesterol condensing effect is currently debated and studied through the use of molecular simulations and experimentally with LB films. We studied the cholesterol condensing effect with self-assembled monolayers by designing molecules to mimic the biological phenomenon. The first type of molecule contains a cholesterol-based single tailgroup with a hydrocarbon methylene spacer and a thiol headgroup. The second type of molecules are designed similar to molecules studied by Lee *et al*. that contain two different tailgroups.[1] The double tailgroup design allows for the formation of a monolayer that is homogenously mixed and contains a multi-component surface yet is comprised of a single-component. With these advantages in mind, novel cholesterol-based molecules containing one and two tailgroups were designed, synthesized, and used to form one-component and two-component self-assembled monolayers (SAMs). The structure and surface interfacial properties of all monolayers were examined by ellipsometry, contact angle goniometry, surface IR spectroscopy, and XPS characterization.

In Chapter 2, a series of single tailgroup cholesterol-based molecules with a structure **CholCnSH**, where n = 2, 3, 4, 5, 6, 9, and 12 were designed and synthesized. The new single-chain cholesterol-based thiols were successfully synthesized and used to

form single-component SAMs on gold. Characterization of all the monolayers in the series revealed that these molecules can be used to generate SAMs at room temperature that are more efficiently packed than films formed from **CholSH**. The SAMs generated from **CholC9SH** and **CholC12SH** have a decreased molecular tilt, increased density, and increased order than the other cholesterol-based SAMs, yet are not as dense or crystalline as a SAM generated from **C18SH**. The addition of the methylene spacer to cholesterol allows for a better formation of a SAM than thiocholesterol. These molecules show potential for use in studying the cholesterol condensing effect as compared to thiocholesterol.

In Chapter 3, a series of cholesterol-based, double tailgroup adsorbates were successfully synthesized and used to form single-component SAMs on gold, where the sulfur headgroup is bound to the gold substrate and the double tailgroups extend away from the surface in a well-organized array. Monolayers of these molecules were successfully formed as determined by the ellipsometric and XPS data. For the SAM generated from **C18C3CholSH**, the resulting film exhibits a surface interface that is a mixture of the two tailgroups, an extended alkyl chain and a chain terminated by a cholesterol-based moiety. This SAM produced contact angle data that fell between that of the single-component SAMs generated from the two individual tailgroups, respectively. The SAMs generated from **C18C3CholSH**, **C18C6CholSH**, and **C18C9CholSH** produce spectra that show the presence of both tailgroups as seen in the PM-IRRAS data. A definite overlap of signals from the extended alkyl chains and the

cholesterol-based moieties are observed. The XPS data show that the SAMs formed from **C18C3CholSH**, **C18C6CholSH**, and **C18C9CholSH** are denser monolayers compared to the SAM formed from **CholSH** and almost as dense as the SAM formed from **C18SH**. Overall, the new double tailgroup series of molecules are capable of producing a well-structured single-component SAM. Further examination of these thiols within a mixed SAM format, along with similarly structured cholesterol-based molecules, will provide insight into the cholesterol condensing effect utilizing self-assembled monolayer films.

In Chapter 4, a series of cholesterol-based, single tailgroup adsorbates were used to form double-component SAMs on gold, where the sulfur headgroup is bound to the gold substrate and the cholesterol-based tailgroup extend away from the surface in a well-organized array. The binary SAMs were generated from a series of mixtures of **C18SH** and **CholC3SH** or **CholC6SH**. Monolayers of these mixtures were successfully formed as determined by the ellipsometric and XPS data. For the binary SAMs generated from a solution composition 0 – 70 % cholesterol-based thiol, the resulting film exhibits a surface interface that is similar to that of a pure SAM generated from C18SH. These SAMs produced contact angle data that mimic a pure SAM generated from normal alkanethiols. The binary SAMs generated from a solution composition of 90 % cholesterol-based thiol exhibits a surface interface that is a mixture of the two solution components, an extended alkyl chain and a chain terminated by a cholesterol-based moiety. The binary SAMs generated from a 50 % solution composition of **CholC3SH** and a 30 % solution composition of **CholC6SH** show an increase in cholesterol-based

thiolates in the surface composition on the PM-IRRAS spectra. A definite overlap of signals from the extended alkyl chains and the cholesterol-based moieties are observed. The XPS data show the binary SAMs formed from mixtures of **C18SH** and **CholC3SH** or **CholC6SH** do not have surface compositions matching that of the developing solution composition, however as the solution composition increases from 70 – 100 % of the cholesterol-based thiol, the surface composition starts to resemble the solution composition. The elemental ratios show the cholesterol condensing effect for the SAMs generated from solution compositions between 0 and 50 % cholesterol-based thiol. Overall, the new single tailgroup series of molecules are capable of producing a well-structured double-component SAM. Further examination of these thiols within a mixed SAM format, focusing on the solution concentrations between 0 – 50 % cholesterol-based thiol, will provide further insight into the cholesterol condensing effect utilizing self-assembled monolayer films.

After analysis of the single-component and binary SAMs, we have shown that it is possible to study the cholesterol condensing effect utilizing self-assembled monolayers. In the binary SAM study, the condensing effect was observed at low solution and surface compositions which disproves the Condensed Complex Model, suggested by Finean.[2-4] The surface composition is approximately 12 % cholesterol-based moiety which does not correlate with the suggested stoichiometric ratios of the Condensed Complex Model (*e.g.*, 1 cholesterol: 2 lipids or 3 cholesterols: 6 lipids). With additional experimentation, the new molecules, both single-chained and double-chained, will provide insight and

potentially support one of the other mechanistic models, Superlattice[5] or Umbrella Model[6], of the cholesterol condensing effect through the use of self-assembled monolayers.

5.2. References

1. Zhang, S.; Jamison, A. C.; Schwartz, D. K.; Lee, T. R. *Langmuir* **2008,** *24*, 10204–10208.
2. Finean, J. *Cell. Mol. Life Sci.* **1953,** *9*, 17–19.
3. Needham, D.; McIntosh, T. J.; Evans, E. *Biochemistry* **1988,** *27*, 4668–4673.
4. Radhakrishnan, A.; McConnell, H. M. *J. Am. Chem. Soc.* **1999,** *121*, 486–487.
5. Chong, P. L. *Proc. Natl. Acad. Sci. U. S. A.* **1994,** *91*, 10069–10073.
6. Huang, J.; Feigenson, G. W. *Biophys. J.* **1999,** *76*, 2142–2157.

Chapter 6. Future Work

6.1. Future Work

Within this dissertation, we present the design and synthesis of single-chain and double-chain cholesterol-based thiols for use in self-assembled monolayers (SAMs). Utilizing binary SAMs with the single-chain cholesterol-based thiol and *n*-octadecanethiol, we were able to show the effects of cholesterol on a trans-extended alkane monolayer. The data in this dissertation need to be verified through repetition of the experiments. The data for the single-component SAMs were collected twice which confirmed the trends however triplicate data collection is preferred. The data for the binary SAMs were only collected once and therefore must be repeated in a similar manner. Future investigations involving the molecules described in this dissertation shall provide more information about the cholesterol condensing effect.

Utilizing the molecules described within this dissertation, an investigation of the lower solution compositions for the synthesis of a binary SAM should provide more information about the cholesterol condensing effect. The binary SAM study showed that SAMs generated from 0 – 50 % solution composition of the cholesterol-based moiety results in denser monolayers as an affect of the cholesterol condensing effect. Further investigations within this narrow range, may be able to provide a more precise solution composition to produce a dense mixed monolayer. An atomic force microscopy study of the binary SAMs investigated in this dissertation, may provide support for the

Superlattice Model based on a topography image. The difference in the length of *n*-alkanethiol and the cholesterol-based thiol will create a topography image that can be used to determine the exact positioning of the molecules. If the molecules within the monolayer are aligned systematically, then the Superlattice Model is supported.[1] A sum frequency generation study of the SAMs generated within this dissertation will also provide more information about the monolayer systems. The data collected through sum frequency generation spectroscopy will support the previously collected data. This additional microscopy data may aid in the understanding of the cholesterol condensing effect.

A future study to be conducted involves the double-chained cholesterol-based thiols and *n*-eicosanethiol for use in a binary SAM, as seen in Figure 6.1 (A). The pure SAM generated from the double-chain cholesterol-based thiols is a well-packed dense monolayer. Thus the binary SAMs generated from these thiols should form a denser monolayer as the alkyl tailgroups will add support for ordering and packing via van der Waals interactions, which will provide more insight into the condensing effect.

Another study to be done will involve the use of both of these molecules for the formation of a ternary SAM, as seen in Figure 6.1 (B). Similar to the work of Zhang *et al*., the double-tailgroup cholesterol-based thiol will be utilized as a linactant, a two-dimensional surfactant, in a SAM formed from *n*-eicosanethiol, the double-chain cholesterol-based thiol, and the single-chain cholesterol-based thiol.[2] The ternary SAMs should form a denser monolayer than the one observed by Zhang which consisted of hydrocarbons and fluorocarbons that are known to phase seperate.[2] Since cholesterols

and normal alkyl chains do not phase separate, the ternary SAMs formed from these cholesterol-based thiols should provide further information about the condensing phenomenon.

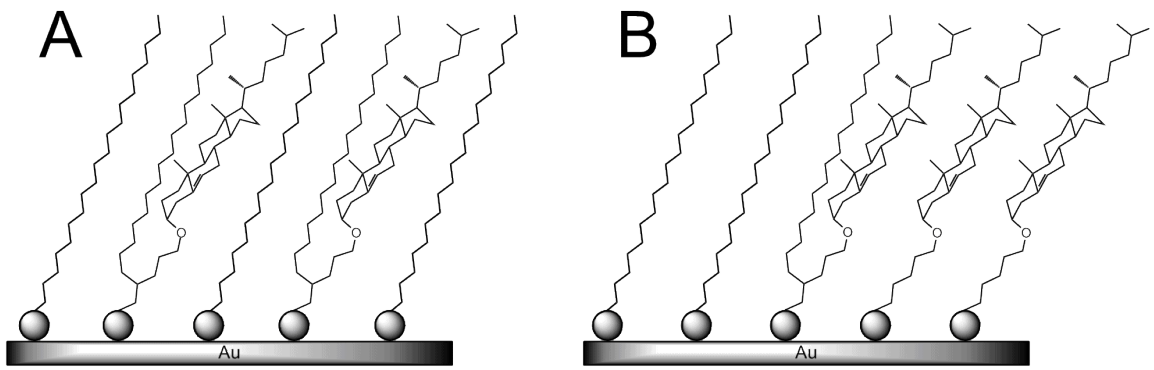

Figure 6.1. Illustrations of the structures of SAMs generated from (A) normal alkanethiols and double-chained cholesterol-based thiols and (B) normal alkanethiols, double-chained cholesterol-based thiols, and single-chain cholesterol-based thiols. Molecular sizes and dimensions are not drawn to scale.

A final study will involve the comparison of SAMs and Langmuir-Blodgett monolayers generated from the new double-chained and single-chained cholesterol-based molecules. Single-chained and double-chained cholesterol-based carboxylic acids were also synthesized that share the same tailgroups as the thiols described in this dissertation. For ternary systems, Trabelsi *et al.* utilized Langmuir monolayers to determine that the double-chained molecules preferentially segregate to the phase boundary of a mixed system.[3] A comparison of the monolayer properties for these cholesterol-based molecules will aid in the understanding of the cholesterol condensing effect.

6.2. References

1. Chong, P. L. *Proc. Natl. Acad. Sci. U. S. A.* **1994,** *91*, 10069–10073.
2. Zhang, S.; Jamison, A. C.; Schwartz, D. K.; Lee, T. R. *Langmuir* **2008,** *24*, 10204–10208.
3. Trabelsi, S.; Zhang, S.; Lee, T. R.; Schwartz, D. K. *Phys. Rev. Lett.* **2008,** *100*, 037802/1–037802/4.

Appendix I. Magnetic Microorganisms: A Novel, Versatile Experiment Utilizing Nanotechnology to Observe Microorganisms for High School Students

Lynn M. Tarkington,[†] William W. Bryan,[†] Elizabeth A. Raska,[‡] Supparesk Rittikulsittichai,[†] Chien-Hung Li,[†] Michael M. Cubacub,[‡] and T. Randall Lee*,[†]

[†] Department of Chemistry, University of Houston, Houston, Texas 77204, United States

[‡] North Shore Senior High School, Houston, Texas 77049, United States

AP.1. Abstract

A laboratory experiment is described in which high school students mimic current research by incorporating nanotechnology into an experiment about microorganisms. This experiment integrates chemistry into a traditional biological laboratory. Magnetic Fe_3O_4 nanoparticles and *Paramecium aurelia* combine to create magnetic microorganisms.

Keywords:

Nanotechnology, Magnetic Nanoparticles, High School/Introductory Biology, Laboratory Instruction, Hands-On learning/Manipulatives, Application of Chemistry in a Biological

Laboratory, Laboratory Equipment/Apparatus, Microorganism, Eukaryotes, Paramecium, Protist

AP.2. Introduction

Nanotechnology is a versatile area of study encompassing medicine, chemistry, biology, engineering, and many other areas.[1] This interdisciplinary field has a lot to offer and should be taught to secondary students to excite and inform students of the possibilities within nanotechnology. This interdisciplinary experiment uses the chemistry and physics of magnetic nanoparticles to magnetically control microorganisms for biological observation and manipulation reflecting research performed in a university research lab.[2-6] The incorporation of leading research topics into required educational material can prove difficult. This experiment provides a method to introduce "new" science into a traditional lesson about microorganisms and protists. This experiment provides an opening for discussions about environmental concerns of nanotechnology and the engineering of nanotechnology.

Nanotechnology is employed in several everyday items including sunscreen, stain-free clothing, make-up, stained glass, and medicine.[1,5,7] This nanotechnology revolution, which consists of particles and materials with at least one dimension in the range of 1 to 100 nm, has occurred due to the distinctive physical properties of the materials caused by the high surface-to-area ratio. For example, these properties are utilized in medicine for the antibacterial properties of nanosilver.[6,8] Scientists are trying

to engineer nanorobots that are small enough to be undetected and can carry a load to a desired location.[3,9] Scientists are modeling nanorobots after microorganisms for their motility, energy source, and size.[8,9]

Paramecium aurelia are fresh water protist typically found in pond scum. These ciliated unicellular microorganisms are a popular species to study in secondary educational biological laboratories for their ability to visualize in an optical microscope, ability to observe organelles, and relatively cheap cost. Eukaryotic organisms have been used for years in research laboratories for photodynamic therapy,[10] toxicology,[11,12] bioaccumulation,[13] and environmental impact.[6,14] Their ability to phagocytise particulate matter and swim at approximately 2,700 μm/second makes *P. aurelia* an attractive model for this study.

In this two-day experiment, the students combine *Paramecia aurelia* with magnetic Fe_3O_4 nanoparticles. In a high school laboratory setting, it is not possible to observe the ingestion of nanoparticles with a basic optical microscope, even on 400x power; however, once internalized, the students can magnetically manipulate the microorganisms and visualize nanoparticle aggregates within the organisms. This manipulation allows the students to observe cilia movement, organelles, and other scientific discoveries associated with microorganisms. The *Paramecia aurelia* stay magnetic for up to one week without cell death when provided with a food source.

AP.3. Experimental Section

Introductory Lecture. An introductory lecture provided the students with the principles needed to fully understand the concepts covered in this experiment. The lecture topics include nanotechnology and polymers. Several examples of nanotechnology were discussed to relate this experiment to the student's every-day lives.

Materials and Equipment. *Paramecium aurelia* were purchased from Carolina Biological Supply Company and used as purchased. A daily aeration is necessary to keep the organisms alive. All other chemicals were purchased from Sigma Aldrich and used without any further purification. Several magnets were purchased from online venders including a grade N42 bar magnet and smaller rare-earth magnets. Necessary equipment includes a Qualitron microcentrifuge that can rotate up to 6,400 rotations per minute (2000 x g) and an optical microscope with 40x, 100x, and 400x magnification. Plastic 1.5 mL microtubes, plastic 5 mL disposable pipettes, and glass slides with cover sheets were used in this experiment.

Magnetic Fe_3O_4 Nanoparticle Synthesis. The targeted magnetic Fe_3O_4 particles can be synthesized by straightforward modification of a procedure reported by Li and co-workers.[15] In this modified procedure, a round-bottomed flask is charged with $FeCl_3.6H_2O$ (2.0 g), which is then dissolved in 15 mL of ethylene glycol followed by the addition of sodium acetate (5.4 g). The latter addition leads to a rapid change in the color

of the solution from orange to brown. The solution is stirred for an additional 30 min and then injected at once into a round-bottomed flask containing a vigorously stirred solution of poly(vinylpyrrolidone) (0.60 g) in 60 mL of ethylene glycol heated to 180 °C. The mixture is then vigorously stirred for 8 h. After cooling the solution to room temperature, the resulting black precipitate is collected using a bar magnet. The particles are purified by repeated cycles of washing and redispersing in ethanol and Milli-Q water. By adjusting the amount of the iron precursor, the diameters of these magnetic Fe_3O_4 particles can be tuned from less than 10 nanometers to several hundred nanometers. The nanoparticles were visualized with SEM and TEM spectroscopy to confirm size (Figure AP.1).

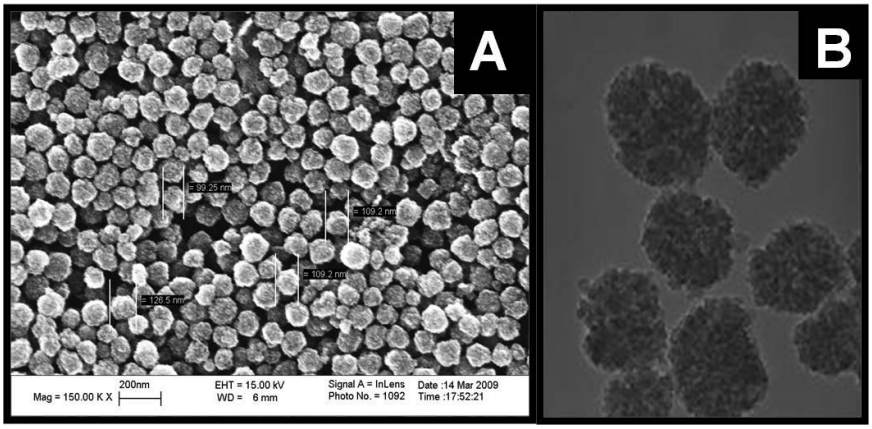

Figure AP.1. SEM (A) and TEM (B) images of Fe_3O_4 nanoparticles.

A similar magnetic Fe_3O_4 nanoparticle solution can also be purchased from Sigma Aldrich (product number 725358).

Experimentation Preformed by Students. Using 1.5 mL microtubes, the students acquired 3 drops of concentrated nanoparticle solution (100 mg/mL in distilled H_2O) and added 10 mg of either poly(ethylene oxide) or poly(vinylpyrrolidone). The students added enough distilled H_2O to fill the microtube and thoroughly mixed the solution by shaking it for 3 minutes. After 5 minutes of centrifugation at highest speed, the students used a grade N42 bar magnet to hold the particles at the bottom of the microtube while pipetting out the liquid. The washing process (add H_2O, mix, centrifuge, remove liquid) must be completed a total of 3 times to prevent any contamination of the polymers to the microorganisms. After the third wash, the students removed the excess liquid leaving the nanoparticles at the bottom of the microtube. The students added approximately 1 mL of microorganism solution to the microtube and incubated overnight to ensure internalization of the nanoparticle by the *Paramecium aurelia.*

On day two of the experiment, the students pipetted a few drops of the incubated solution onto a glass slide and observed the microorganisms under an optical microscope. The rare-earth magnets were used to control the *P. aurelia* while on the glass slide. The grade N42 bar magnet will pull the nanoparticle out of the organism causing cell death. A digital camera was used to take pictures of the microorganisms. After all observations were made, the students cleaned up the slides with soap and water and disposed of any remaining nanoparticle solution in a labeled waste bottle. All microorganisms were disposed of with bleach/water mixture.

Closing Lecture. A final lecture was prepared to ensure the students completed the experiment and learned the concepts that were being taught. The lecture allowed the students to share their findings and propose questions about further experiments. Environmental concerns and the future of nanotechnology were covered in the closing lecture.

AP.4. Hazards

All chemicals used are listed as irritants and must be handled with appropriate personal protective equipment (goggles, lab aprons, gloves) as indicated in the material safety data sheets (MSDS). The nanoparticles are relatively safe yet must be disposed of properly. Labeled waste containers should be made available for any waste solutions. The rare-earth magnets and bar magnets used for magnetic nanoparticle manipulation are powerful and should be handled with care to avoid pinching. The microorganisms introduce potential hazard and should be disposed of properly with bleach. It is advised that all working surfaces be wiped down with a 25 % bleach/water solution to prevent illness caused by microorganisms. For additional safety and hazard information of all chemicals and organisms please refer to the MSDS provided by the vendors.

AP.5. Results and Discussion

After 12 hours of incubation, *Paramecium aurelia* were able to be magnetically manipulated. Figure AP.2 shows *P. aurelia* after internalization of the magnetic Fe_3O_4 nanoparticles at 12 hours and 4 days. After one day incubation, the Fe_3O_4 nanoparticles appear to have aggregated together either through self attraction of the particle to itself or through the organism's digestive process, phagocytosis.

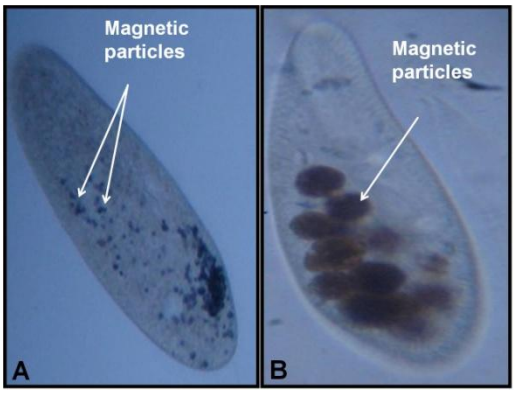

Figure AP.2. Viewed with 400x power on an optical microscope, *Paramecium aurelia* after internalization of Fe_3O_4 nanoparticles at 12 hours incubation (A) and 4 days incubation (B).

This experiment was performed by 40 groups of 4 – 6 Advanced Placement® biology students. The students were able to take a picture of their organisms and show the attraction of the organism to a magnet (Figure AP.3).

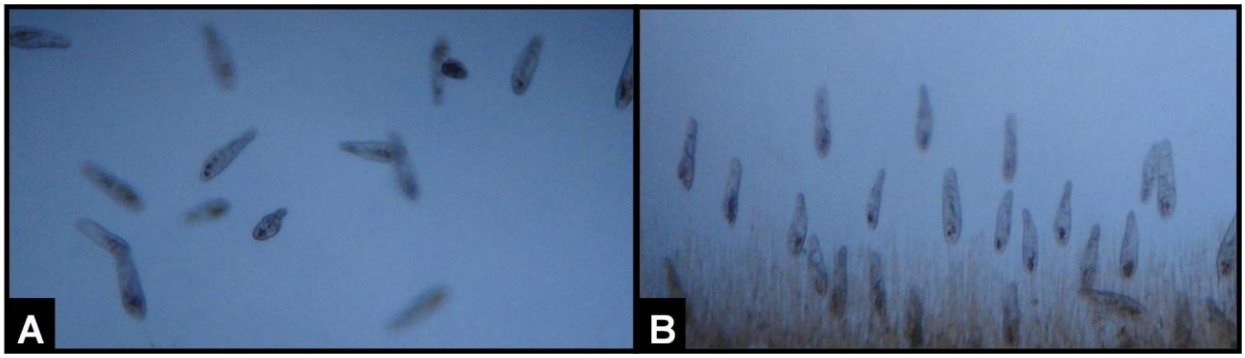

Figure AP.3. Viewed under an optical microscope at 40x power, *Paramecium aurelia* swimming freely (A) and being controlled with a magnet located at the bottom of the picture (B). Nanoparticle waste is also attracted to the magnet as seen in B.

AP.6. Conclusions

Nanotechnology was introduced and utilized in a basic experiment that most students can perform. In a two-day experiment, the students were able to observe microorganisms and experience a portion of relevant research. Many students described this experiment as "cool" and questioned what else they could expose to magnetic nanoparticles for manipulation. Several students expanded this experiment, different types of microorganisms and/or different types of nanoparticles, for use as a senior research project and as a science fair project.

AP.7. Associated Content

AP. 7.1. Laboratory Student Handout

Focus Questions: We use nanotechnology in several every-day items, so what happens when nanoparticles and microorganisms combine?

Learning objectives:

- to determine the effect of the addition of iron oxide (Fe_3O_4) nanoparticles to a solution containing microorganisms
- to observe *Paramecium aurelia*
- to be able to explain what is nanotechnology

The goal of this investigation is to develop an understanding of how nanoparticles interact with *Paramecium aurelia*. Through the use of magnetic Fe_3O_4 nanoparticles, you should be able to control the microorganisms so that you can observe cilia movement, organelles, and possibly budding.

During this experiment you will develop a hypothesis, test that hypothesis, and make notes of all observations. After the experiment, you should be able to identify all parts of *Paramecium aurelia* and be able to postulate concerns regarding nanotechnology.

LABORATORY SAFETY

In this laboratory, you will work with *Paramecium aurelia* and Fe_3O_4 nanoparticles.

- *Work surface*: any work surface that may become contaminated (such as countertops, etc.) must be cleaned *with a* 25 % bleach/water solution to avoid future contamination.
- *Waste*: All waste containing Fe_3O_4 nanoparticles must be carefully poured into the labeled waste bottle. All solutions containing microorganisms must be placed in the bleach/water bucket for disposal. NOTHING should be poured down the sink drain.
- *Protective gloves*: Wear gloves while handling the microorganisms. Do not touch, eat or drink your microorganism samples as they can make you sick.
- *Eyewear* - safety goggles should be worn at all times while in the laboratory.

EXPERIMENTAL PROCEDURE

Day 1:

1. Obtain the following materials and bring them to your bench:

   2 - Disposable pipettes
   1 - Beaker with 50 mL distilled water
   1 - Labeled waste beaker
   1 - Marker
   1 - grade N42 bar magnet
   1 - Microtube

2. Label the microtube according to your group number and class period.
3. Obtain 3 drops of concentrated magnetic nanoparticle solution in your microtube.

4. Add 10 mg of either poly(ethylene oxide) or poly(vinylpyrrolidone) to the microtube.
5. Using a pipette, fill the microtube with water till full (~ 1.5 mL).
6. Close the lid and shake for 3 minutes. Shake it vigorously to thoroughly mix.
7. Place in the centrifuge and spin for 5 minutes on the highest setting.
8. Carefully remove the microtube from the centrifuge and place the tip on the N43 bar magnet.
9. Carefully remove the liquid from the microtube with the other pipette. Be sure to leave the brown nanoparticle pellet at the bottom of the microtube.
10. Repeat steps 5 – 9 two more times. Three total washings are necessary.
11. After the third wash, remove all possible liquid without removing the brown nanoparticle pellet.
12. Add ~ 1.5 mL solution from the microorganism container. Be sure to use the liquid at the bottom of the cup near the food source to ensure several *Paramecium aurelia*.
13. Close the lid and gently mix the microtube. Do not shake too vigorously or you will kill the organisms.
14. When the nanoparticle pellet is no longer visible, open the lid and place in a tube rack for incubation overnight.

Day 2:

1. Obtain the following materials and bring them to your bench:

   1 - Disposable pipette Your microtube

1 - Optical microscope 1 - Rare-earth magnet

1 - Glass slide 1 - Cover slip

2. Close the lid to the microtube and gently mix.
3. With a disposable pipette, place 1 – 2 drops of nanoparticle/microorganism solution onto the slide.
4. Cover with a cover slip.
5. Place under the optical microscope and observe.
6. Use a rare-earth magnet to manipulate the microorganisms.
7. After observing, rinse the slide and slide cover with the 25 % bleach/water solution. Be careful with the bleach.
8. Place the clean slide and slide cover on the front bench for other groups to use.
9. When done with the experiment, pour the nanoparticle/microorganism solution into the 25 % bleach/water waste bottle.
10. Wipe up the bench with 25 % bleach/water solution.

REQUIRED OBSERVATIONS:

- Draw *Paramecium aurelia* as you see it under the microscope on all three powers (40x, 100x, and 400x).
- Label all possible organelles for the organism.
- Count the number of organisms in your sample.
- Count the number of organisms that are magnetic and non-magnetic.
- Describe the nanoparticle waste in the sample.

AP.7.2. Teaching Guide for Introductory Lecture

Through this experiment, the students will learn about nanoparticles and microorganisms as they combine the two and observe what happens. The lesson begins with a brief talk about nanoparticles and exactly how small nano is. During the talk, the teacher will demonstrate the making of nanoparticles through an online demonstration and current, every-day use of nanoparticles. The lesson continues with a brief talk about microorganisms. A prior homework assignment involving reading about microorganisms is necessary for the students to follow the lecture and experiment.

The lecture is written as if talking directly to the students. An answer to each question asked the students is provided in the parentheses following the question.

Introduction Lecture. What is nanotechnology? (Nanotechnology is any material with at least one dimension in the nanometer scale.) Exactly how small is nano? (Nano is 10^{-9} or one billionth of a meter. It is smaller than micro and larger than pico.) Nano is 10 to the minus what? (10^{-9}) Can you see nano with your bare eyes? (No. A microscope is needed to observe items on the nano scale.) Name everyday items that contain nanoparticles? (Sunscreen, make-up, stained glass, Dockers Stain resistant pants, anti-bacterial band-aids, etc.) We use nanotechnology in our everyday lives. But then what? (Open ended question. There is no correct or wrong answer to this question.) What happens to these particles as they are used and disposed of? (After disposal, nanomaterials can enter our environment through proper and improper trash disposal.)

The silver nanoparticles on band-aids and nanoparticles on stain-free pants wash off after time. So where to these particles go? (When washed down the sink drain, these particles are introduced into our water systems. When thrown away in the trash, these nanoparticles are introduced into our environment.) Like almost everything in our society, nanoparticles end up in our garbage which in turn ends up in our environment. But then what? (Open ended question. There is no correct or wrong answer to this question.) Will nanoparticles hurt our food cycle? (Possibly. It is unsure if nanoparticles bioaccumulate or are lethal after prolonged exposure.) What is the first energy level of an environment after the sun? (Primary producers.) What eats primary producers? (Primary consumers.) Name a few primary consumers? (Several answers are correct: microorganisms, all herbivores, etc.) What happens to microorganisms when they ingest nanoparticles? (Lead question, let the students answer but do not provide a definite answer.) Can microorganisms ingest nanoparticles? If microorganisms can ingest nanoparticles, what happens to the secondary consumers as they feed on the microorganisms? (Lead question, let students think about it but do not provide a definite answer.) Eventually nanoparticles will be included in our diet, will it harm us? Are nanoparticles toxic to humans? (We don't know for sure.) Scientists are studying the effects of nanoparticles on humans and it make take twenty to fifty years to find out.

So how do we make nanoparticles? (A chemical reaction must occur to produce materials on the nano scale.) Is it as simple as taking a block of silver or gold and trying to break it up into really, really small pieces? (No.) Chemicals on the nano level have different properties than chemicals on the bulk level. We make nanoparticles from atoms

of silver, gold, and other materials. It is a chemical reaction that creates these small particles. What color is solid gold? (Yellow.) What color are gold atoms? (The color depends on the chemical composition: potassium gold is yellow to clear.) What color are gold nanoparticles? (Gold based nanoparticles are red, purple, and blue: it depends on the particles size and coagulation.) Let's look at this internet website that shows the making of gold nanoparticles, http://mrsec.wisc.edu/Edetc/nanolab/gold/index.html. (This website shows a procedure for making gold nanoparticles from the Journal of Chemical Education in 2004 volume 81 pages 544A–544B.)

Can we use nanoparticles just as they are, or do we have to coat them in something? (Yes and no, it depends on what you are going to do with them.) Today, we will coat our particles with a polymer. What is a polymer? (Polymers are large molecules consisting of repeating units.) What in this classroom is made out of polymers? (Several answers are possible depending on items inside the classroom.) Several things in a classroom are made with polymers. Plastics make up a huge portion of our daily items, from toys to cars to pens. So why do you think we have to coat the nanoparticles in a polymer coating? (Lead question, let students think about it but do not provide a definite answer.) Polymers are used as a coating on many everyday items because they keep us safe. For this same reason, we will use two different types of polymers to coat the nanoparticles. This coating protects the microorganism from any possible toxic effect of the nanoparticle.

Before we start the lab, let's review what you will be doing. First we will coat the magnetic microparticles with a polymer. The coating process involves 3 washings: Add

polymer, centrifuge, remove as much liquid as possible, add clean water, mix, centrifuge, remove as much liquid as possible, add clean water, mix, centrifuge, remove as much liquid as possible, add clean water, mix, centrifuge, and remove as much liquid as possible. Use a magnet to retain as many particles as possible at the bottom of the microtube. After the particles have been coated, they are ready to be mixed with the microorganisms. Let the microorganisms incubate with the particles for at least one day to ensure ingestion. Observe the results.

Any questions before we begin the experiment?

Lesson Background.

- For a review article on nanotechnology: "Rise of the nanomachine: the evolution of a revolution in medicine", Park, H.H.; Jamison, A.C.; Lee, T.R. Nanomedicine 2007, 2(4), 425–439.
- For a Virtual lab on making nanoparticles and a general review of nanotechnology: http://www.mrsec.wisc.edu/Edetc/index.html

  The procedure for making gold nanoparticles is from the following reference:

  McFarland, A. D.; Haynes, C. L.; Mirkin, C. A.; Van Duyne, R. P.; Godwin, H. A. *J. Chem. Ed.* **2004**, *81*, 544A–544B.

AP.7.3. Teaching Guide for Closing Lecture

The closing lecture is to ensure that the students learned the concepts taught during this experiment. It is used as a direct and immediate method of assessment.

The lecture is written as if talking directly to the students. An answer to each question asked the students is provided in the parentheses following the question.

Lesson Closure. So what happened to the microorganisms? (The organisms should have ingested the nanoparticles and be able to be manipulated by a magnet.) Did they ingest the particles? (Yes.) If so, did they live or die? (All organisms should have survived.) If they died, what conclusions can you make about your experiment? (The experiment is not a failure however something went wrong during the procedure.) If they lived, what conclusions can you make about your experiment? (The students' hypothesis should be supported by the data collected during the experiment.) Compare your results with your classmates. Does anyone have pictures to share with the rest of the class? (Allow the students to share their recently acquired knowledge.) Now, what conclusions can you make? (Their conclusions should be supportive of a hypothesis that the organisms will ingest the nanoparticles and be magnetically manipulated.) What can you say about your hypothesis? (The data should support the hypothesis.) Did the results support or not support your hypothesis? (The data should support the hypothesis.)

Knowing what we now know about microorganisms and nanoparticles, what environmental impacts do nanoparticles cause? (Lead question, let students think about it

but do not provide a definite answer.) Should we continue to use nanoparticles in our everyday lives? (Lead question, let students think about it but do not provide a definite answer.) Do you think we can go smaller than nano? (Lead question, let students think about it but do not provide a definite answer.) Would we want to go smaller than nano? (Lead question, let students think about it but do not provide a definite answer.)

AP.7.4. Additional Assessment

Each student must write up a complete lab report including 5 references, all observations made during the experiment, and answer the following questions:

1. Are microorganisms considered primary consumers or primary producers? (The answer depends on the type of microorganism. Some protists and bacteria produce their own food thus they are primary producers. *Paramecium aurelia* uses cilia to move food into its oral groove thus it is a primary consumer.) Are all microorganisms primary consumers? (No, it depends on the type of microorganism.) What type of consumers are *Paramecium aurelia*: primary or secondary? (*Paramecium aurelia* are primary consumers and eat bacteria, algae, and yeasts.)
2. Besides polymers, what else can be used to coat a nanoparticle? (Several answers are acceptable; other metals, nonmetals, molecules, etc.) What other polymers can be used to coat the nanoparticles? (Any water soluble polymer is acceptable.)

3. This experiment uses iron oxide (Fe_3O_4) nanoparticles, what other materials can nanoparticles be made out of? (Several answers are acceptable; carbon, gold, silver, etc.)
4. What are some implications of this experiment? (Implications of this experiment include environmental effects and bioaccumulation.) Why are we testing this idea? (This experiment introduces nanotechnology while learning about microorganisms. We want to learn what happens when the two are combines and think about possible effects nanotechnology might create.)
5. How does nanotechnology improve our way of life? (Several answers are acceptable. Nanotechnology makes our life better in several ways through the miniaturization of technology (smaller cell phones, computers, etc.), improved cancer treatments, and stain-free clothing.)
6. Provide 2 other examples of nanotechnology. And explain why they are important. (Several answers are acceptable. Medicine, beauty products, cell phones, computers, stain-free clothing, food, paints, sports equipment, etc.)

AP.8. Acknowledgment

We would like to thank the NSF GK-12 Program, College of Engineering, University of Houston, Houston, TX for their financial support.

AP.9. References

(1) Mahmoudi, M.; Azadmanesh, K.; Shokrgozar, M. A.; Journeay, W. S.; Laurent, S. *Chem. Rev.* **2011**, *111*, 3407–3432.

(2) Wilhelm, C.; Gazeau, F.; Bacri, J. C. *Phys. Rev. E.* **2003**, *67*, 061908–061901/061912.

(3) Kim, D. H.; Cheang, U. K.; Kohidai, L.; Byun, D.; Kim, M. J. *Appl. Phys. Lett.* **2010**, *97*, 173702–173701/173703.

(4) Akin, D.; Sturgis, J.; Ragheb, K.; Sherman, D.; Burkholder, K.; Robinson, J. P.; Bhunia, A. K.; Mohammed, S.; Bashir, R. *Nature Nanotech.* **2007**, *2*, 441–449.

(5) Ochsenkuhn, M. A.; Jess, P. R. T.; Stoquert, H.; Dholakia, K.; Campbell, C. J. *ACS Nano* **2009**, *3*, 3613–3621.

(6) Kvitek, L.; Vanickova, M.; Panacek, A.; Soukupova, J.; Dittrich, M.; Valentova, E.; Prucek, R.; Bancirova, M.; Milde, D.; Zboril, R. *J. Phys. Chem. B* **2009**, *113*, 4296–4300.

(7) Park, H. H.; Jamison, A. C.; Lee, T. R. *Nanomedicine* **2007**, *2*, 425–439.

(8) Freitas, R. A. *J. Comput. Theor. Nanosci.* **2005**, *2*, 1–25.

(9) Sanni, M. L.; Kamal, R. A.; Kanj, M. Y. *Saudi Aramco Journal of Technology* **Spring 2008**, 44–52.

(10) Detty, M. R.; Gibson, S. L.; Wagner, S. J. *J. Med. Chem.* **2004**, *47*, 3910–3911.

(11) Brayner, R.; Dahoumane, S. A.; Yepremian, C.; Djediat, C.; Meyer, M.; Coute, A.; Fievet, F. *Langmuir* **2010**, *26*, 6522–6528.

(12) Haga, N.; Haneda, K. *Jpn. J. Protozool.* **2007**, *40*, 139–146.

(13) Morgalev, Y. N.; Khoch, N. S.; Morgaleva, T. G.; Gulik, E. S.; Borilo, G. A.; Bulatova, U. A.; Morgalev, S. Y.; Ponyavina, E. V. *Nanotechnology in Russia* **2010**, *5*, 851–856.

(14) Ghafari, P.; St-Denis, C. H.; Power, M. E.; Jin, X.; Tsou, V.; Mandal, H. S.; Bols, N. C.; Tang, X. S. *Nature Nanotech.* **2008**, *3*, 347–351.

(15) Deng, H. L., X.; Peng, Q.; Wang, X.; Chen, J.; Li, Y. *Angew. Chem. Int. Ed.* **2005**, *44*, 2782.

Appendix II. Synthesis of Cholesterol-based Carboxylic Acids for Use in Langmuir-Blodgett Monolayers

AP.10. Introduction

The two main pathways for monolayer formation include Langmuir-Blodgett monolayers and self-assembled monolayers. Langmuir-Blodgett monolayers are formed at the air-water interface, allowed to equilibrate while mobile on the water interface, and transferred to a solid substrate where as self-assembled monolayers are formed at the solid-liquid interface and have a lesser ability to move once adsorbed onto the metal substrate. Therefore the headgroups of molecules used to form Langmuir-Blodgett monolayers are hydrophilic (*e.g.*, carboxylic acids in water) while the headgroups of molecules used to form self-assembled monolayers can be less hydrophilic and are typically chosen based on their ability to bind strongly with the metal interface (*e.g.*, thiolate on gold). After formation, the monolayers have similar physical properties and can thus be compared.

In order to study the difference in the monolayer formation for cholesterol-based adsorbates, we have synthesized targeted single-chained and double-chained carboxylic acids for use in Langmuir-Blodgett monolayers to correlate with the thiols previously discussed in this dissertation for use in self-assembled monolayers.

AP.11. Synthesis of Single-chained Cholesterol-based Carboxylic Acids

Materials. Tetrahydrofuran (THF) was purchased from Mallinckrodt Baker, Inc, distilled over calcium hydride, and stored under argon. Anhydrous dioxane, methanol, cholesterol, 1,3-propanediol, 1,4-butanediol, 1,5-pentanediol, 1,6-hexanediol, 1,9-nonanediol, and triethylamine (NEt_3) were purchased from Aldrich Chemical Co. and used as received. *p*-Toluenesulfonyl chloride (TsCl) was purchased from Acros Organics and used as received. Column chromatography was performed using silica gel (40 – 64 μm) and thin-layer chromatography (TLC) was carried out using 200 μm thick silica gel plates, which both were purchased from Sorbent Technologies, Inc. The eluted TLC plates were developed with a molybdenum blue stain followed by heating. Nuclear Magnetic Resonance (NMR) spectra were recorded on a JOEL ECA-500 spectrometer operating at 500 MHz. The data were obtained in chloroform-d ($CDCl_3$) and referenced to δ 7.26 ppm for ^{1}H NMR spectra and 77.00 ppm for ^{13}C NMR spectra.

Analysis of Starting Materials. Reference information for the initial reagents was analyzed by ^{1}H NMR spectroscopy and TLC. These data were used as a baseline to judge the progress of the reactions. *Cholesterol*. ^{1}H NMR (500 MHz, $CDCl_3$): δ 0.66 (s, 3 H), 0.86 – 1.57 (m, 36 H), 1.82 (m, 3 H), 1.99 (dd, J = 12.72 Hz, 2 H), 2.25 (m, 2 H), 3.50 (m, 1 H), 5.34 (m, 1 H). TLC: R_f = 0.73.

Synthesis of Single-chained Cholesterol-based Carboxylic Acids. The general synthetic route for this series of single-chain linactants containing carboxylic acid is outlined in Scheme AP.1.

Scheme AP.1. Preparation of a Series of Single-chained Cholesterol-based Carboxylic Acids, where n = 3, 4, 5, 6, and 9.

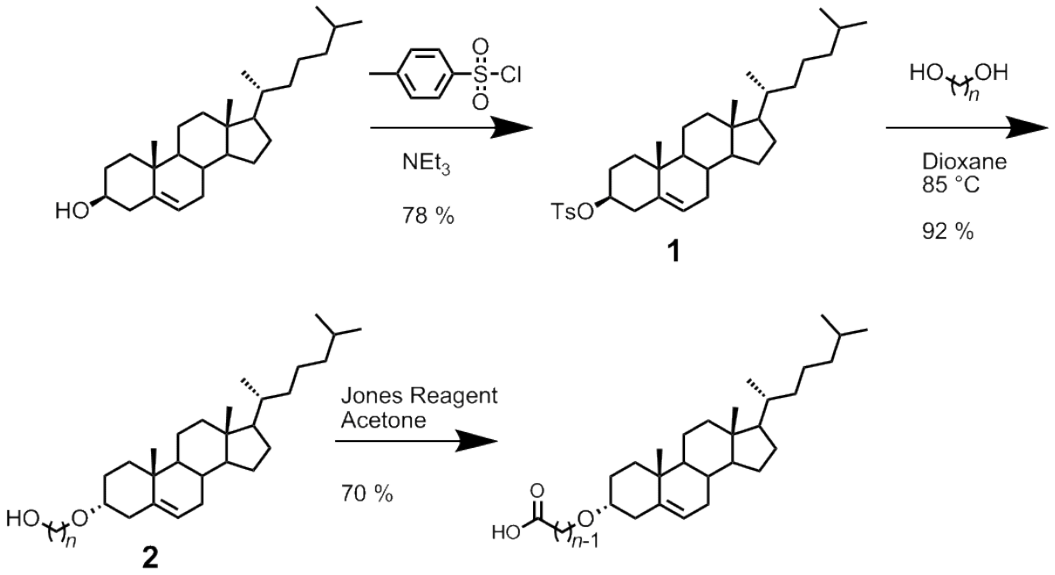

*Cholesterol tosylate (**1**).* Cholesterol tosylate was synthesized by combining 18.09 g of cholesterol (46.78 mmol) and 37.71 g *p*-toluenesulfonyl chloride (197.8 mmol) in 60.0 mL of triethylamine (430 mmol). After purging with nitrogen, the reaction stirred overnight at room temperature. TLC confirmed that a reaction occurred. The reaction was worked up by the addition of 150 mL of dichloromethane and 150 mL water. The organic layer was washed with 2 × 100 mL of each of the following solutions: 1N hydrochloric acid, water, and brine. The organic layer was dried with anhydrous sodium

sulfate, filtered, and the solvent was reduced under vacuum to yield a yellow liquid. The product was precipitated by the addition of methanol and filtered to collect a white solid. Yield: 19.76 g (36.54 mmol, 78 %). TLC (80 % hexane: 20 % ethyl acetate): R_f = 0.62. Crude ^{1}H NMR (500 MHz, $CDCl_3$): δ 0.61 (s, 3 H), 0.86 – 1.58 (m, 34 H), 1.69 (m, 1 H), 1.81 (m, 3 H), 2.00 (m, 2 H), 2.25 (m, 1 H), 2.43 (m, 4 H), 4.31 (m, 1 H), 5.29 (m, 1 H), 7.32 (d, *J* = 7.90 Hz, 2 H), 7.79 (d, *J* = 8.25 Hz, 2 H).

C*holest-5-en-3β-oxypropan-3-ol (**2**).* Cholest-5-en-3β-oxypropan-3-ol was synthesized by combining 1.115 g of tosylate **1** (2.061 mmol) and 5.00 mL of 1,3-propanediol (69.2 mmol) in 24.0 mL of anhydrous dioxane. The reaction was heated to 85 ºC for 4 hours under nitrogen. TLC confirmed that a reaction occurred. The reaction was worked up by the addition of 50 mL of dichloromethane and 50 mL water. The organic layer was washed with 2 × 100 mL of each of the following solutions: water, 1N hydrochloric acid, and brine. The organic layer was dried with anhydrous sodium sulfate, filtered, and the solvent was removed under vacuum to yield a yellow solid. The crude compound was purified by column chromatography (99 % hexane: 1 % ethyl acetate – 70 % hexane: 30 % ethyl acetate) to provide a white solid. Yield: 0.842 g (1.89 mmol, 92 %). TLC (80 % hexane: 20 % ethyl acetate): R_f = 0.20. ^{1}H NMR (500 MHz, $CDCl_3$): δ 0.67 (s, 3 H), 0.85 – 1.58 (m, 35 H), 1.78 – 2.05 (m, 7 H), 2.15 (m, 1 H), 2.37 (m, 1 H), 2.59 (t, *J* = 5.15 Hz, 1 H), 3.17 (m, 1 H), 3.67 (m, 2 H), 3.87 (q, *J* = 5.50 Hz, 2 H), 5.34 (m, 1 H).

C*holest-5-en-3β-yl-3-carboxypropyl ether*. Cholest-5-en-3β-yl-3-carboxypropyl ether was synthesized by dissolving 0.771 g of alcohol **2** (1.60 mmol) in 5.00 mL of

anhydrous acetone. Jones reagent (12.5 g $Na_2Cr_2O_7 \bullet 2H_2O$, 25 mL concentrated sulfuric acid, and 75 mL water) was added dropwise until an orange color was sustained. 2-Propanol was added to neutralize the excess Jones reagent. The green Cr^{+4} salts were removed by filtration, and the solvent was removed under vacuum. Purification was achieved via column chromatography (99 % hexanes: 1 % ethyl acetate – 70 % hexane: 30 % ethyl acetate). Yield: 0.182 g (0.397 mmol, 25 %). TLC (80 % hexane: 20 % ethyl acetate): $R_f = 0.39$. ^{1}H NMR (500 MHz, $CDCl_3$): δ 0.66 (s, 3 H), 0.85 – 2.02 (m, 50 H), 2.23 (m, 1 H), 2.38 (m, 1 H), 2.64 (t, *J* = 5.73 Hz, 3 H), 3.26 (m, 1 H), 5.35 (m, 1 H). ^{13}C NMR (500 MHz, $CDCl_3$): δ 11.95, 18.81, 19.46, 21.15, 22.66, 22.92, 23.92, 24.38, 28.11, 28.33, 29.81, 31.96, 32.00, 35.32, 35.88, 36.28, 36.93, 37.24, 38.99, 39.60, 39.86, 42.40, 50.24, 56.24, 56.85, 63.14, 79.67, 121.90, 140.72, 179.80.

C*holest-5-en-3β-yl-4-carboxybutyl ether*. Yield: 0.274 g (0.580 mmol, 31 %). TLC (80 % hexane: 20 % ethyl acetate): $R_f = 0.40$. ^{1}H NMR (500 MHz, $CDCl_3$): δ 0.66 (s, 3 H), 0.85 – 2.02 (m, 50 H), 2.23 (m, 1 H), 2.37 (m, 1 H), 2.64 (t, *J* = 6.87 Hz, 3 H), 3.27 (m, 1 H), 5.35 (m, 1 H). ^{13}C NMR (500 MHz, $CDCl_3$): δ 11.95, 18.80, 19.47, 21.16, 22.67, 22.92, 23.91, 24.38, 28.11, 28.32, 29.81, 31.96, 32.01, 35.32, 35.88, 36.28, 36.93, 37.25, 38.99, 39.60, 39.86, 42.41, 50.22, 56.24, 56.86, 63.15, 79.66, 121.83, 140.89, 179.82.

C*holest-5-en-3β-yl-5-carboxypentyl ether*. Yield: 0.322 g (0.662 mmol, 38 %). TLC (80 % hexane: 20 % ethyl acetate): $R_f = 0.42$. ^{1}H NMR (500 MHz, $CDCl_3$): δ 0.67 (s, 3 H), 0.85 – 2.02 (m, 52 H), 2.40 (m, 1 H), 2.37 (m, 1 H), 2.64 (t, *J* = 6.85 Hz, 3 H), 3.27 (m, 1 H), 5.35 (m, 1 H). ^{13}C NMR (500 MHz, $CDCl_3$): δ 11.95, 18.82, 19.46, 21.16,

22.66, 22.93, 23.92, 24.39, 28.11, 28.33, 29.82, 31.97, 32.00, 35.33, 35.88, 36.28, 36.93, 37.27, 38.99, 39.60, 39.85, 42.42, 50.22, 56.25, 56.87, 63.13, 79.67, 121.84, 140.88, 179.87.

C*holest-5-en-3β-yl-6-carboxyhexyl ether.* Yield: 0.511 g (1.02 mmol, 62 %). TLC (80 % hexane: 20 % ethyl acetate): R_f = 0.44. ^{1}H NMR (500 MHz, $CDCl_3$): δ 0.67 (s, 3 H), 0.85 – 2.02 (m, 46 H), 2.19 (m, 1 H), 2.37 (t, *J* = 7.45 Hz, 3 H), 3.13 (m, 1 H), 3.48 (m, 2 H), 5.35 (m, 1 H). ^{13}C NMR (500 MHz, $CDCl_3$): δ 11.95, 18.81, 19.46, 21.16, 22.65, 22.93, 23.92, 24.39, 28.11, 28.33, 29.81, 31.98, 32.01, 35.32, 35.89, 36.28, 36.92, 37.26, 38.99, 39.61, 39.85, 42.42, 50.22, 56.24, 56.87, 63.14, 79.67, 121.84, 140.89, 179.90.

C*holest-5-en-3β-yl-9-carboxynonyl ether.* Yield: 0.422 g (0.778 mmol, 50 %). TLC (80 % hexane: 20 % ethyl acetate): R_f = 0.46. ^{1}H NMR (500 MHz, $CDCl_3$): δ 0.67 (s, 3 H), 0.85 – 2.02 (m, 46 H), 2.20 (m, 1 H), 2.35 (t, *J* = 7.45 Hz, 3 H), 3.13 (m, 1 H), 3.47 (m, 2 H), 5.34 (m, 1 H). ^{13}C NMR (500 MHz,$CDCl_3$): δ 11.95, 18.81, 19.47, 21.16, 22.66, 22.93, 23.92, 24.38, 28.11, 28.33, 29.81, 31.97, 32.00, 35.33, 35.88, 36.28, 36.94, 37.26, 38.99, 39.62, 39.85, 42.40, 50.22, 56.24, 56.88, 63.14, 79.68, 121.84, 140.89, 179.92.

AP.12. Synthesis of Double-chained Cholesterol-based Carboxylic Acids

Materials. Tetrahydrofuran (THF) was purchased from Mallinckrodt Baker, Inc, distilled over calcium hydride, and stored under argon. Anhydrous dioxane, anhydrous

N,*N*-dimethylformamide (DMF), methanol, cholesterol, 1,3-propanediol, 1,6-hexanediol, 1,9-nonanediol, sodium iodide (NaI), and triethylamine (NEt_3) were purchased from Aldrich Chemical Co. and used as received. Methanesulfonyl chloride (MsCl) and *p*-toluenesulfonyl chloride (TsCl) were purchased from Acros Organics and used as received. Column chromatography was performed using silica gel (40 – 64 μm) and thin-layer chromatography (TLC) was carried out using 200 μm-thick silica gel plates, which both were purchased from Sorbent Technologies, Inc. The eluted TLC plates were developed with a molybdenum blue stain followed by heating. Nuclear Magnetic Resonance (NMR) spectra were recorded on a JOEL ECA-500 spectrometer operating at 500 MHz. The data were obtained in chloroform-d ($CDCl_3$) and referenced to δ 7.26 ppm for ^{1}H NMR spectra and 77.00 ppm for ^{13}C NMR spectra.

Synthesis of Double-chained Cholesterol-based Carboxylic Acids. The synthetic strategy used to prepare the targeted double-chain cholesterol-based carboxylic acids is shown in Scheme AP.2. The complete experimental details of each synthetic step are provided as follows.

Scheme AP.2. Preparation of a Series of Double-chained Cholesterol-based Carboxylic Acids, where n = 3, 6, and 9.

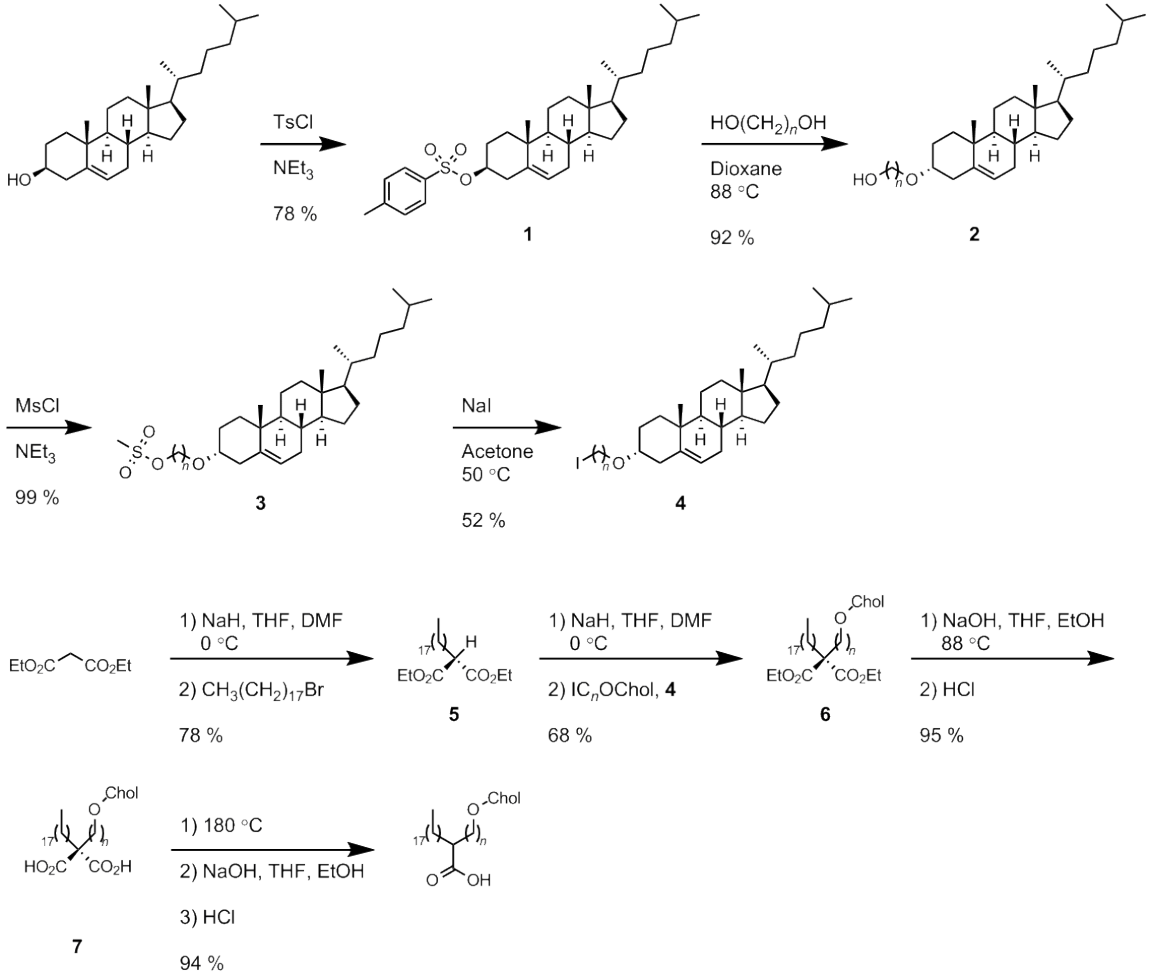

*Cholesterol tosylate (**1**).* Cholesterol tosylate was synthesized by combining 18.09 g of cholesterol (46.78 mmol) and 37.71 g *p*-toluenesulfonyl chloride (197.8 mmol) in 60.0 mL of triethylamine (430 mmol). After purging with nitrogen, the reaction was allowed to stir overnight at room temperature. TLC confirmed that a reaction occurred. The reaction was worked up by the addition of 150 mL of dichloromethane and 150 mL

water. The organic layer was washed with 2 × 100 mL of each of the following solutions: 1N hydrochloric acid, water, and brine. The organic layer was dried with anhydrous sodium sulfate, filtered, and the solvent was reduced under vacuum to yield a yellow liquid. The product was precipitated by the addition of methanol and filtered to collect a white solid. Yield: 19.76 g (36.54 mmol, 78 %). TLC (80 % hexane: 20 % ethyl acetate): R_f = 0.62. Crude ^{1}H NMR (500 MHz, $CDCl_3$): δ 0.61 (s, 3 H), 0.86 – 1.58 (m, 34 H), 1.69 (m, 1 H), 1.81 (m, 3 H), 2.00 (m, 2 H), 2.25 (m, 1 H), 2.43 (m, 4 H), 4.31 (m, 1 H), 5.29 (m, 1 H), 7.32 (d, *J* = 7.90 Hz, 2 H), 7.79 (d, *J* = 8.25 Hz, 2 H).

C*holest-5-en-3β-oxypropan-3-ol (**2**).* Cholest-5-en-3β-oxypropan-3-ol was synthesized by combining 1.115 g of tosylate **1** (2.061 mmol) and 5.00 mL of 1,3-propanediol (69.2 mmol) in 24.0 mL of anhydrous dioxane. The reaction was heated to 85 ºC for 4 hours under nitrogen. TLC confirmed that a reaction occurred. The reaction was worked up by the addition of 50 mL of dichloromethane and 50 mL water. The organic layer was washed with 2 × 100 mL of each of the following solutions: water, 1N hydrochloric acid, and brine. The organic layer was dried with anhydrous sodium sulfate, filtered, and the solvent was removed under vacuum to yield a yellow solid. The crude compound was purified by column chromatography (99 % hexane: 1 % ethyl acetate – 70 % hexane: 30 % ethyl acetate) to provide a white solid. Yield: 0.842 g (1.89 mmol, 92 %). TLC (80 % hexane: 20 % ethyl acetate): R_f = 0.20. ^{1}H NMR (500 MHz, $CDCl_3$): δ 0.67 (s, 3 H), 0.85 – 1.58 (m, 35 H), 1.78 – 2.05 (m, 7 H), 2.15 (m, 1 H), 2.37 (m, 1 H), 2.59 (t, *J* = 5.15 Hz, 1 H), 3.17 (m, 1 H), 3.67 (m, 2 H), 3.87 (q, *J* = 5.50 Hz, 2 H), 5.34 (m, 1 H).

C*holest-5-en-3β-oxypropan-3-mesylate (**3**)*. A solution of the alcohol **2** (1.2148 g, 2.7315 mmol) in triethylamine (6.00 mL, 43.0 mmol) was prepared under nitrogen and allowed to stir for 1 hour. Methanesulfonyl chloride (0.65 mL, 8.4 mmol) was added dropwise over 5 minutes to the stirred mixture. After the addition was completed, stirring was continued for 4 hours at room temperature. The reaction was quenched by the addition of ice-cold water (200 mL). The mixture was extracted with dichloromethane (3 × 100 mL). The organic phase was washed with water (2 × 100 mL) and 2 × 100 mL of each of the following solutions: 1N hydrochloric acid, water, and brine. The organic layer was dried over anhydrous sodium sulfate, filtered, and the solvent was removed under vacuum to yield a yellow solid. The crude product was used directly in the next step without further purification. Yield: 1.42 g (2.72 mmol, 99 %). TLC (80 % hexane: 20 % ethyl acetate): R_f = 0.25. Crude ^{1}H NMR (500 MHz, $CDCl_3$): δ 0.64 (s, 3 H), 0.85 – 1.62 (m, 37 H), 1.80 – 2.02 (m, 7 H), 2.15 (m, 1 H), 2.34 (m, 1 H), 3.00 (s, 3 H), 3.13 (m, 1 H), 3.57 (m, 2 H), 4.34 (t, *J* = 6.19 Hz, 2 H), 5.34 (m, 1 H).

C*holest-5-en-3β-oxypropan-3-iodide (**4**)*. The mesylate **3** (1.416 g, 2.708 mmol) was dissolved in degassed ethanol (24 mL) and added to a reaction flask containing sodium iodide (0.983 g, 8.61 mmol). The reaction mixture was heated to 88 °C for 4 hours under nitrogen. The reaction was worked up by addition of cool water (50 mL) and the mixture extracted with dichloromethane (3 × 100 mL). The organic phases were combined and washed with water (3 × 100 mL) and brine (1 × 100 mL), dried over anhydrous sodium sulfate, filtered, and the solvent was removed under vacuum to yield a light yellow solid. The crude product was purified by column chromatography (99 %

hexane: 1 % ethyl acetate) to give a white solid. Yield: 0.900 g (1.62 mmol, 66 %). TLC (80 % hexane: 20 % ethyl acetate): R_f = 0.79. ^{1}H NMR (500 MHz, $CDCl_3$): δ 0.67 (s, 3 H), 0.84 – 1.60 (m, 37 H), 1.78 – 2.02 (m, 7 H), 2.15 (m, 1 H), 2.37 (m, 4 H), 2.96 (t, *J* = 6.87 Hz, 2 H), 3.17 (m, 1 H), 3.51 (m, 2 H), 5.34 (m, 1 H).

Diethyl 2-octadecylmalonate (**5**). A solution of sodium hydride (5.246 g, 131.1 mmol; 60% dispersion in mineral oil) in tetrahydrofuran (50 mL) and N,N-dimethylformamide (24 mL) was prepared at 0 °C under an atmosphere of nitrogen. To this stirred solution maintained at 0 °C, diethyl malonate (18.50 mL, 121.9 mmol) was added slowly. Stirring was continued for 15 minutes at room temperature, and then bromooctadecane (20.09 g, 60.25 mmol) was added. The reaction mixture was stirred at room temperature overnight and then concentrated under reduced pressure. The resultant oil was suspended in water (100 mL), and extracted with ethyl acetate (2 × 150 mL). The organic layer was washed with water (2 × 100 mL) and brine (1 × 100 mL). The organic layer was dried over anhydrous sodium sulfate, filtered, and concentrated under reduced pressure to provide brown oil. The crude compound was purified by column chromatography (95 % hexane: 5 % ethyl acetate) to give a white solid. Yield: 39.37 g (95.41 mmol, 78 %). TLC (80 % hexane: 20 % ethyl acetate): R_f = 0.74. ^{1}H NMR (500 MHz, $CDCl_3$): δ 0.88 (t, *J* = 6.87 Hz, 3 H), 1.22 – 1.32 (m, 40 H), 1.88 (m, 2 H), 3.31 (t, *J* = 7.56 Hz, 1 H), 4.19 (m, 4 H).

Diethyl 2-(cholest-5-en-3β-oxypropane)-2-octadecylmalonate (**6**). A solution of sodium hydride (0.790 g, 19.8 mmol) in tetrahydrofuran (16 mL) and N,N-dimethylformamide (2 mL) was prepared at 0 °C under an atmosphere of nitrogen. To

this solution diester **5** (5.035 g, 12.20 mmol) was added slowly. The mixture was stirred at room temperature for 15 minutes, and then iodide **4** (6.796 g, 12.25 mmol) was transferred into the mixture via syringe. The reaction mixture was stirred at room temperature overnight and then concentrated under vacuum. The resultant oil was suspended in water (100 mL), and extracted with ethyl acetate (2 × 100 mL). The organic layer was washed with water (2 × 50 mL) and brine (1 × 100 mL), dried over anhydrous sodium sulfate, filtered, and concentrated under reduced pressure. The yellow oil was purified by column chromatography (95 % hexane: 5 % dichloromethane) to give a colorless oil. Yield: 6.98 g (8.32 mmol, 68 %). TLC (80 % hexane: 20 % ethyl acetate): R_f = 0.77. ^{1}H NMR (500 MHz, $CDCl_3$): δ 0.63 (s, 3 H), 0.78 – 1.70 (m, 84 H), 1.75 – 2.01 (m, 10 H), 2.12 (m, 1 H), 2.29 (m, 1 H), 3.07 (m, 1 H), 3.39 (t, *J* = 6.30 Hz, 2 H), 4.13 (q, *J* = 6.87 Hz, 4 H), 5.27 (m, 1 H).

2-(Cholest-5-en-3β-oxypropane)-2-octadecylmalonic acid (**7**). Malonate **6** (6.984 g, 8.321 mmol) and sodium hydroxide (7.5454 g, 188.64 mmol) were dissolved in ethanol (100 mL) with dry tetrahydrofuran (15 mL). After purging with nitrogen, the reaction mixture was refluxed for 12 hours at 88 °C. The reaction mixture was then cooled in an ice bath and concentrated hydrochloric acid was added until the mixture was acidic. The product was extracted into ethyl acetate (3 × 50 mL), washed with water (2 × 50 mL) and once with brine (50 mL). The organic phase was dried over anhydrous sodium sulfate, filtered, and the solvent was evaporated under vacuum to yield a white solid. The crude product was used directly in the next step without any purification. Yield: 6.17 g (7.88 mmol, 95 %). TLC (80 % hexane: 20 % ethyl acetate): R_f = 0.05.

Crude ^{1}H NMR (500 MHz, $CDCl_3$): δ 0.66 (s, 3 H), 0.80 – 1.73 (m, 72 H), 1.77 – 2.07 (m, 9 H), 2.22 (m, 1 H), 2.36 (m, 1 H), 3.30 (m, 1 H), 3.62 (t, J = 5.73 Hz, 2 H), 5.34 (m, 1 H).

2-(C*holest-5-en-3β-oxypropane)-2-eicosanoic acid*. Crude malonic acid **7** (6.171 g, 7.879 mmol) was placed in a flask fitted with a reflux condenser and purged with argon for 10 minutes. The starting material was then heated to 180 °C until gasses were no longer evolving through an oil bubbler. The flask was then cooled to room temperature, and sodium hydroxide (5.617 g, 140.4 mmol) along with tetrahydrofuran (11 mL) and ethanol (100 mL) were added to the flask. The mixture was refluxed for 12 hours at 88 °C. The mixture was then cooled to room temperature, and concentrated hydrochloric acid was added until the mixture was acidic. The product was extracted into ethyl acetate (3 × 50 mL), washed with water (2 × 50 mL) and once with brine (50 mL). The organic phase was dried over anhydrous sodium sulfate, filtered, and the solvent was evaporated under vacuum to yield a yellow solid. The crude compound was purified by column chromatography (90 % hexane: 10 % ethyl acetate – 60 % hexane: 40 % ethyl acetate) to provide a white solid. Yield: 5.45 g (7.37 mmol, 94 %). TLC (80 % hexane: 20 % ethyl acetate): R_f = 0.48. ^{1}H NMR (500 MHz, $CDCl_3$): δ 0.66 (s, 3 H), 0.80 – 1.73 (m, 76 H), 1.76 – 2.05 (m, 5 H), 2.17 (m, 1 H), 2.33 (m, 1 H), 3.11 (m, 1 H), 3.45 (t, J = 4.58 Hz, 2 H), 5.31 (m, 1 H). ^{13}C NMR (500 MHz, $CDCl_3$): δ 11.94, 14.26, 18.83, 19.45, 21.18, 22.68, 22.83, 22.92, 24.00, 24.39, 27.46, 27.97, 28.10, 28.36, 28.46, 28.87, 29.55, 29.65, 29.81, 29.85, 29.91, 31.97. 32.09, 32.22, 25.93, 35.93, 36.32, 36.94. 37.37, 39.18, 39.63, 39.90, 42.39, 45.36, 50.29, 56.30, 56.87, 67.23, 79.24, 121.58, 140.90, 182.44.

2-(C*holest-5-en-3β-oxyhexane)-2-eicosanoic acid.* Yield: 3.250 g (4.160 mmol, 54 %). TLC (80% Hex: 20% EA): R_f = 0.48. ^{1}H NMR (500 MHz, $CDCl_3$): δ 0.63 (s, 3 H), 0.86 - 1.64 (m, 82 H), 1.77 – 2.10 (m, 4 H), 2.18 (m, 1 H), 2.35 (m, 1 H), 3.13 (m, 1 H), 3.44 (t, *J* = 6.31 Hz, 2 H), 5.33 (m, 1 H). ^{13}C NMR (500 MHz, $CDCl_3$): δ 11.94, 14.27, 18.83, 19.45, 21.18, 22.68, 22.83, 22.93, 24.01, 24.39, 27.46, 27.98, 28.10, 28.37, 28.46, 28.88, 29.55, 29.65, 29.81, 29.85, 29.92, 31.97. 32.09, 32.22, 25.93, 35.93, 36.33, 36.94. 37.37, 39.18, 39.63, 39.90, 42.39, 45.36, 50.30, 56.30, 56.87, 67.24, 79.24, 121.58, 140.91, 182.46.

2-(C*holest-5-en-3β-oxynonane)-2-eicosanoic acid.* Yield: 3.250 g (3.947 mmol, 37 %). TLC (80% Hex: 20% EA): R_f = 0.59. ^{1}H NMR (500 MHz, $CDCl_3$): δ 0.69 (s, 3 H), 0.86 - 1.64 (m, 89 H), 1.76 – 2.13 (m, 5 H), 2.18 (m, 1 H), 2.32 (m, 1 H), 3.13 (m, 1 H), 3.44 (t, *J* = 6.30 Hz, 2 H), 5.32 (m, 1 H). ^{13}C NMR (500 MHz, $CDCl_3$): δ 11.94, 14.27, 18.83, 19.46, 21.18, 22.69, 22.83, 22.94, 24.01, 24.39, 27.47, 27.98, 28.10, 28.38, 28.46, 28.88, 29.55, 29.65, 29.81, 29.86, 29.92, 31.97. 32.10, 32.23, 25.93, 35.93, 36.34, 36.94. 37.37, 39.19, 39.63, 39.90, 42.40, 45.36, 50.30, 56.32, 56.87, 67.24, 79.24, 121.58, 140.91, 182.50.

AP.12. Conclusions

These single-chained and double-chained cholesterol-based carboxylic acids were successfully synthesized and characterized by NMR spectroscopy. For the single-chained series, n = 3, 4, 5, 6, and 9. For the double-chained series, the cholesterol-

containing tailgroup has n = 3, 6, and 9 and the other tailgroup is an alkyl chain with 18 carbons. These novel molecules will be used to form pure and mixed Langmuir-Blodgett monolayers. The data collected from the Langmuir-Blodgett monolayers will be compared to the data collected from the self-assembled monolayers generated from the corresponding thiols.